Electronic Supplementary Material (ESI) for ChemComm.

Supporting Information

Bis(perchlorocatecholato)silane and Heteroleptic Bidonors: Hidden Frustrated Lewis Pairs by Ring Strain

Deborah Hartmann, Sven Braner and Lutz Greb*

Table of contents

1. Materials and Methods

Unless stated otherwise, all manipulations were carried out under a dry argon atmosphere by using standard Schlenk techniques to prevent oxidation and hydrolysis of the sensitive compounds. Solvents were degassed prior to use with three freeze-pump-thaw cycles and were stored in sealed Schlenk ampulla over activated molecular sieve (3 or 4 Å, respectively) under a dry argon atmosphere. All glassware, syringes, magnetic stirring bars and needles were thoroughly dried. The commercially available chemicals were used as received. Bis-sulfolane adduct **1**·(sulfolane)$_2$,[1] and 2-((dimethyl-amino)methyl)pyridine[2] were prepared according the literature. All air sensitive compounds were stored in a glove box (Sylatech Y-05-G-7986) under N_2 atmosphere. Purity and identity of the compounds were confirmed by high resolution multinuclear NMR spectroscopy and single crystal X-Ray diffraction (SCXRD). ^{1}H-, ^{13}C-, ^{29}Si and ^{31}P NMR spectra were collected with a *Bruker BZH 200/52*, a *Bruker DPX 200*, a *Bruker Avance II 400* or a *Bruker Avance III 600* NMR spectrometer and referenced to the solvent in use. NMR data is reported as follows: chemical shift δ [ppm], multiplicity (s = singlet, d = doublet, t = triplet, m = multiplet, and combinations), scalar spin-spin coupling constant [Hz] as $^{X}J_{A\text{-}B}$ (X = number of chemical bonds between coupled nuclei; A, B = coupled nuclei), integration value. NMR spectra were processed and plotted with MestReNova 14.2.[3] Mass analysis of the obtained products was attempted by various methods (ESI, LIFDI, EI) but remained unsuccessful. Elemental analysis was not performed.

2. Synthetic Procedures

2.1 Synthesis of $Si(cat^{Cl})_2(pyNMe_2)$ (**1-A**)

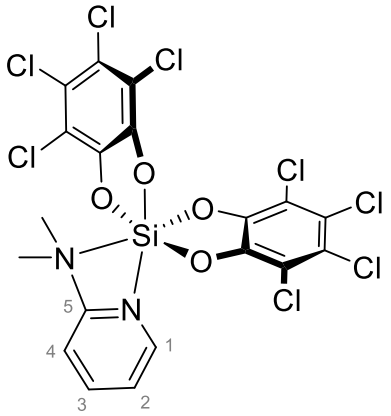

To a suspension of $Si(cat^{Cl})_2$·$(sulfolane)_2$ (0.31 g, 0.42 mmol, 1.00 eq.) in 12 ml dichloromethane, 2-(dimethylamino)pyridine (0.05 g, 0.42 mmol, 1.00 eq.) was added dropwise and the reaction mixture was stirred for 1 hour. A weakly cloudy off-white solution was obtained. 12 ml pentane were added and the precipitate was filtered off, washed two times with 10 ml dichloromethane:pentane 1:1 and dried *in vacuo*. The product was obtained as a colorless solid (0.24 g, 0.37 mmol, 91 %).
Suitable colorless single-crystals for SCXRD were obtained by gaseous diffusion of pentane into a saturated solution of chlorobenzene at −40 °C.

^{1}H NMR (600 MHz, CD_2Cl_2) δ = 8.40 (*pseudo*-t, $^3J_{H-H}$ = 7.7 Hz, 1H, H_{py}-1), 8.26 (d, $^3J_{H-H}$ = 5.3 Hz, 1H, H_{py}-4), 7.74 (m, 2H, H_{py}-2, H_{py}-3), 3.08 (s, 6H, CH_3).

^{13}C NMR (151 MHz, CD_2Cl_2) δ = 157.1 (C_{py}-5), 146.9 (C_{py}-1), 145.6 (*ipso*-C_{cat}), 142.1 (C_{py}-3), 127.5 (C_{py}-2), 122.4 (*ortho*-C_{cat}), 118.2 (C-4), 115.6 (*meta*-C_{cat}), 47.8 (2C, CH_3).

^{29}Si NMR (119 MHz, CD_2Cl_2) δ = −134.1.

^{29}Si NMR (79 MHz, *o*-DCB) δ = −133.8.

2.2 Synthesis of $Si(cat^{Cl})_2(pyCH_2NMe_2)$ (**1-B**)

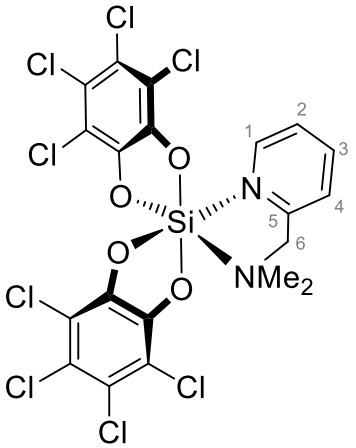

To a suspension of $Si(cat^{Cl})_2$·$(sulfolane)_2$ (25 mg, 33 µmol, 1.00 eq.) in 0.5 ml CD_2Cl_2 was added 2-((dimethylamino)methyl)pyridine (4.5 mg, 33 µmol, 1.00 eq.). Dissolution of the poorly soluble starting material indicated complete reaction. The product was not isolated and contains 2 eq. of sulfolane.

Suitable colorless single-crystals for SCXRD were obtained by gaseous diffusion of pentane into a saturated solution of dichloromethane at −40 °C.

^{1}H NMR (600 MHz, CD_2Cl_2) δ = 8.96 (d, $^3J_{H-H}$ = 5.5 Hz, 1H, H_{py}-1), 8.14 (td, $^3J_{H-H}$ = 7.7, 1.6 Hz, 1H, H_{py}-3), 7.69 (t, $^3J_{H-H}$ = 6.7 Hz, 1H, H_{py}-2), 7.57 (dd, $^3J_{H-H}$ = 7.8, 1.2 Hz, 1H, H_{py}-4), 4.89 (d, $^2J_{H-H}$ = 15.3 Hz, 1H, CH_2), 3.87 (d, $^2J_{H-H}$ = 15.3 Hz, 1H, CH_2), 3.11 (s, 3H, CH_3), 2.32 (s, 3H, CH_3).

^{13}C NMR (151 MHz, CD_2Cl_2) δ = 149.8 (C_{py}-5), 147.0 (C_{py}-1), 146.2 (*ipso*-C_{cat}), 146.1 (*ipso*-C_{cat}), 145.5 (*ipso*-C_{cat}), 145.4 (*ipso*-C_{cat}), 143.5 (C_{py}-3), 126.4 (C_{py}-2), 124.0 (C_{py}-4), 122.1 (*ortho*-C_{cat}), 121.8 (*ortho*-C_{cat}), 121.7 (*ortho*-C_{cat}), 121.2 (*ortho*-C_{cat}), 115.7 (*meta*-C_{cat}), 115.4 (*meta*-C_{cat}), 115.3 (*meta*-C_{cat}), 115.1 (*meta*-C_{cat}), 63.5 (CH_2), 50.1 (CH_3), 49.0 (CH_3).

^{29}Si NMR (119 MHz, CD_2Cl_2) δ = −140.2.

^{29}Si NMR (119 MHz, *o*-DCB) δ = −139.9.

2.3 Synthesis of $Si(cat^{Cl})_2(pyPPh_2)$ (**1-C**)

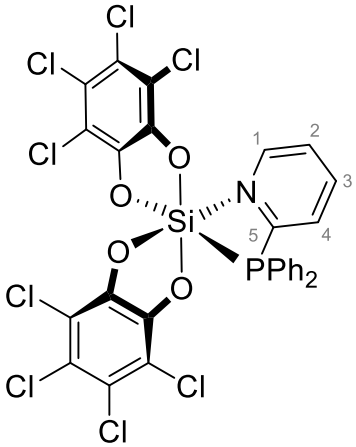

To a suspension of $Si(cat^{Cl})_2$·(sulfolane)$_2$ (170 mg, 224 µmol, 1.00 eq.) in 20 ml dichloromethane was added a solution of 2-(diphenylphosphine)pyridine (59 mg, 224 µmol, 1.00 eq.) in 5 ml dichloromethane. The reaction mixture was stirred over night and the precipitate was washed three times with 5 ml dichloromethane:pentane 1:1 and dried *in vacuo*. The product was collected as a colorless solid (150 mg, 192 µmol, 85 %).
Suitable colorless single-crystals for SCXRD were obtained by gaseous diffusion of pentane into a saturated solution of dichloromethane at −40 °C.

^{1}H NMR (400 MHz, CD_2Cl_2) δ = 8.64 (d, $^3J_{H-H}$ = 5.7, 1H, H_{py}-1), 8.23 (*pseudo*-t, $^3J_{H-H}$ = 7.9, 1H, H_{py}-3), 7.92 (d, $^3J_{H-H}$ = 7.6, 1H, H_{py}-4), 7.81 (bs, 1H, H_{py}-2), 7.55 - 7.49 (m, 2H, *para*-H_{phenyl}), 7.49 - 7.43 (m, 4H, *meta*-H_{phenyl}), 7.49 - 7.35 (m, 4H, *ortho*-H_{phenyl}).

^{13}C NMR (151 MHz, CD_2Cl_2) δ = 145.2 (C_{py}-1), 145.2 (*ipso*-C_{cat}), 143.4 (C_{py}-3), 133.7 (*meta*-C_{phenyl}), 132.4 (C_{py}-4), 132.0 (*para*-C_{phenyl}), 129.7 (d, ^1J= 9.3 Hz, *ortho*-C_{phenyl}), 143.4 (C_{py}-2), 122.9 (*ortho*-C_{cat}), 116.3 (*meta*-C_{cat}).
Due to bad solubility, the signals of C_{phenyl} and C_{py} are better visible in the ^{13}C-HSCQ experiment as cross-correlation peaks. Therefore, the *ipso*-C_{phenyl} and the C_{py}-5 signals were not observed.

^{31}P NMR (243 MHz, CD_2Cl_2) δ = 12.1.*

^{29}Si NMR could not be obtained due to bad solubility in common organic solvents.

*for comparison, the shift of the free base: **^{31}P NMR** (243 MHz, CD_2Cl_2) δ = −4.0.

2.4 Synthesis of $Si(cat^{Cl})_2(pyCH_2PPh_2)$ (**1-D**)

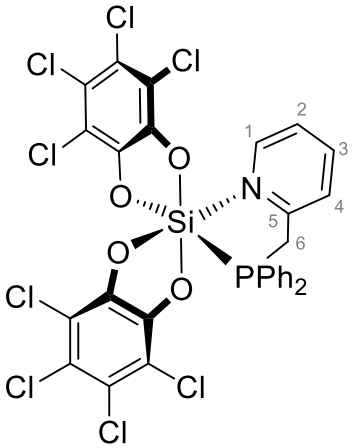

To a suspension of $Si(cat^{Cl})_2$·(sulfolane)$_2$ (230 mg, 303 µmol, 1.00 eq.) in 10 ml chlorobenzene was added a solution of 2-((diphenylphosphino)methyl)pyridine (84 mg, 303 µmol, 1.00 eq.) in 5 ml chlorobenzene. A weakly cloudy yellow solution was obtained. 15 ml pentane were added and the precipitate was filtered off, washed two times with 5 ml pentane and dried *in vacuo*. The product was collected as a colorless solid (235 mg, 295 µmol, 97 %).
Suitable colorless single-crystals for SCXRD were obtained by gaseous diffusion of pentane into a saturated solution of dichloromethane at −40 °C and from a saturated chlorobenzene solution at room temperature.

^{1}H NMR (600 MHz, CD_2Cl_2) δ = 9.20 (dd, J_{H-H} = 6.0, 1.9 Hz, 1H, H_{py}-1), 8.06 (ddd, J_{H-H} = 7.5, 7.5, 1.0 Hz, 1H, H_{py}-3), 7.64 (ddd, J_{H-H} = 7.5, 5.9, 1.4 Hz, 1H, H_{py}-2), 7.59 (d, $^3J_{H-H}$ = 7.8 Hz, 1H, H_{py}-4), 7.53 (td, J_{H-H} = 7.2, 1.6 Hz, 2H, *para*-H_{phenyl}), 7.46 – 7.41 (m, 4H, *ortho*-H_{phenyl}), 7.42 – 7.33 (m, 4H, *meta*-H_{phenyl}), 4.10 (d, $^2J_{H-P}$ = 11.0 Hz, 2H, CH_2).

^{13}C NMR (151 MHz, CD_2Cl_2) δ = 151.6 (C_{py}-5), 148.5 (C_{py}-1), 145.6 (*ipso*-C_{cat}), 142.9 (C_{py}-3), 133.2 (d, $^3J_{C-P}$ = 10.6 Hz, 4C, *meta*-C_{phenyl}), 132.5 (*para*-C_{phenyl}), 129.6 (d, $^2J_{C-P}$ = 10.3 Hz, 4C, *ortho*-C_{phenyl}), 127.6 (d, $^3J_{C-P}$ = 5.3 Hz, C_{py}-4), 125.3 (C_{py}-2), 124.9 (*ipso*-C_{phenyl}), 121.9 (*ortho*-C_{cat}), 115.9 (meta-C_{cat}), 31.3 (d, $^1J_{C-P}$ = 27.0 Hz, CH_2 (C_{py}-6)).

^{31}P NMR (243 MHz, CD_2Cl_2) δ = −14.4.*

^{29}Si NMR (119 MHz, CD_2Cl_2) δ = −136.9 (d, $^1J_{Si-P}$ = 161.5 Hz).

*for comparison, the shift of the free base: **^{31}P NMR** (243 MHz, CD_2Cl_2) δ = −11.0.

2.5 Reaction of **1-(donor)** with aldehydes

The following section describes procedures for the reaction of **1**-(donor) with aldehydes. Isolation of the products was not attempted, but successful reaction confirmed by multi-nuclear NMR spectroscopy, and if possible, SCXRD. Hence, the samples may contain residuals of sulfolane or excessive donor or substrate.

2.5.1 Reaction of **1-C** + paraformaldehyde

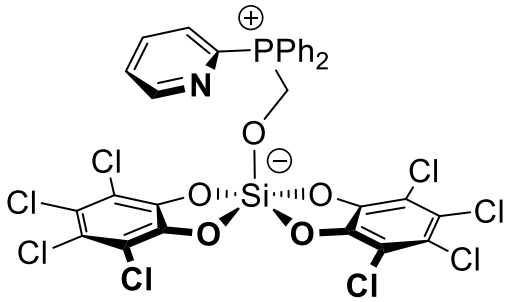

To a suspension of $Si(cat^{Cl})_2(sulfolane)_2$ (22.8 mg, 30.0 µmol, 1.00 eq.) in 0.5 ml CD_2Cl_2 **C** (7.90 mg, 30.0 µmol, 1.00 eq.) and paraformaldehyde (0.9 mg, 30.0 µmol, 1.00 eq.) were added. The suspension remained turbid, indicating the poor solubility of the formed product or incomplete reaction (even after 4 weeks). The product was not isolated and the NMR contains 2 eq. of sulfolane.

^{1}H NMR (600 MHz, CD_2Cl_2) δ = 8.78 (d, J_{H-H} = 4.8 Hz, 1H, H_{py}-1), 7.91 – 7.85 (m, 1H, H_{py}-4), 7.76 – 7.72 (m, 2H, *para*-H_{phenyl}), 7.65 – 7.59 (m, 4H, *ortho*-H_{phenyl}; 2H, H_{py}-2, H_{py}-3), 7.59 – 7.53 (m, 4H, *meta*-H_{phenyl}), 5.49 (d, $^2J_{H-P}$ = 2.1 Hz, 2H, $CH_{2\text{-aldehyde}}$).

^{13}C NMR (151 MHz, CD_2Cl_2) δ = 152.5 (d, $^3J_{C-P}$ = 19.5 Hz, C_{py}-1), 148.3 (C_{py}-5), 145.6 (*ipso*-C_{cat}), 138.0 (d, $^2J_{C-P}$ = 9.9 Hz, C_{py}-2), 135.7 (d, $^4J_{C-P}$ = 3.1 Hz, *para*-C_{phenyl}), 134.4 (d, $^2J_{C-P}$ = 9.3 Hz, *ortho*-C_{phenyl}), 131.8 (d, $^3J_{C-P}$ = 22.7 Hz, C_{py}-3), 130.4 (d, $^3J_{C-P}$ = 12.5 Hz, *meta*-C_{phenyl}), 128.6 (d, $^4J_{C-P}$ = 3.6 Hz, C_{py}-2), 121.7 (*ortho*-C_{cat}), 115.5 (d, $^1J_{C-P}$ = 83.7 Hz, *ipso*-C_{phenyl}), 114.9 (*meta*-C_{cat}), 59.2 (d, $^1J_{C-P}$ = 69.7 Hz, $CH_{2\text{-aldehyde}}$).

^{31}P NMR (162 MHz, CD_2Cl_2) δ = 13.7.

^{29}Si NMR (120 MHz, CD_2Cl_2) δ = −102.6 (d, $^3J_{Si-P}$ = 11.9 Hz).

2.5.2 Reaction of **1-D** + *p*-Me-benzaldehyde

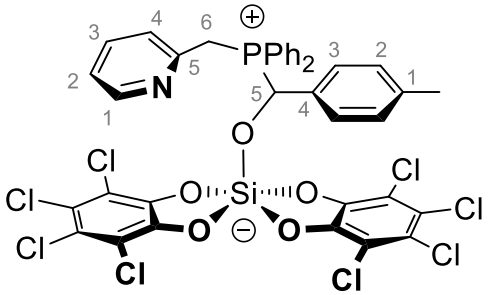

To a suspension of $Si(cat^{Cl})_2(pyCH_2PPh_2)$ (28.0 mg, 35.1 µmol, 1.00 eq.) in 0.5 ml CD_2Cl_2 *p*-Me-benzaldehyde (4.2 mg, 35.1 µmol, 1.00 eq.) was added. The suspension became clear indicating the complete consumption of the poorly soluble starting material and a quantitative formation of the product. The product was isolated as a white solid by precipitation with pentane (27.4 mg, 85 %).
Suitable colorless single-crystals for SCXRD were obtained by gaseous diffusion of pentane into a saturated solution of dichloromethane at −40 °C.

^{1}H NMR (600 MHz, CD_2Cl_2) δ = 8.49 (ddd, J_{H-H} = 4.9, 1.8, 0.9 Hz, 1H, H_{py}-1), 7.75 (*pseudo*-tq, J_{H-H} = 7.5, 1.5 Hz, 1H, *para*-$H_{phenyl-a}$), 7.61 – 7.54 (m, 1H, *para*-$H_{phenyl-b}$), 7.54 – 7.48 (m, 1H, H_{py}-3), 7.54 – 7.48 (m, 2H, *ortho*-$H_{phenyl-b}$), 7.54 – 7.48 (m, 2H, *meta*-$H_{phenyl-a}$), 7.43 (ddd, J_{H-H} = 11.3, 8.3, 1.3 Hz, 2H, *ortho*-$H_{phenyl-a}$), 7.41 – 7.32 (m, 2H, *meta*-$H_{phenyl-b}$), 7.18 (*pseudo*-ddt, J_{H-H} = 7.5, 5.0, 1.2 Hz, 1H, H_{py}-2), 6.94 (d, $^3J_{H-H}$ = 1.9 Hz, 1H, H_{py}-4), 6.94 (d, $^2J_{H-P}$ = 8.2 Hz, 1H, $H_{aldehyde}$-5), 6.78 – 6.72 (m, 4H, $H_{aldehyde}$-2, $H_{aldehyde}$-3), 4.03 – 3.91 (m, 2H, CH_2), 2.16 (d, $^4J_{H-H}$ = 2.4 Hz, 3H, $CH_{3-aldehyde}$).

^{13}C NMR (151 MHz, CD_2Cl_2) δ = 149.9 (C_{py}-1), 149.4 (d, $^2J_{C-P}$ = 7.2 Hz, C_{py}-5), 146.3 (*ipso*-C_{cat}), 144.9 (*ipso*-C_{cat}), 140.5 ($C_{aldehyde}$-1), 140.4 ($C_{aldehyde}$-4), 137.9 (C_{py}-3), 135.3 (d, $^4J_{C-P}$ = 3.0 Hz, *para*-$C_{phenyl-a}$), 134.9 (d, $^2J_{C-P}$ = 8.0 Hz, *ortho*-$C_{phenyl-a}$), 134.7 (d, $^4J_{C-P}$ = 3.0 Hz, *para*-$C_{phenyl-b}$), 133.8 (d, $^2J_{C-P}$ = 8.6 Hz, *ortho*-$C_{phenyl-b}$), 129.8 (d, $^3J_{C-P}$ = 18.2 Hz, *meta*-$C_{phenyl-b}$), 129.6 (d, $^3J_{C-P}$ = 17.8 Hz, *meta*-$C_{phenyl-a}$), 129.0 (d, $^4J_{C-P}$ = 2.9 Hz, $C_{aldehyde}$-2), 127.9 (d, $^3J_{C-P}$ = 5.4 Hz, $C_{aldehyde}$-3), 124.8 (d, $^3J_{C-P}$ = 7.8 Hz, C_{py}-4), 123.6 (C_{py}-2), 122.0 (*ortho*-C_{cat}), 120.8 (*ortho*-C_{cat}), 117.2 (d, $^1J_{C-P}$ = 81.7 Hz, *ipso*-$C_{phenyl-b}$), 116.1 (d, $^1J_{C-P}$ = 80.5 Hz, *ipso*-$C_{phenyl-a}$), 114.9 (*meta*-C_{cat}), 114.6 (*meta*-C_{cat}), 72.0 (d, $^1J_{C-P}$ = 67.5 Hz, $C_{aldehyde}$-5), 29.9 (d, $^1J_{C-P}$ = 51.4 Hz, CH_2), 21.1 (d, $^6J_{C-P}$ = 1.3 Hz, $CH_{3-aldehyde}$).

^{31}P NMR (243 MHz, CD_2Cl_2) δ = 23.9.

^{29}Si NMR (119 MHz, CD_2Cl_2) δ = −101.9 (d, $^3J_{Si-P}$ = 21.8 Hz).

2.5.3 Reaction of **1-(PPh$_3$)** + *p*-NO$_2$-benzaldehyde

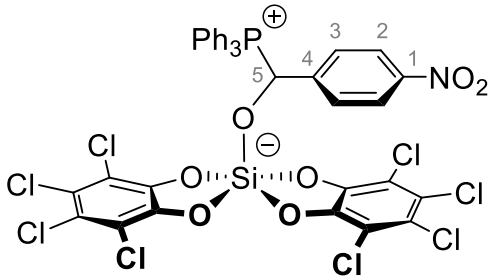

To a suspension of Si(cat^{Cl})$_2$(sulfolane)$_2$ (15.5 mg, 20.4 µmol, 1.00 eq.) in 0.5 ml CD_2Cl_2 PPh_3 (5.4 mg, 20.4 µmol, 1.00 eq.) and *p*-NO$_2$-benzaldehyde (3.1 mg, 20.4 µmol, 1.00 eq.) were added. The suspension became clear indicating the complete consumption of the poorly soluble starting material and quantitative formation of the aldehyde-activation product. The product was not isolated and the NMR contains 2 eq. of sulfolane.
Suitable colorless single-crystals for SCXRD were obtained by gaseous diffusion of pentane into a saturated solution of dichloromethane at −40 °C.

^{1}H NMR (600 MHz, CD_2Cl_2) δ = 7.83 (d, $^3J_{H-H}$ = 8.7 Hz, 2H, $H_{aldehyde}$-2), 7.80 – 7.76 (m, 3H, *para*-C_{phenyl}), 7.59 – 7.55 (m, 6H, *ortho*-C_{phenyl}), 7.48 – 7.42 (m, 6H, *meta*-C_{phenyl}), 7.08 (dd, $^3J_{H-H}$ = 8.9, $^4J_{H-P}$ = 2.2 Hz, 2H, $H_{aldehyde}$-3), 6.58 (d, $^2J_{H-P}$ = 3.3 Hz, 1H, $H_{aldehyde}$-5).

^{13}C NMR (151 MHz, CD_2Cl_2) δ = 148.7 (d, $^5J_{C-P}$ = 3.2 Hz $C_{aldehyde}$-1) 145.9 (*ipso*-C_{cat}), 144.6 (*ipso*-C_{cat}), 140.3 ($C_{aldehyde}$-4), 136.0 (d, $^4J_{C-P}$ = 3.0 Hz, *para*-C_{phenyl}), 134.9 (d, $^3J_{C-P}$ = 8.9 Hz, *meta*-C_{phenyl}), 130.6 (d, $^2J_{C-P}$ = 12.4 Hz, *ortho*-C_{phenyl}), 129.6 (d, $^3J_{C-P}$ = 5.2 Hz, $C_{aldehyde}$-3) , 123.5 (d, $^4J_{C-P}$ = 2.6 Hz, $C_{aldehyde}$-2), 122.4 (*ortho*-C_{cat}), 121.2 (*ortho*-C_{cat}), 115.3 (d, $^1J_{C-P}$ = 82.7 Hz, *ipso*-C_{phenyl}), 115.2 (*meta*-C_{cat}), 114.7 (*meta*-C_{cat}), 74.2 (d, $^1J_{C-P}$ = 69.8 Hz, $C_{aldehyde}$-5).

^{31}P NMR (243 MHz, CD_2Cl_2) δ = 21.7.

^{29}Si NMR (119 MHz, CD_2Cl_2) δ = −102.3 (d, $^3J_{Si-P}$ = 19.8 Hz).

2.6 General procedure for the reaction of **1-(donor)** with aldehydes at NMR scale

The following reactions were performed at NMR scale, according to the following general procedure:

To a suspension of $Si(cat^{Cl})_2 \cdot (sulfolane)_2$ (20.0 mg, 26.3 µmol, 1.00 eq.) in 0.5 ml dichloromethane or *ortho*-dichlorobenzene were added one equivalent of a bidentate Lewis base/two equivalents of a monodentate Lewis base and one equivalent of paraformaldehyde or *para*-substituted benzaldehyde. The occurrence of a reaction was judged by the clearing of the suspension and/or characteristic NMR shifts (for example the former-aldehydic carbon/proton signals in ^{13}C and ^{1}H NMR).
Suitable colorless single-crystals for SCXRD were obtained by gaseous diffusion of pentane into a saturated solution of dichloromethane or *ortho*-dichlorobenzene at −40 °C (dichloromethane) or room temperature (*ortho*-dichlorobenzene).

2.6.1 Reaction of **1-A** + paraformaldehyde

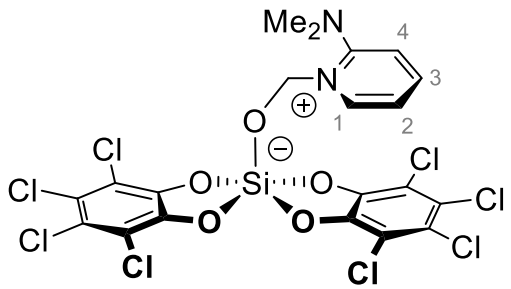

After mixing of the compounds a colorless suspension was obtained.

^{1}H NMR (400 MHz, CD_2Cl_2) δ = 8.35 (dd, $J_{H\text{-}H}$ = 6.7, 1.8 Hz, 1H, H_{py}-1), 7.75 (ddd, $J_{H\text{-}H}$ = 8.9, 7.1, 1.8 Hz, 1H, H_{py}-3), 7.03 (td, $J_{H\text{-}H}$ = 6.9, 1.3 Hz, 1H, H_{py}-2), 6.95 (dt, $J_{H\text{-}H}$ = 8.9, 0.9 Hz, 1H, H_{py}-4), 5.73 (s, 2H, $CH_{2\text{-aldehyde}}$), 3.10 (s, 6H, CH_3).

^{29}Si NMR (80 MHz, CD_2Cl_2) δ = −103.1.

2.6.2 Reaction of **1-D** + paraformaldehyde

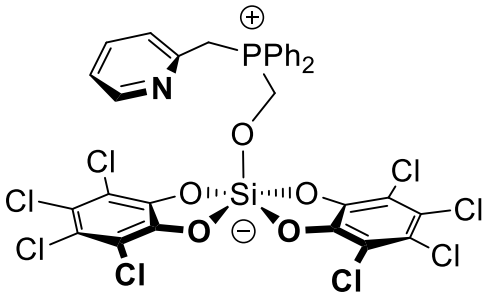

After mixing of the compounds a colorless suspension was obtained. ^{1}H NMR was indicating formation of the desired product beside some unidentified side-products.

^{1}H NMR (400 MHz, CD_2Cl_2) δ = 8.23 (d, $^{3}J_{H\text{-}H}$ = 5.0 Hz, 1H, H_{py}-1), 7.65 (td, $J_{H\text{-}H}$ = 7.7, 1.9 Hz, 2H, *para*-H_{phenyl}), 7.60 – 7.56 (m, 1H, H_{py}-3), 7.57 – 7.53 (m, 4H, *meta*-H_{phenyl}), 7.50 – 7.44 (m, 4H, *ortho*-H_{phenyl}), 7.18 (d, $^{3}J_{H\text{-}H}$ = 7.9 Hz, 1Hz, H_{py}-4), 7.15 – 7.09 (m, 1H, H_{py}-2), 5.28 (d, $^{2}J_{H\text{-}P}$ = 2.1 Hz, 2H, $CH_{2\text{-aldehyde}}$), 4.36 (d, $^{2}J_{H\text{-}P}$ = 14.4 Hz, 2H, $CH_{2\text{-py}}$).

^{31}P NMR (162 MHz, CD_2Cl_2) δ = 21.3.

^{29}Si NMR (79 MHz, CD_2Cl_2) δ = −102.3.

2.6.3 Reaction of **1-(PPh_3)** + paraformaldehyde

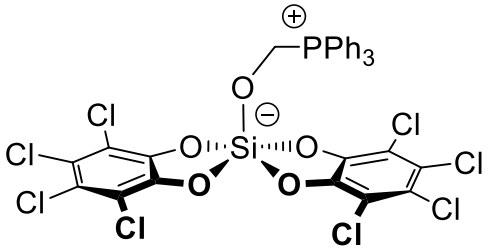

After mixing of the compounds a colorless suspension was obtained.

^{1}H NMR (400 MHz, CD_2Cl_2) δ = 7.78 – 7.73 (m, 3H, *para*-H_{phenyl}), 7.60 – 7.51 (m, 12H, *ortho*-H_{phenyl}, *meta*-H_{phenyl}), 5.39 (d, $^{2}J_{H\text{-}P}$ = 1.6 Hz, 2H, $CH_{2\text{-aldehyde}}$).

^{31}P NMR (243 MHz, CD_2Cl_2) δ = 17.7.

^{29}Si NMR (119 MHz, CD_2Cl_2) δ = −102.9.

2.6.4 Reaction of **1-C** + *p*-Me-benzaldehyde

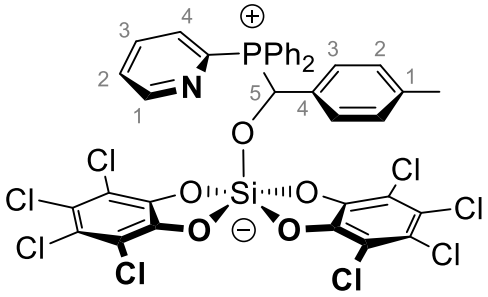

After mixing of the compounds a colorless solution was obtained immediately.

Suitable colorless single-crystals for SCXRD were obtained by gaseous diffusion of pentane into a saturated solution of dichloromethane at −40 °C.

^{1}H NMR (400 MHz, CD_2Cl_2) δ = 8.85 (d, $^{3}J_{H\text{-}H}$ = 4.6 Hz, 1H, H_{py}-1), 7.79 – 7.69 (m, 5H), 7.65 – 7.55 (m, 2H), 7.54 – 7.43 (m, 4H), 7.23 (ddd, $J_{H\text{-}H}$ = 11.6, 8.4, 1.3 Hz, 2H), 6.82 – 6.69 (m, 4H), 6.65 (d, $^{2}J_{H\text{-}P}$ = 3.3 Hz, 1H, $H_{aldehyde}$-5), 2.16 (d, J = 2.4 Hz, 3H, $CH_{3\text{-}aldehyde}$).

^{31}P NMR (162 MHz, CD_2Cl_2) δ = 15.8.

^{29}Si NMR (79 MHz, CD_2Cl_2) δ = −102.3 (d, $^{3}J_{Si\text{-}P}$ = 22.3 Hz).

2.6.5 Reaction of **1-(PPh$_3$)** + *p*-Me-benzaldehyde

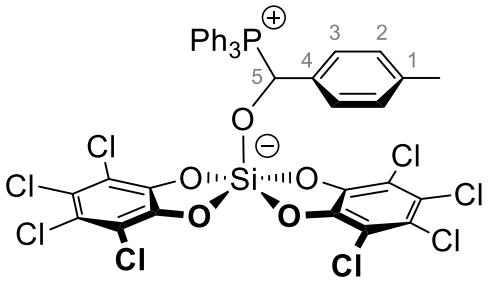

After mixing of the compounds for several minutes a colorless solution was obtained.

Suitable colorless single-crystals for SCXRD were obtained by gaseous diffusion of pentane into a saturated solution of dichloromethane at −40 °C.

^{1}H NMR (600 MHz, CD_2Cl_2) δ = 7.72 (dd, $J_{H\text{-}H}$ = 7.6, 1.8 Hz, 3H, *para*-H_{phenyl}), 7.53 (*pseudo*-td, $J_{H\text{-}H}$ = 7.9, 3.5 Hz, 6H, H_{phenyl}), 7.48 – 7.39 (m, 6H, H_{phenyl}), 6.83 – 6.71 (m, 4H, $H_{aldehyde}$), 6.40 (s, 1H, $H_{aldehyde}$-5), 2.18 (s, 3H, $CH_{3\text{-}aldehyde}$).

^{31}P NMR (243 MHz, CD_2Cl_2) δ = 20.2.

^{29}Si NMR (79 MHz, CD_2Cl_2) δ = −102.3 (d, $^{3}J_{Si\text{-}P}$ = 21.3 Hz).

2.7 Reaction of **1-A** + *p*-X-benzaldehyde

After mixing of the compounds, colored solutions (for X = Me and H: orange, F: red, NO_2: yellow, OMe: purple-dark red) along with colorless solids were obtained.

For X = H, F and Ome suitable colorless single-crystals for SCXRD were obtained by gaseous diffusion of pentane into a saturated solution of dichloromethane at −40 °C.

2.8 Synthesis of $Si(cat^{Cl})_2(pyCH_2NMe_2)$ (**1-(hppH)$_2$**)

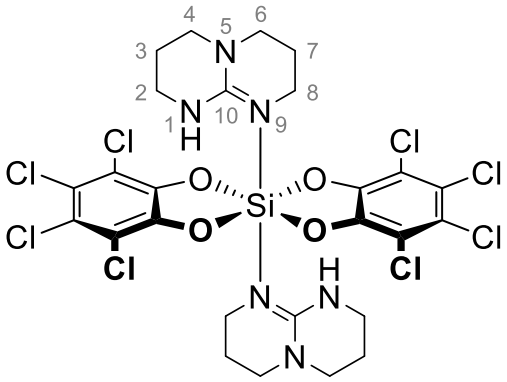

To a suspension of $Si(cat^{Cl})_2(sulfolane)_2$ (10.0 mg, 13.2 µmol, 1.00 eq.) in 0.5 ml dichloromethane or *ortho*-dichlorobenzene hppH (3.7 mg, 31.3 µmol, 2.00 eq.) was added (hppH = 1,3,4,6,7,8-hexahydro-2*H*-pyrimido[1,2-*a*]pyrimidine). The suspension was stirred for 1 d but poor solubility of the desired product inhibited complete dissolution. The product was not isolated and the NMR contains 2 eq. of the byproduct sulfolane.

Suitable colorless single-crystals for SCXRD were obtained by gaseous diffusion of hexane into a saturated solution of dichloromethane at −40 °C.

^{1}H NMR: No NMR in deuterated solvent was conducted.

^{13}C NMR (151 MHz, *o*-DCB) δ = 154.2 (C_{hppH}-10), 146.8 (*ipso*-C_{cat}), 120.8 (*ortho*-C_{cat}), 115.7 (*meta*-C_{cat}), 48.2 (C_{hppH}-4/8), 47.4 (C_{hppH}-4/8), 42.2 (C_{hppH}-2/6), 38.7 (C_{hppH}-2/6), 22.7 (C_{hppH}-3/7), 22.1 (C_{hppH}-3/7).

^{29}Si NMR (119 MHz, *o*-DCB) δ = −151.0.

2.9 Dehydrogenative coupling of dimethylamine borane

Dimethylamine borane (15.5 mg, 263.1 µmol, 1.00 eq.) was dissolved in 0.5 ml *ortho*-dichlorobenzene:C_6D_6 (99:1) and 5 mol% catalyst (**1-A**, **1-B**, **1-(sulfolane)$_2$** or **A**) was added. The mixture was heated in a NMR tube to 100 °C and followed immediately *in situ* by ^{11}B NMR spectroscopy. The extent of reaction ξ was determined by integration of the ^{11}B NMR signals (for this data see Table 2 in the main part). Figure S2.1 exemplary shows the course of the reaction catalyzed by **1-A**. The dehydrogenation is accompanied by the formation of (μ-NMe_2)B_2H_5 (δ = – 17.5 ppm) and minor byproducts at δ = 2.1 and 9.2 ppm.

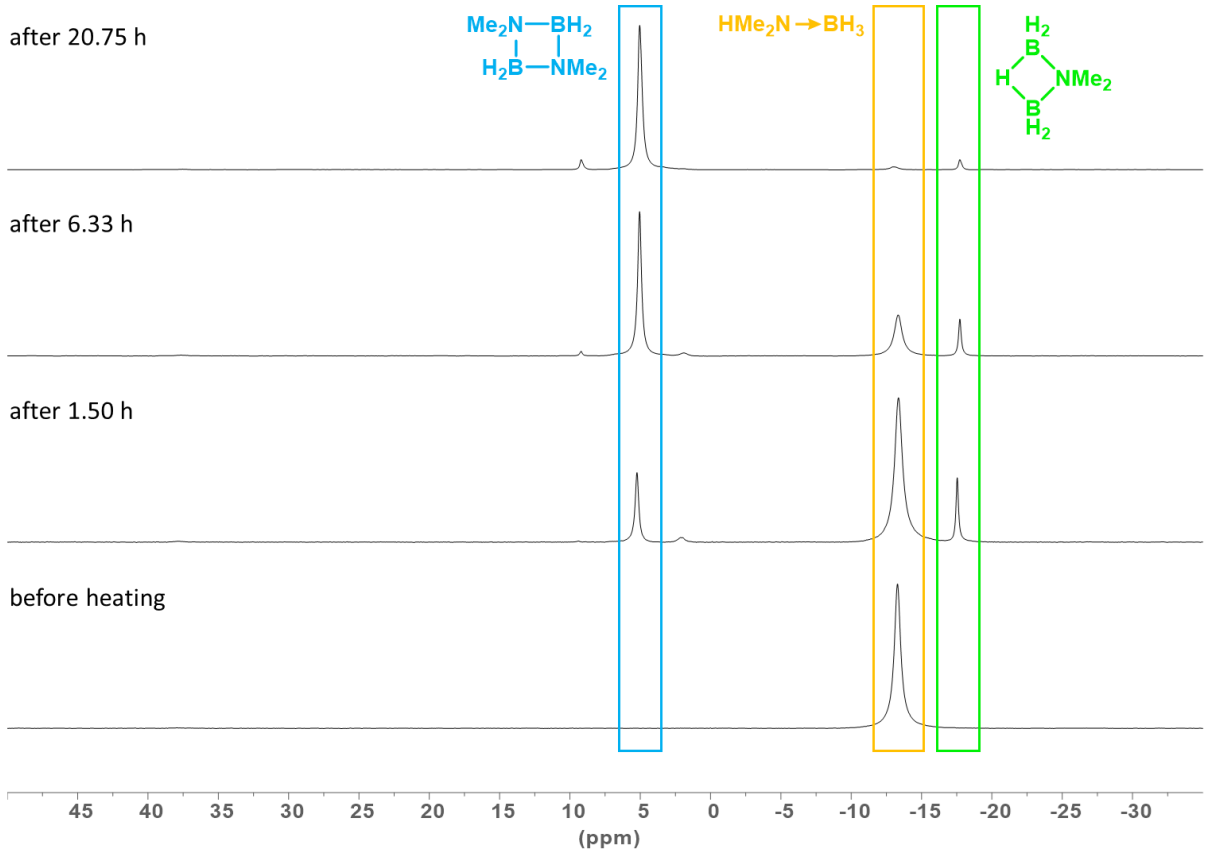

Fig. S2.1: ^{11}B{^{1}H} NMR spectra (64 MHz, *ortho*-dichlorobenzene:C_6D_6 (99:1), RT) of the dehydrogenative coupling of HMe_2N-BH_3 (δ = −13.4 ppm, orange) with 5 mol% **1-A** at 100 °C. Stacked spectra resemble different reaction times. Respective ^{11}B NMR shifts of the product $(Me_2N\text{-}BH_2)_2$: δ = 5.2 ppm (blue) and the byproduct (μ-NMe_2)B_2H_5: δ = −17.5 ppm (green).

3. Single Crystal X-Ray Diffraction

Suitable crystals for single-crystal structure determination were taken directly from the mother liquor, taken up in perfluorinated polyether oil and fixed on a cryo loop. Full shells of intensity data were collected at low temperature with a Bruker D8 Venture diffractometer, dual source (Mo-or Cu-K_α radiation, microfocus X-ray tube, Photon III detector). Data were processed with the standard Bruker (SAINT, APEX3) software package.[4, 5] Multiscan absorption correction was applied using the SADABS program.[6, 7] The structures were solved by intrinsic phasing[8, 9] and refined using the SHELXTL software package (Version 2014/6 and 2018/3).[10-13] Graphical handling of the structural data during solution and refinement was performed with OLEX2[14] and shelXle.[15] All non-hydrogen atoms were given anisotropic displacement parameters. Hydrogen atoms bound to carbon were input at calculated positions and refined with a riding model.

For data visualization, Mercury 2020.3.0 was used.[16-19] The thermal displacement ellipsoids are shown at the probability level of 50 %. CCDC numbers 2091065, 2091068, 2091070-2091079, 2091082 and 2091083 contain the supplementary crystallographic data for this paper. These data can be obtained free of charge from the Cambridge Crystallographic Data Centre's and FIZ Karlsruhe's joint Access Service via https://www.ccdc.cam.ac.uk/structures/.

Electron density attributed to solvent of crystallization (dichloromethane, chlorobenzene, fluorobenzene or *o*-difluorobenzene) which could not be modelled was removed from the structures of **1-C**, ([**1**-O-**1**][$C_{21}H_{25}N_4F$]), **1-(*p*-Me-BA)-C** and **1-(BA)-C** with the BYPASS procedure,[20, 21] as implemented in PLATON (squeeze/hybrid).[22, 23] Partial structure factors from the solvent masks were included in the refinement as separate contributions to F_{calc}.

For Si(cat^{Cl})$_2$pyPPh$_2$ (**1-C**), 120 electrons were found in a volume of 374 Å^3 in one void per unit cell. This is consistent with the presence of 3 CH_2Cl_2 per unit cell (1.5 per formula unit) which account for 126 electrons per unit cell.

For [(cat^{Cl})$_2$Si-O-Si(cat^{Cl})$_2$][$C_{21}H_{25}N_4F$] ([**1**-O-**1**][$C_{21}H_{25}N_4F$]), 257 electrons were found in a volume of 691 Å^3 in one void per unit cell. This is consistent with the presence of 6 CH_2Cl_2 per unit cell (3 per formula unit) which account for 252 electrons per unit cell.

For Si(cat^{Cl})$_2$pyPPh$_2$·(*p*-Me-BA) (**1-(*p*-Me-BA)-C**), 332 electrons were found in a volume of 1028 Å^3 in one void per unit cell. This is consistent with the presence of 8 CH_2Cl_2 per unit cell (1 per formula unit) which account for 336 electrons per unit cell.

For Si(cat^{Cl})$_2$pyPPh$_2$·(BA) (**1-(BA)-C**), 88 electrons were found in a volume of 362 Å^3 in one void per unit cell. This is consistent with the presence of 2 CH_2Cl_2 per unit cell (0.5 per formula unit) which account for 84 electrons per unit cell.

3.1 Compound Si(cat^{Cl})$_2$pyNMe$_2$ (**1-A**)

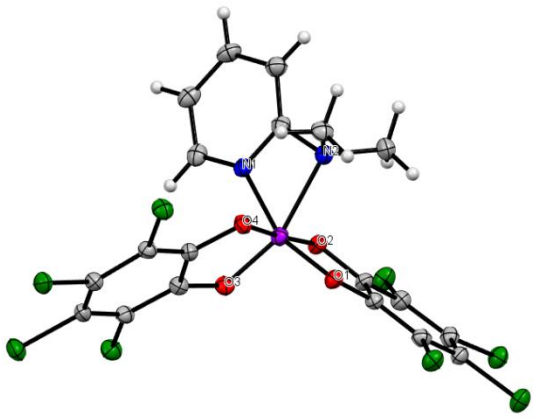

Identification code	**mo_dh302h2_0m**
Empirical formula	$C_{19}H_{10}Cl_8N_2O_4Si$
Formula weight	641.98
Temperature/K	100.0
Crystal system	monoclinic
Space group	C2/c
a/Å	14.3910(13)
b/Å	8.8970(8)
c/Å	36.446(3)
α/°	90
β/°	93.241(3)
γ/°	90
Volume/Å^3	4659.0(7)
Z	8
ρ_{calc}g/cm^3	1.831
μ/mm^{-1}	1.052
F(000)	2560.0
Crystal size/mm^3	0.344 × 0.239 × 0.182
Radiation	Mo-K_α (λ = 0.71073)
2Θ range for data collection/°	4.478 to 57.5
Index ranges	-19 ≤ h ≤ 19, -12 ≤ k ≤ 12, -49 ≤ l ≤ 45
Reflections collected	89708
Independent reflections	6036 [R_{int} = 0.0676, R_{sigma} = 0.0273]
Data/restraints/parameters	6036/0/309
Goodness-of-fit on F^2	1.152
Final R indexes [I>=2σ (I)]	R_1 = 0.0478, wR_2 = 0.1161
Final R indexes [all data]	R_1 = 0.0564, wR_2 = 0.1220
Largest diff. peak/hole / e Å^{-3}	0.78/-0.55
CCDC number	2091065

3.2 Compound Si(cat^{Cl})$_2$pyCH$_2$NMe$_2$ (**1-B**)

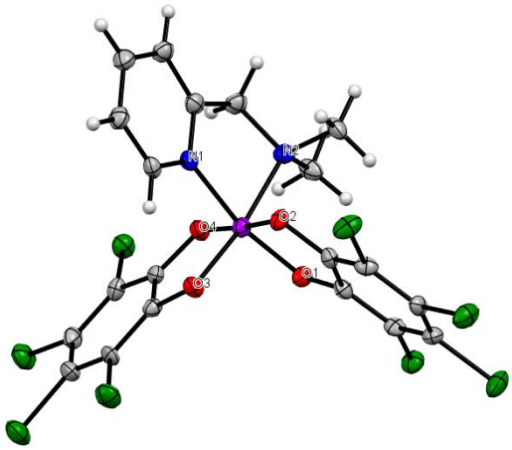

Identification code	**dh177B_P21c**
Empirical formula	$C_{22}H_{16}Cl_{12}N_2O_4Si$
Formula weight	825.86
Temperature/K	100
Crystal system	monoclinic
Space group	$P2_1/c$
a/Å	16.942(3)
b/Å	12.536(3)
c/Å	15.917(3)
α/°	90
β/°	112.19(3)
γ/°	90
Volume/Å^3	3130.2(13)
Z	4
ρ_{calc}g/cm^3	1.752
μ/mm^{-1}	1.135
F(000)	1648.0
Crystal size/mm^3	0.5 × 0.2 × 0.2
Radiation	Mo-K_α (λ = 0.71073)
2Θ range for data collection/°	4.16 to 54.2
Index ranges	-21 ≤ h ≤ 21, -16 ≤ k ≤ 16, -20 ≤ l ≤ 20
Reflections collected	13294
Independent reflections	6902 [R_{int} = 0.0812, R_{sigma} = 0.1038]
Data/restraints/parameters	6902/0/372
Goodness-of-fit on F^2	1.026
Final R indexes [I>=2σ (I)]	R_1 = 0.0560, wR_2 = 0.1111
Final R indexes [all data]	R_1 = 0.1155, wR_2 = 0.1300
Largest diff. peak/hole / e Å^{-3}	0.82/-0.99
CCDC number	2091068

3.3 Compound $Si(cat^{Cl})_2pyPPh_2$ (**1-C**)

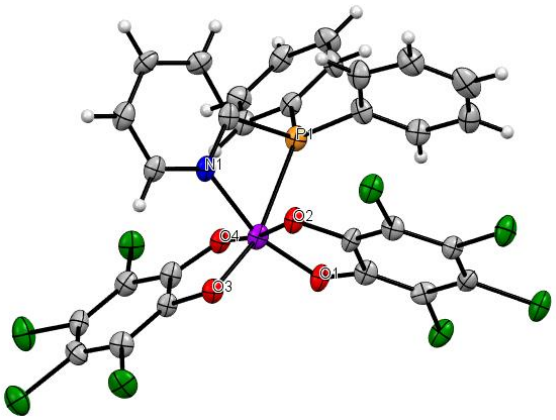

Identification code	**mo_dhsb11_0m**
Empirical formula	$C_{29}H_{14}Cl_8NO_4PSi$
Formula weight	783.07
Temperature/K	100.0
Crystal system	triclinic
Space group	P-1
a/Å	12.5198(17)
b/Å	12.5964(18)
c/Å	12.8616(17)
α/°	63.404(5)
β/°	83.620(5)
γ/°	86.982(5)
Volume/Å^3	1802.5(4)
Z	2
ρ_{calc}g/cm^3	1.443
μ/mm^{-1}	0.736
F(000)	784.0
Crystal size/mm^3	0.168 × 0.049 × 0.029
Radiation	Mo-K_α (λ = 0.71073)
2Θ range for data collection/°	4.594 to 53.206
Index ranges	-15 ≤ h ≤ 15, -14 ≤ k ≤ 15, -16 ≤ l ≤ 16
Reflections collected	28255
Independent reflections	7420 [R_{int} = 0.1164, R_{sigma} = 0.1124]
Data/restraints/parameters	7420/0/397
Goodness-of-fit on F^2	0.973
Final R indexes [I>=2σ (I)]	R_1 = 0.0570, wR_2 = 0.1207
Final R indexes [all data]	R_1 = 0.1129, wR_2 = 0.1423
Largest diff. peak/hole / e Å^{-3}	0.48/-0.58
CCDC number	2091070

3.4 Compound $Si(cat^{Cl})_2pyCH_2PPh_2$ (**1-D**)

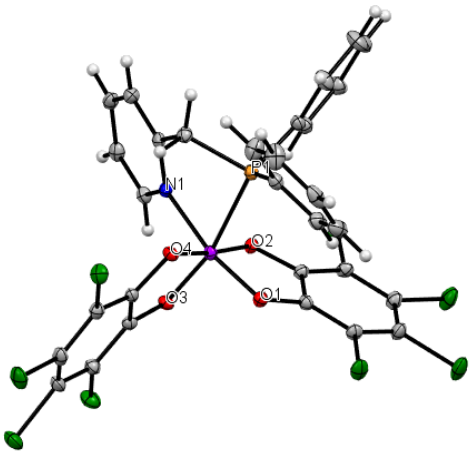

Identification code	**mo_dh301_0ma**	**mo_dh416_0m**
Empirical formula	$C_{30}H_{16}Cl_8NO_4PSi$	$C_{32}H_{20}Cl_{12}NO_4PSi$
Formula weight	797.10	966.95
Temperature/K	100.0	100.0
Crystal system	monoclinic	triclinic
Space group	$P2_1/c$	P-1
a/Å	23.136(4)	8.7056(5)
b/Å	12.559(2)	11.1906(6)
c/Å	24.311(4)	20.7094(10)
α/°	90	77.511(2)
β/°	115.803(6)	89.089(2)
γ/°	90	75.072(2)
Volume/Å^3	6360.0(19)	1901.61(18)
Z	8	2
ρ_{calc}g/cm^3	1.665	1.689
μ/mm^{-1}	0.836	0.987
F(000)	3200.0	968.0
Crystal size/mm^3	0.116 × 0.086 × 0.074	0.41 × 0.329 × 0.17
Radiation	Mo-K_α (λ = 0.71073)	Mo-K_α (λ = 0.71073)
2Θ range for data collection/°	3.722 to 56.076	3.944 to 60.118
Index ranges	$-30 \le h \le 30$, $-15 \le k \le 15$, $-28 \le l \le 28$	$-11 \le h \le 12$, $-15 \le k \le 15$, $-28 \le l \le 29$
Reflections collected	115559	36496
Independent reflections	13044 [R_{int} = 0.0784, R_{sigma} = 0.0337]	10828 [R_{int} = 0.0368, R_{sigma} = 0.0354]
Data/restraints/parameters	13044/0/811	10828/0/460
Goodness-of-fit on F^2	1.079	1.028
Final R indexes [I>=2σ (I)]	R_1 = 0.0956, wR_2 = 0.1757	R_1 = 0.0312, wR_2 = 0.0692
Final R indexes [all data]	R_1 = 0.1255, wR_2 = 0.1971	R_1 = 0.0391, wR_2 = 0.0729
Largest diff. peak/hole / e Å^{-3}	0.78/-0.90	0.57/-0.65
CCDC number	2091082	2091071

3.5 Compound Si(cat^{Cl})$_2$pyNMe$_2$·H$_2$CO (**1-(OCH$_2$)-A**)

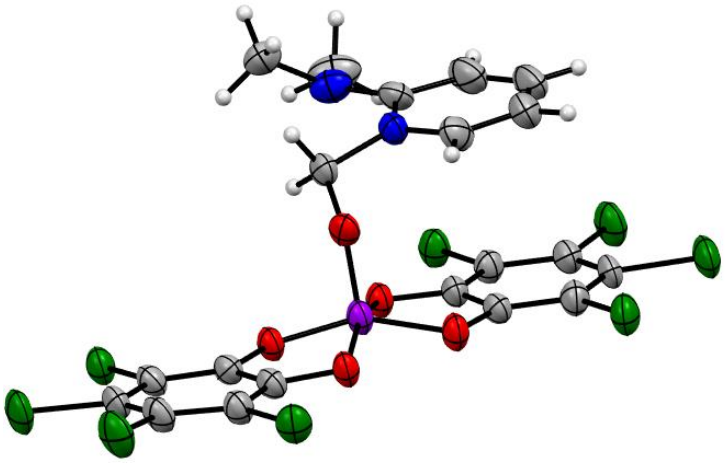

Identification code	**mo_dh390_0m**
Empirical formula	$C_{20}H_{12}Cl_8N_2O_5Si$
Formula weight	672.01
Temperature/K	100.0
Crystal system	monoclinic
Space group	$P2_1/c$
a/Å	14.3396(13)
b/Å	9.8161(11)
c/Å	18.6371(17)
α/°	90
β/°	108.642(4)
γ/°	90
Volume/Å3	2485.7(4)
Z	4
ρcalcg/cm3	1.796
μ/mm-1	0.993
F(000)	1344.0
Crystal size/mm3	0.126 × 0.104 × 0.045
Radiation	Mo-K_α (λ = 0.71073)
2Θ range for data collection/°	4.614 to 52.93
Index ranges	-17 ≤ h ≤ 17, -12 ≤ k ≤ 10, -23 ≤ l ≤ 23
Reflections collected	34627
Independent reflections	5023 [Rint = 0.0886, Rsigma = 0.0556]
Data/restraints/parameters	5023/0/327
Goodness-of-fit on F2	1.017
Final R indexes [I>=2σ (I)]	R1 = 0.0629, wR2 = 0.1556
Final R indexes [all data]	R1 = 0.1017, wR2 = 0.1857
Largest diff. peak/hole / e Å-3	0.61/-0.52
CCDC number	2091072

3.6 Compound [(cat^{Cl})$_2$Si-O-Si(cat^{Cl})$_2$][$C_{21}H_{25}N_4F$] ([**1**-O-**1**][$C_{21}H_{25}N_4F$])

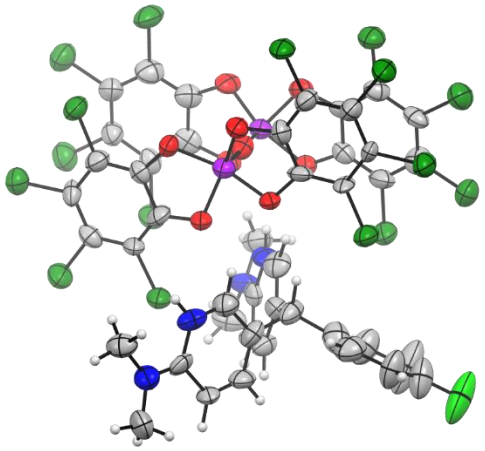

Identification code	**mo_dhsb52_0m**
Empirical formula	$C_{45}H_{25}Cl_{16}FN_4O_9Si_2$
Formula weight	1408.07
Temperature/K	100
Crystal system	triclinic
Space group	P-1
a/Å	13.35(2)
b/Å	14.77(4)
c/Å	16.46(3)
α/°	86.32(7)
β/°	78.14(3)
γ/°	82.12(7)
Volume/Å3	3144(12)
Z	2
ρcalcg/cm3	1.488
μ/mm-1	0.790
F(000)	1408.0
Crystal size/mm3	0.74 × 0.112 × 0.1
Radiation	Mo-K_α (λ = 0.71073)
2Θ range for data collection/°	4.258 to 47.056
Index ranges	-14 ≤ h ≤ 14, -16 ≤ k ≤ 16, -18 ≤ l ≤ 18
Reflections collected	23797
Independent reflections	9126 [Rint = 0.1713, Rsigma = 0.2143]
Data/restraints/parameters	9126/0/674
Goodness-of-fit on F2	0.939
Final R indexes [I>=2σ (I)]	R1 = 0.0858, wR2 = 0.1856
Final R indexes [all data]	R1 = 0.1995, wR2 = 0.2430
Largest diff. peak/hole / e Å-3	0.50/-0.44
CCDC number	2091073

3.7 Compound $Si(cat^{Cl})_2pyPPh_2 \cdot$(*p*-Me-BA) (**1-(*p*-Me-BA)-C**)

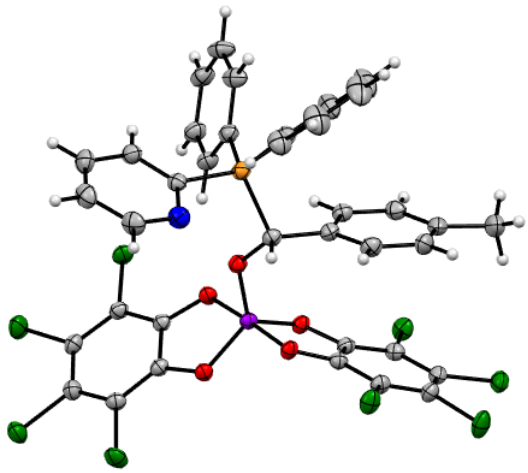

Identification code	**mo_dh410_0m**	**mo_dhsb43_0ma**
Empirical formula	$C_{37}H_{22}Cl_8NO_5PSi$	$C_{39}H_{26}Cl_{12}NO_5PSi$
Formula weight	903.21	1073.07
Temperature/K	100.0	100.0
Crystal system	monoclinic	orthorhombic
Space group	C2/c	$Pna2_1$
a/Å	33.002(6)	15.5399(11)
b/Å	15.336(3)	16.4844(12)
c/Å	18.448(4)	17.4224(11)
α/°	90	90
β/°	119.585(7)	90
γ/°	90	90
Volume/Å3	8120(3)	4463.0(5)
Z	8	4
ρcalcg/cm3	1.478	1.597
μ/mm-1	0.667	0.852
F(000)	3648.0	2160.0
Crystal size/mm3	0.581 × 0.428 × 0.398	0.31 × 0.24 × 0.15
Radiation	Mo-K_α (λ = 0.71073)	Mo-K_α (λ = 0.71073)
2Θ range for data collection/°	4.368 to 56.798	4.294 to 55.132
Index ranges	-44 ≤ h ≤ 43, -20 ≤ k ≤ 20, -24 ≤ l ≤ 24	-20 ≤ h ≤ 20, -21 ≤ k ≤ 21, -22 ≤ l ≤ 22
Reflections collected	138258	239193
Independent reflections	10166 [Rint = 0.0751, Rsigma = 0.0286]	10295 [Rint = 0.0954, Rsigma = 0.0274]
Data/restraints/parameters	10166/0/479	10295/1/533
Goodness-of-fit on F2	1.026	1.061
Final R indexes [I>=2σ (I)]	R1 = 0.0341, wR2 = 0.0857	R1 = 0.0269, wR2 = 0.0634
Final R indexes [all data]	R1 = 0.0440, wR2 = 0.0927	R1 = 0.0308, wR2 = 0.0654
Largest diff. peak/hole / e Å-3	0.42/-0.42	0.32/-0.38
Flack parameter	-	0.015(15)
CCDC number	2091074	2091083

3.8 Compound Si(cat^{Cl})$_2$pyPPh$_2$·(BA) (**1-(BA)-C**)

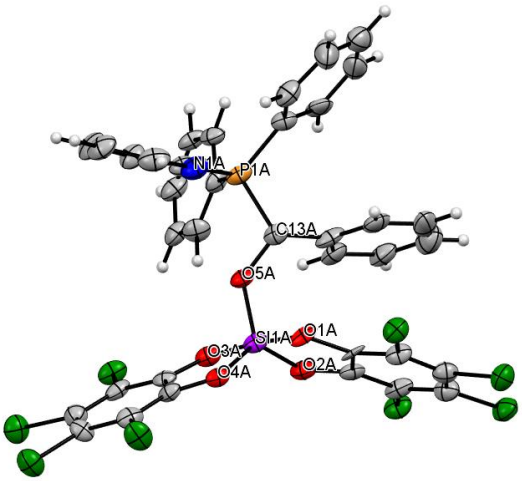

Identification code	**P-1_a**
Empirical formula	$C_{36.5}H_{21}Cl_9NO_5PSi$
Formula weight	931.65
Temperature/K	100.0
Crystal system	triclinic
Space group	P-1
a/Å	15.162(2)
b/Å	16.186(2)
c/Å	18.463(3)
α/°	109.982(5)
β/°	90.192(5)
γ/°	107.734(6)
Volume/Å3	4026.6(10)
Z	4
ρcalcg/cm3	1.537
μ/mm-1	0.739
F(000)	1876.0
Crystal size/mm3	0.124 × 0.116 × 0.059
Radiation	Mo-K_α (λ = 0.71073)
2Θ range for data collection/°	3.908 to 49.998
Index ranges	-19 ≤ h ≤ 19, -20 ≤ k ≤ 19, 0 ≤ l ≤ 23
Reflections collected	14102
Independent reflections	14102 [Rint = ?, Rsigma = 0.1871]
Data/restraints/parameters	14102/0/964
Goodness-of-fit on F2	1.045
Final R indexes [I>=2σ (I)]	R1 = 0.0827, wR2 = 0.2036
Final R indexes [all data]	R1 = 0.1742, wR2 = 0.2379
Largest diff. peak/hole / e Å-3	0.73/-0.75
CCDC number	2091075

3.9 Compound Si(cat^{Cl})$_2$pyCH$_2$PPh$_2$·(*p*-Me-BA) (**1-(*p*-Me-BA)-D**)

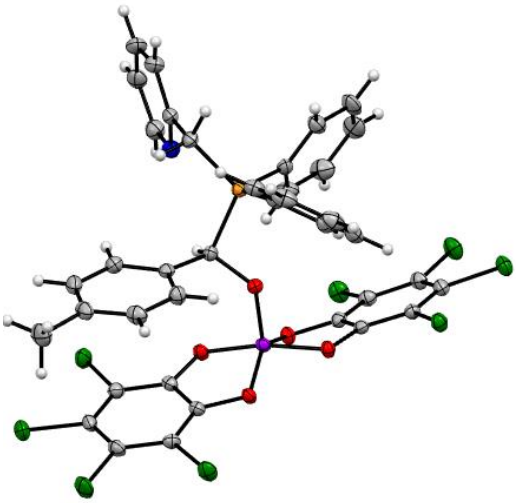

Identification code	**mo_dh415_0m**
Empirical formula	$C_{40}H_{28}Cl_{12}NO_5PSi$
Formula weight	1087.09
Temperature/K	100.0
Crystal system	monoclinic
Space group	$P2_1/n$
a/Å	12.6888(10)
b/Å	17.8472(12)
c/Å	20.3151(17)
α/°	90
β/°	90.872(3)
γ/°	90
Volume/Å3	4600.0(6)
Z	4
ρcalcg/cm3	1.570
μ/mm-1	0.827
F(000)	2192.0
Crystal size/mm3	0.288 × 0.117 × 0.09
Radiation	Mo-K_α (λ = 0.71073)
2Θ range for data collection/°	3.938 to 52.85
Index ranges	-15 ≤ h ≤ 15, -22 ≤ k ≤ 22, -25 ≤ l ≤ 25
Reflections collected	64408
Independent reflections	9452 [Rint = 0.0742, Rsigma = 0.0423]
Data/restraints/parameters	9452/26/552
Goodness-of-fit on F2	1.033
Final R indexes [I>=2σ (I)]	R1 = 0.0361, wR2 = 0.0791
Final R indexes [all data]	R1 = 0.0529, wR2 = 0.0879
Largest diff. peak/hole / e Å-3	0.76/-0.45
CCDC number	2091076

3.10 Compound Si(cat^{Cl})$_2$PPh$_3$·(*p*-Me-BA) (**1-(*p*-Me-BA)-PPh$_3$**)

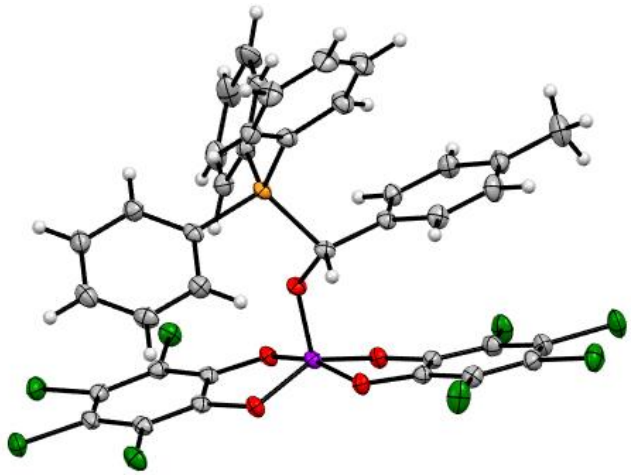

Identification code	**mo_dh400_0m**
Empirical formula	$C_{39}H_{25}Cl_{10}O_5PSi$
Formula weight	987.15
Temperature/K	100.0
Crystal system	triclinic
Space group	P-1
a/Å	11.9675(9)
b/Å	12.4047(10)
c/Å	16.8129(13)
α/°	94.060(3)
β/°	106.632(3)
γ/°	117.844(3)
Volume/Å3	2052.1(3)
Z	2
ρcalcg/cm3	1.598
μ/mm-1	0.792
F(000)	996.0
Crystal size/mm3	0.271 × 0.103 × 0.08
Radiation	Mo-K_α (λ = 0.71073)
2Θ range for data collection/°	4.006 to 54.524
Index ranges	-15 ≤ h ≤ 15, -15 ≤ k ≤ 15, -21 ≤ l ≤ 21
Reflections collected	83194
Independent reflections	9087 [Rint = 0.0528, Rsigma = 0.0259]
Data/restraints/parameters	9087/1/516
Goodness-of-fit on F2	1.042
Final R indexes [I>=2σ (I)]	R1 = 0.0331, wR2 = 0.0804
Final R indexes [all data]	R1 = 0.0390, wR2 = 0.0844
Largest diff. peak/hole / e Å-3	0.72/-0.60
CCDC number	2091077

3.11 Compound Si(cat^{Cl})$_2$PPh$_3$·(*p*-NO$_2$-BA) (**1-(*p*-NO$_2$-BA)-PPh$_3$**)

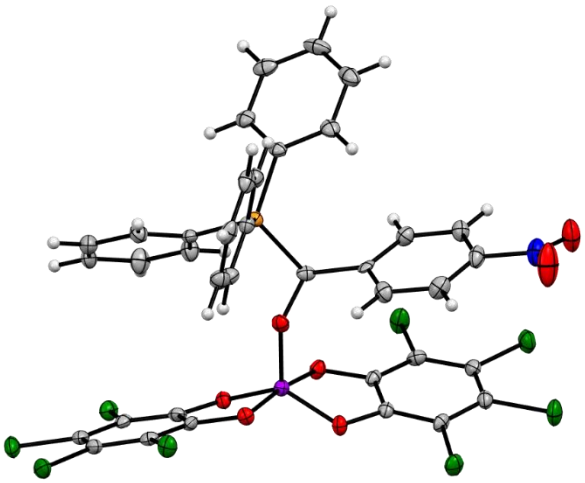

Identification code	**mo_dh431_0m_4**
Empirical formula	$C_{77}H_{46}Cl_{22}N_2O_{14}P_2Si_2$
Formula weight	2121.18
Temperature/K	100.0
Crystal system	triclinic
Space group	P-1
a/Å	11.1778(8)
b/Å	11.9331(9)
c/Å	17.3665(12)
α/°	83.309(3)
β/°	88.887(2)
γ/°	67.403(3)
Volume/Å3	2123.2(3)
Z	1
ρcalcg/cm3	1.659
μ/mm-1	0.837
F(000)	1066.0
Crystal size/mm3	0.22 × 0.186 × 0.104
Radiation	Mo-K_α (λ = 0.71073)
2Θ range for data collection/°	3.948 to 49.992
Index ranges	-12 ≤ h ≤ 13, -12 ≤ k ≤ 14, -20 ≤ l ≤ 20
Reflections collected	6981
Independent reflections	6981 [Rint = ?, Rsigma = 0.0668]
Data/restraints/parameters	6981/477/550
Goodness-of-fit on F2	1.055
Final R indexes [I>=2σ (I)]	R1 = 0.0530, wR2 = 0.1134
Final R indexes [all data]	R1 = 0.0743, wR2 = 0.1207
Largest diff. peak/hole / e Å-3	0.56/-0.42
CCDC number	2091078

3.12 Compound $Si(cat^{Cl})_2(hppH)_2$ (**1-(hppH)$_2$**)

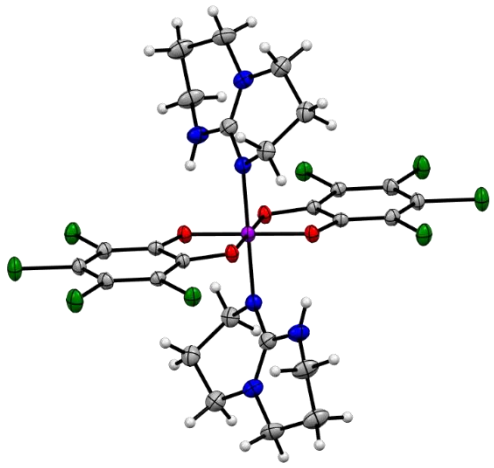

Identification code	**mo_dh457B_2_0m**
Empirical formula	$C_{26}H_{26}Cl_8N_6O_4Si$
Formula weight	798.22
Temperature/K	100.0
Crystal system	triclinic
Space group	P-1
a/Å	8.4949(8)
b/Å	8.5627(7)
c/Å	11.6916(9)
α/°	110.389(3)
β/°	91.093(3)
γ/°	90.987(4)
Volume/Å^3	796.75(12)
Z	1
ρ_{calc}g/cm^3	1.664
μ/mm^{-1}	0.790
F(000)	406.0
Crystal size/mm^3	0.209 × 0.075 × 0.05
Radiation	Mo-K_α (λ = 0.71073)
2Θ range for data collection/°	4.798 to 57.528
Index ranges	-11 ≤ h ≤ 11, -11 ≤ k ≤ 11, -15 ≤ l ≤ 15
Reflections collected	15996
Independent reflections	4071 [R_{int} = 0.0281, R_{sigma} = 0.0249]
Data/restraints/parameters	4071/151/208
Goodness-of-fit on F^2	1.065
Final R indexes [I>=2σ (I)]	R_1 = 0.0362, wR_2 = 0.0921
Final R indexes [all data]	R_1 = 0.0422, wR_2 = 0.0950
Largest diff. peak/hole / e Å^{-3}	0.56/-0.40
CCDC number	2091079

4. Computational Section

Geometry optimizations and single point energy calculations have been performed with ORCA 4.2.3.[24] The structures of all involved compounds were optimized with the PBEh-3c/def2-mSVP as implemented in ORCA, using *grid5* settings.[25] All calculated structures have been confirmed as energetic minima on the potential energy surface by analytical calculation of harmonic frequencies at the PBEh-3c level, revealing only positive Hessian eigenvalues, or one negative in case of the transition state. Enthalpies at 298.15 K have been calculated at the same level of theory by using the rigid-rotor harmonic oscillator (RRHO) approximation,[26] as implemented in ORCA. The following input line was used:

```
! PBEh-3c Grid5 OPT TightSCF FREQ
```

Final single point enthalpies were obtained on PW6B95[27]-D3(BJ)/def2-QZVPP[28-30] including Grimme's semi-empirical dispersion correction (D3)[31] with Becke-Johnson damping function (BJ).[32-34]
In all DFT computations, the resolution-of-identity[35] and "chain of spheres"[36] approximation in the form of RIJCOSX was used in combination with matching auxiliary basis sets (def2/J).[37]

```
! PW6B95 D3BJ def2-QZVPP RIJCOSX def2/J grid5 finalgrid7 gridx6 TightSCF
```

Solvation free energies were obtained by COSMO-RS in dichloromethane as implemented in ADF[38] based on BP86/TZP[39] single point energy calculations for the electrostatic solute-solvent interaction on the PBEh-3c gas-phase structures.[40-43] The following input line was used:

The numerical data and a summary of all the relevant values can be found in tables S4.1-10.

4.1 Reaction of **1-A** with formaldehyde

As a first reaction step the dissociation of one of the two donor sites was considered necessary. Ring opening by Si-NMe_2-bond dissociation (see Fig. S4.1) is thermodynamically favored and proceeds *via* a slightly lower energetic pathway than ring opening by Si-py-bond cleavage (see Fig. S4.2). Opening of the Si-NMe_2-bond is followed by coordination of the formaldehyde *via* an easily accessible transition state ($\Delta G^* = 109.0$ kJ mol^{-1}). **INT2** converts through a slightly lower transition states to final product **1-(OCH_2)-A** by concerted Si-N-bond elongation and C=O insertion in the binding pocket.

The second conceivable pathway proceeds in a similar fashion. After ring opening by Si-py-bond cleavage, the formaldehyde coordinates to the silicon center. Subsequently, the base **A** rotates along the Si-NMe_2-bond until the N(py) reaches spatial proximity to attack the aldehydic carbon atom, yielding the thermodynamic minimum **1-(OCH_2)-A** without another reaction barrier.

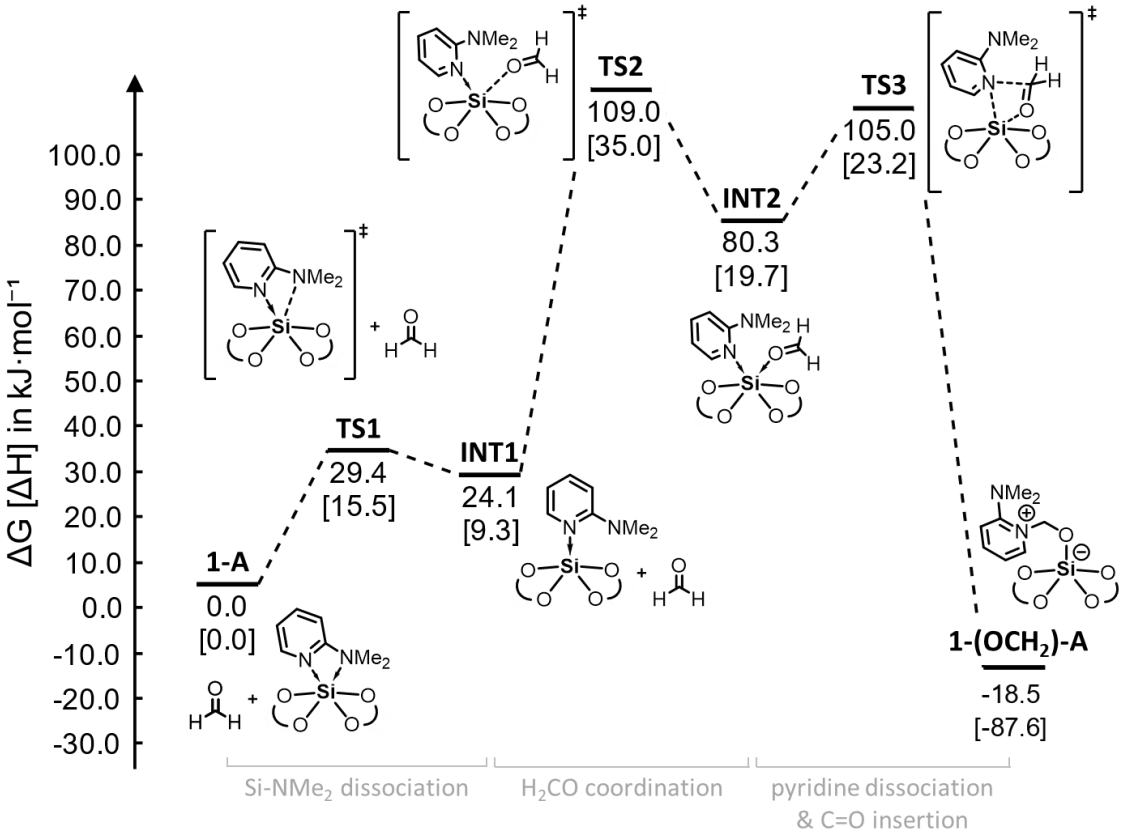

Fig. S4.1: Reaction coordinate for the formaldehyde activation with **1-A** using density functional theory. Calculations were carried out at the PW6B95-D3(BJ)/def2-QZVPP//PBEh-3c level of theory. The given values are free enthalpies and were obtained after considering the solvent environment (CH_2Cl_2) with the COSMO-RS scheme. The values in square brackets correspond to gas phase enthalpies.

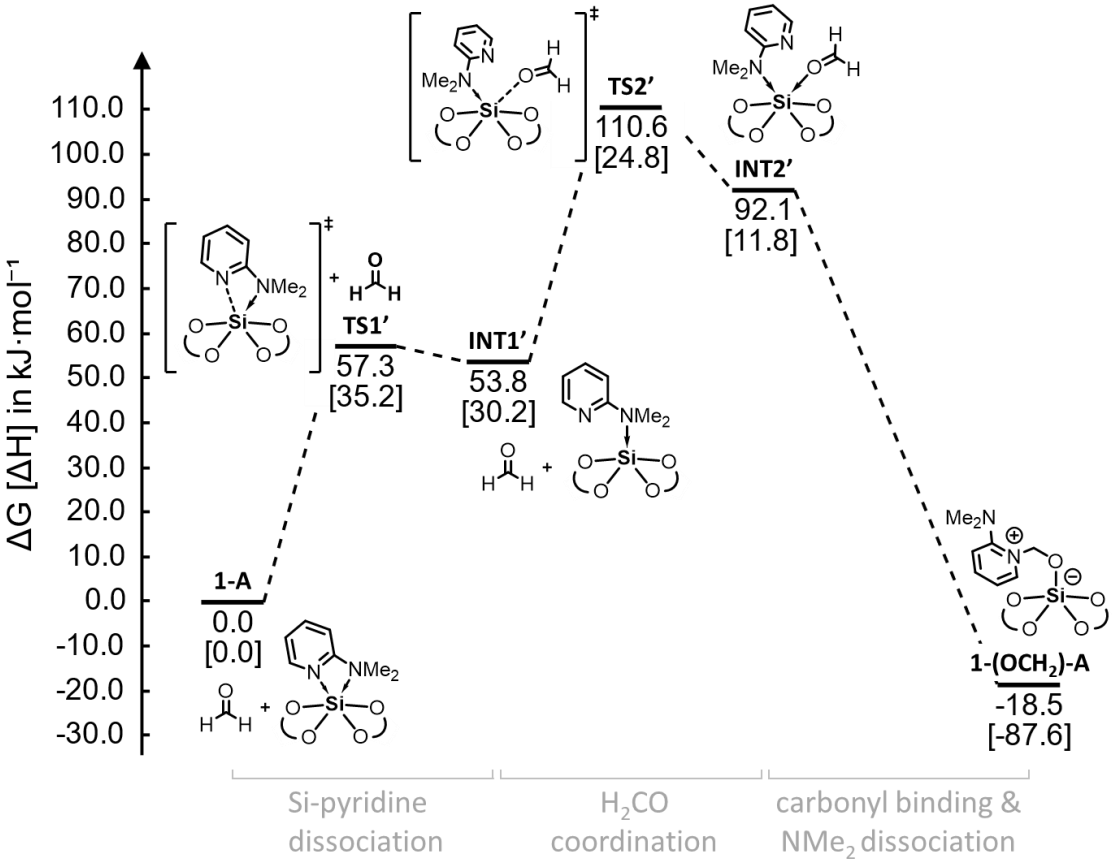

Fig. S4.2: Reaction coordinate for the formaldehyde activation with **1-A** *via* the high-energetic pathway using density functional theory. Calculations were carried out at the PW6B95-D3(BJ)/def2-QZVPP//PBEh-3c level of theory. The given values are free enthalpies and were obtained after considering the solvent environment (CH_2Cl_2) with the COSMO-RS scheme. The values in square brackets correspond to gas phase enthalpies.

Table S4.1: Summary of the energies relative to the ground state **1-A + H_2CO**, obtained by PBEh-3c, PW6B95 and PW6B95 incl. COSMO RS

Compound	ΔH (PBEh-3c)	ΔG (PBEh-3c)	ΔH (PW6B95)	ΔG (PW6B95)	ΔH (PW6B95) + COSMO RS	ΔG (PW6B95) + COSMO RS
1-A + H_2CO	0.00	0.00	0.00	0.00	0.00	0.00
TS1 + H_2CO	20.72	21.72	15.53	16.53	29.60	29.38
INT1 + H_2CO	20.76	17.56	9.29	6.09	29.10	24.08
TS2	33.92	82.45	34.98	83.51	72.38	109.03
INT2	18.52	67.84	19.70	69.03	41.44	80.25
TS3	31.47	83.90	23.22	75.64	63.10	104.98
1-(OCH_2)-A	-87.27	-31.07	-87.62	-31.41	-66.33	-18.50
energies for higher energetic path						
TS1' + H_2CO	45.70	51.44	35.22	40.95	51.96	57.25
INT1' + H_2CO	41.85	43.25	30.23	31.63	52.34	53.79
TS2'	34.03	84.35	24.80	75.12	70.76	110.63
INT2'	19.65	72.64	11.77	64.76	49.60	92.15

Table S4.2: Numerical data for the involved structures in the reaction of **1-A** and formaldehyde (H_2CO), obtained by PBEh-3c, PW6B95 and PW6B95 incl. COSMO RS.

	Compound	Final Gibbs free energy [Eh]	Final entropy term [Eh]	Final entropy term [kJ mol^{-1}]	Total enthalpy H [Eh]	Total correction [Eh]	Total correction [kJ mol^{-1}]	final singlepoint energy [Eh]	final singlepoint energy [kJ mol^{-1}]	H [kJ mol^{-1}] = E_{el} (SP) + total corr. (FREQ) + k_BT	G [kJ mol^{-1}] = H - final entropy term (FREQ)	ΔH [kJ mol^{-1}]	ΔG (295.15K) [kJ mol^{-1}]	H [kJ mol^{-1}]	G (295.15K) [kJ mol^{-1}]
		PBEh-3c Grid5 OPT TightSCF FREQ						PW6B95/def2-QZVPP				COSMO RS		solvent corr. values	
absolute values	H_2CO	-114.245036	0.025446	66.81	-114.219591	0.030515	80.12	-114.689604	-301117.51	-301037.39	-301104.20	-19.65	-10.50	-301057.04	-301114.70
	1-A	-5104.713327	0.090483	237.56	-5104.622844	0.307982	808.61	-5117.040161	-13434787.10	-13433978.49	-13434216.05	-129.88	-120.68	-13434108.37	-13434336.74
	TS1	-5104.705052	0.090101	236.56	-5104.614951	0.306664	805.15	-5117.032927	-13434768.10	-13433962.96	-13434199.52	-115.80	-107.83	-13434078.76	-13434307.35
	INT1	-5104.706638	0.091701	240.76	-5104.614937	0.308118	808.96	-5117.036760	-13434778.17	-13433969.20	-13434209.96	-110.06	-102.69	-13434079.26	-13434312.66
	TS2	-5218.926959	0.097445	255.84	-5218.829514	0.340387	893.69	-5231.718330	-13735874.59	-13734980.90	-13735236.75	-112.12	-105.66	-13735093.03	-13735342.41
	INT2	-5218.932524	0.097141	255.04	-5218.835383	0.341839	897.50	-5231.725603	-13735893.68	-13734996.19	-13735251.23	-127.78	-119.96	-13735123.97	-13735371.19
	TS3	-5218.926407	0.095960	251.94	-5218.830447	0.340806	894.79	-5231.723230	-13735887.45	-13734992.67	-13735244.61	-109.64	-101.85	-13735102.31	-13735346.46
	1-(OCH_2)-A	-5218.970196	0.094520	248.16	-5218.875676	0.344804	905.28	-5231.769443	-13736008.79	-13735103.50	-13735351.67	-128.23	-118.27	-13735231.74	-13735469.94
	energies for higher energetic path														
	TS1‘	-5104.693734	0.088297	231.82	-5104.605437	0.307075	806.22	-5117.025841	-13434749.50	-13433943.27	-13434175.10	-113.14	-104.39	-13434056.41	-13434279.48
	INT1‘	-5104.696853	0.089949	236.16	-5104.606904	0.308285	809.40	-5117.028949	-13434757.66	-13433948.26	-13434184.42	-107.77	-98.53	-13434056.03	-13434282.95
	TS2‘	-5218.926236	0.096763	254.05	-5218.829473	0.340850	894.90	-5231.722672	-13735885.99	-13734991.09	-13735245.14	-103.56	-95.66	-13735094.65	-13735340.80
	INT2‘	-5218.930696	0.095745	251.38	-5218.834952	0.342610	899.52	-5231.729394	-13735903.64	-13735004.12	-13735255.49	-111.70	-103.80	-13735115.81	-13735359.29
summed values	1-A + H_2CO	-5218.958363	0.115929	304.37	-5218.842435	0.338498	888.73	-5231.729765	-13735904.61	-13735015.88	-13735320.26	-149.53	-131.18	-13735165.41	-13735451.44
	TS1 + H_2CO	-5218.950089	0.115547	303.37	-5218.834541	0.337179	885.26	-5231.722530	-13735885.62	-13735000.35	-13735303.72	-135.45	-118.33	-13735135.81	-13735422.05
	INT1 + H_2CO	-5333.215232	0.119966	314.97	-5187.243403	0.375320	985.40	-5346.459047	-14037126.30	-14036140.90	-14036455.87	-147.88	-128.77	-14036288.78	-14036584.64
	TS2	-5218.926959	0.097445	255.84	-5218.829514	0.340387	893.69	-5231.718330	-13735874.59	-13734980.90	-13735236.75	-112.12	-105.66	-13735093.03	-13735342.41
	INT2	-5218.932524	0.097141	255.04	-5218.835383	0.341839	897.50	-5231.725603	-13735893.68	-13734996.19	-13735251.23	-127.78	-119.96	-13735123.97	-13735371.19
	TS3	-5218.926407	0.095960	251.94	-5218.830447	0.340806	894.79	-5231.723230	-13735887.45	-13734992.67	-13735244.61	-109.64	-101.85	-13735102.31	-13735346.46
	1-(OCH_2)-A	-5218.970196	0.094520	248.16	-5218.875676	0.344804	905.28	-5231.769443	-13736008.79	-13735103.50	-13735351.67	-128.23	-118.27	-13735231.74	-13735469.94
	energies for higher energetic path														
	1-A + H_2CO	-5218.958363	0.115929	304.37	-5218.842435	0.338498	888.73	-5231.729765	-13735904.61	-13735015.88	-13735320.26	-149.53	-131.18	-13735165.41	-13735451.44
	TS1‘ + H_2CO	-5218.938770	0.113743	298.63	-5218.825028	0.337590	886.34	-5231.715444	-13735867.01	-13734980.67	-13735279.30	-132.79	-114.89	-13735113.45	-13735394.19
	INT1‘ + H_2CO	-5218.941890	0.115395	302.97	-5218.826494	0.338801	889.52	-5231.718553	-13735875.17	-13734985.65	-13735288.62	-127.42	-109.02	-13735113.07	-13735397.65
	TS2‘	-5218.926236	0.096763	254.05	-5218.829473	0.340850	894.90	-5231.722672	-13735885.99	-13734991.09	-13735245.14	-103.56	-95.66	-13735094.65	-13735340.80
	INT2‘	-5218.930696	0.095745	251.38	-5218.834952	0.342610	899.52	-5231.729394	-13735903.64	-13735004.12	-13735255.49	-111.70	-103.80	-13735115.81	-13735359.29
	1-(OCH_2)-A	-5218.970196	0.094520	248.16	-5218.875676	0.344804	905.28	-5231.769443	-13736008.79	-13735103.50	-13735351.67	-128.23	-118.27	-13735231.74	-13735469.94

4.2 Reaction of **1-B** with formaldehyde

As a first reaction step the dissociation of the two donor sites is possible. Ring opening by Si-NMe_2-bond dissociation (black) is slightly thermodynamically favored compared to the corresponding reaction pathway through initial Si-pyridine bond dissociation (grey).

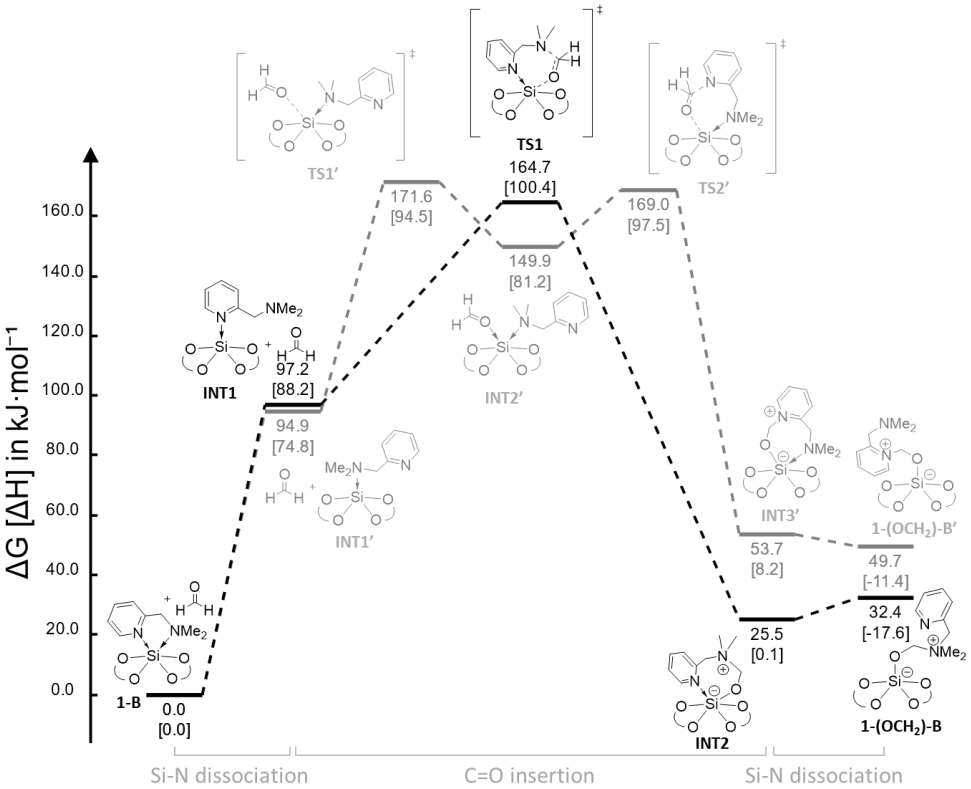

Fig. S4.3: Reaction coordinate for the formaldehyde activation with **1-B** using density functional theory. Calculations were carried out at the PW6B95-D3(BJ)/def2-QZVPP//PBEh-3c level of theory. The given values are free enthalpies and were obtained after considering the solvent environment (CH_2Cl_2) with the COSMO-RS scheme. The values in square brackets correspond to gas phase enthalpies. Ring opening by Si-NMe_2-bond cleavage (black) is slightly thermodynamically favored compared to the corresponding reaction pathway through initial Si-pyridine bond dissociation.

Table S4.3: Summary of the energies relative to the ground state **1-B + H_2CO**, obtained by PBEh-3c, PW6B95 and PW6B95 incl. COSMO RS

Compound	ΔH (PBEh-3c)	ΔG (PBEh-3c)	ΔH (PW6B95)	ΔG (PW6B95)	ΔH (PW6B95) + COSMO RS	ΔG (PW6B95) + COSMO RS
1-B + H_2CO	0.00	0.00	0.00	0.00	0.00	0.00
INT1 + H_2CO	97.99	89.79	88.23	80.02	106.55	97.15
TS1	100.80	149.57	100.37	149.14	125.02	164.74
INT2	-10.72	44.93	0.12	55.78	-25.32	25.46
1-(OCH_2)-B	-28.24	21.41	-17.62	32.04	-10.27	32.42
energies for alternate path via Si-py dissociation						
1-B + H_2CO	0.00	0.00	0.00	0.00	0.00	0.00
INT1' + H_2CO	82.27	78.79	74.85	71.37	98.06	94.93
TS1'	96.04	145.91	94.55	144.42	132.21	171.62
INT2'	83.38	132.44	81.20	130.25	109.99	149.89
TS2'	100.85	155.35	97.49	151.98	124.43	169.04
INT3'	-2.19	55.67	8.17	66.02	0.01	53.67
1-(OCH_2)-B'	-26.49	23.73	-11.39	38.82	7.11	49.74

Table S4.4: Numerical data for the involved structures in the reaction of **1-B** and formaldehyde (H_2CO), obtained by PBEh-3c, PW6B95 and PW6B95 incl. COSMO RS.

	Compound	Final Gibbs free energy [Eh]	Final entropy term [Eh]	Final entropy term [kJ mol^{-1}]	Total enthalpy H [Eh]	Total correction [Eh]	Total correction [kJ mol^{-1}]	final singlepoint energy [Eh]	final singlepoint energy [kJ mol^{-1}]	H [kJ mol^{-1}] = E_{el} (SP) + total corr. (FREQ) + k_BT	G [kJ mol^{-1}] = H - final entropy term (FREQ)	ΔH [kJ mol^{-1}]	ΔG (295.15K) [kJ mol^{-1}]	H [kJ mol^{-1}]	G (295.15K) [kJ mol^{-1}]
		! PBEh-3c Grid5 OPT TightSCF FREQ						PW6B95/def2-QZVPP				COSMO RS		solvent corrected values	
absolute vailues	H_2CO	-114.245036	0.025446	66.81	-114.219591	0.030515	80.12	-114.689604	-301117.51	-301037.39	-301104.20	-19.65	-10.50	-301057.04	-301114.70
	1-B	-5143.925369	0.090844	238.51	-5143.834525	0.339662	891.78	-5156.440762	-13538233.36	-13537341.58	-13537580.09	-132.24	-123.47	-13537473.82	-13537703.56
	INT1	-5143.891170	0.093969	246.72	-5143.797201	0.338551	888.87	-5156.406047	-13538142.22	-13537253.35	-13537500.07	-113.91	-106.34	-13537367.27	-13537606.41
	TS1	-5258.113438	0.097714	256.55	-5258.015724	0.371930	976.50	-5271.093888	-13839255.10	-13838278.60	-13838535.15	-127.24	-118.37	-13838405.84	-13838653.52
	INT2	-5258.153291	0.095091	249.66	-5258.058200	0.376033	987.27	-5271.136174	-13839366.13	-13838378.85	-13838628.51	-177.33	-164.29	-13838556.18	-13838792.80
	1-(OCH_2)-B	-5258.162251	0.097379	255.67	-5258.064873	0.376248	987.84	-5271.143146	-13839384.43	-13838396.59	-13838652.26	-144.55	-133.59	-13838541.13	-13838785.84
	energies for alternate path via Si-py dissociation														
	H_2CO	-114.245036	0.025446	66.81	-114.219591	0.030515	80.12	-114.689604	-301117.51	-301037.39	-301104.20	-19.65	-10.50	-301057.04	-301114.70
	1-B	-5143.925369	0.090844	238.51	-5143.834525	0.339662	891.78	-5156.440762	-13538233.36	-13537341.58	-13537580.09	-132.24	-123.47	-13537473.82	-13537703.56
	INT1'	-5143.895358	0.092168	241.99	-5143.803190	0.339242	890.68	-5156.411834	-13538157.41	-13537266.73	-13537508.72	-109.02	-99.91	-13537375.75	-13537608.63
	TS1'	-5258.114831	0.097294	255.45	-5258.017537	0.372366	977.65	-5271.096543	-13839262.07	-13838284.43	-13838539.87	-114.23	-106.77	-13838398.65	-13838646.64
	INT2'	-5258.119963	0.097606	256.26	-5258.022357	0.373605	980.90	-5271.102867	-13839278.68	-13838297.78	-13838554.04	-123.10	-114.33	-13838420.87	-13838668.37
	TS2'	-5258.111236	0.095533	250.82	-5258.015704	0.372687	978.49	-5271.095745	-13839259.98	-13838281.49	-13838532.31	-124.94	-116.91	-13838406.43	-13838649.22
	INT3'	-5258.149202	0.094254	247.46	-5258.054948	0.375874	986.86	-5271.132952	-13839357.66	-13838370.81	-13838618.27	-160.04	-146.33	-13838530.85	-13838764.60
	1-(OCH_2)-B'	-5258.161367	0.097162	255.10	-5258.064205	0.375011	984.59	-5271.139539	-13839374.96	-13838390.37	-13838645.47	-133.38	-123.05	-13838523.75	-13838768.52
summed values	1-B + H_2CO	-5258.170405	0.116290	305.32	-5258.054115	0.370177	971.90	-5271.130366	-13839350.87	-13838378.97	-13838684.29	-151.89	-133.97	-13838530.86	-13838818.26
	INT1 + H_2CO	-5258.136206	0.119415	313.52	-5258.016791	0.369067	968.98	-5271.095651	-13839259.73	-13838290.75	-13838604.27	-133.56	-116.84	-13838424.31	-13838721.11
	TS1	-5258.113438	0.097714	256.55	-5258.015724	0.371930	976.50	-5271.093888	-13839255.10	-13838278.60	-13838535.15	-127.24	-118.37	-13838405.84	-13838653.52
	INT2	-5258.153291	0.095091	249.66	-5258.058200	0.376033	987.27	-5271.136174	-13839366.13	-13838378.85	-13838628.51	-177.33	-164.29	-13838556.18	-13838792.80
	1-(OCH_2)-B	-5258.162251	0.097379	255.67	-5258.064873	0.376248	987.84	-5271.143146	-13839384.43	-13838396.59	-13838652.26	-144.55	-133.59	-13838541.13	-13838785.84
	energies for alternate path via Si-py dissociation														
	1-B + H_2CO	-5258.170405	0.116290	305.32	-5258.054115	0.370177	971.90	-5271.130366	-13839350.87	-13838378.97	-13838684.29	-151.89	-133.97	-13838530.86	-13838818.26
	INT1' + H_2CO	-5258.140395	0.117614	308.80	-5258.022780	0.369757	970.80	-5271.101437	-13839274.92	-13838304.13	-13838612.92	-128.67	-110.41	-13838432.80	-13838723.33
	TS1'	-5258.114831	0.097294	255.45	-5258.017537	0.372366	977.65	-5271.096543	-13839262.07	-13838284.43	-13838539.87	-114.23	-106.77	-13838398.65	-13838646.64
	INT2'	-5258.119963	0.097606	256.26	-5258.022357	0.373605	980.90	-5271.102867	-13839278.68	-13838297.78	-13838554.04	-123.10	-114.33	-13838420.87	-13838668.37
	TS2'	-5258.111236	0.095533	250.82	-5258.015704	0.372687	978.49	-5271.095745	-13839259.98	-13838281.49	-13838532.31	-124.94	-116.91	-13838406.43	-13838649.22
	INT3'	-5258.149202	0.094254	247.46	-5258.054948	0.375874	986.86	-5271.132952	-13839357.66	-13838370.81	-13838618.27	-160.04	-146.33	-13838530.85	-13838764.60
	1-(OCH2)-B'	-5258.161367	0.097162	255.10	-5258.064205	0.375011	984.59	-5271.139539	-13839374.96	-13838390.37	-13838645.47	-133.38	-123.05	-13838523.75	-13838768.52

4.3 Reaction of **1-(py)$_2$** with formaldehyde

Dissociation of the first equivalent pyridine (pathway to the left) is accessible for entropic reason but the enthalpy considerably large. Additionally, the occourence of a termolecular reaction between **1-(py)**, **py**, and **OCH$_2$** renders this pathway entropically disfavoured. Concerted Si-pyridine dissociation and C=O insertion proceeds through a high-energy transition state, leading to **INT1**. The subsequent release of the second equivalent pyridine is slightly endergonic (ΔG = 6.1 kJ mol^{-1}).

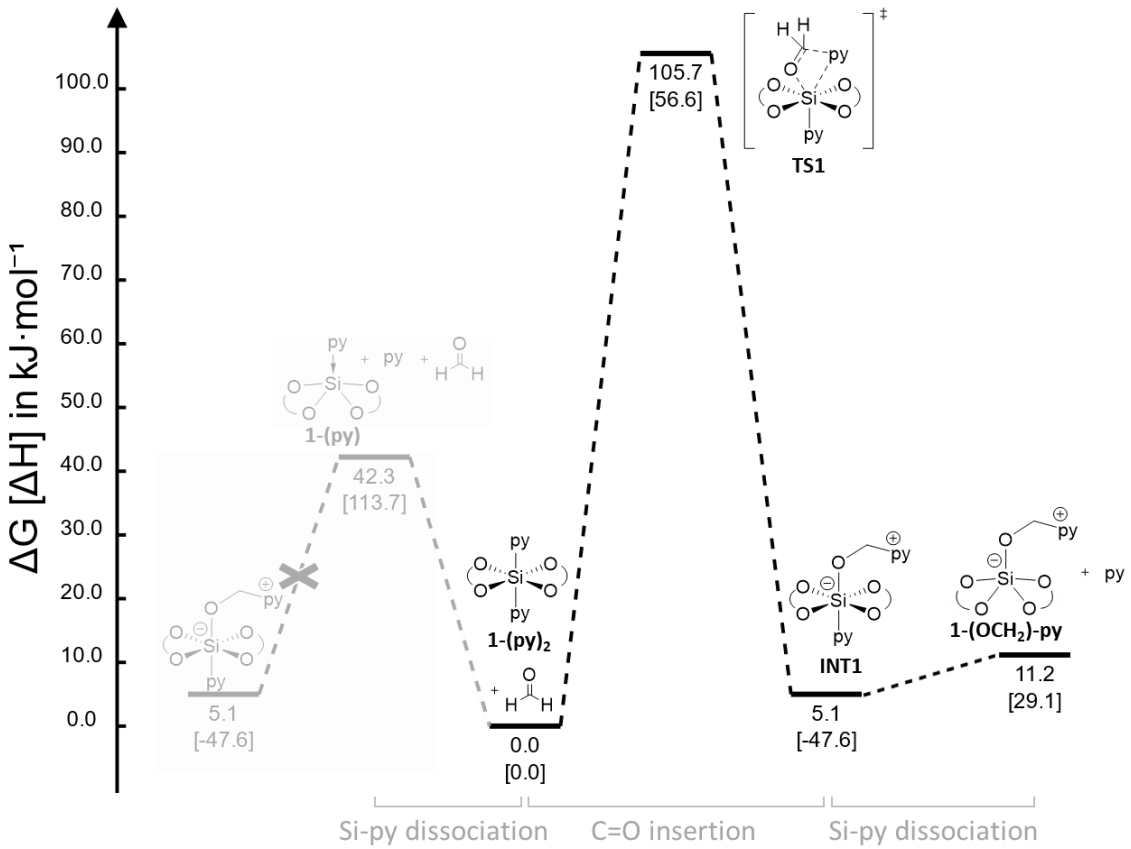

Fig. S4.4: Reaction coordinate for the formaldehyde activation with **1-(py)$_2$** using density functional theory. Calculations were carried out at the PW6B95-D3(BJ)/def2-QZVPP//PBEh-3c level of theory. The given values are free enthalpies and were obtained after considering the solvent environment (CH_2Cl_2) with the COSMO-RS scheme. The values in square brackets correspond to gas phase enthalpies. Dissociation of the first equivalent pyridine (pathway to the left) is energetically accessible but no reaction pathway from the mono-adduct was found. Concerted Si-pyridine dissociation and C=O insertion proceeds through a high-energy transition state.

Table S4.5: Summary of the energies relative to the ground state **1-(py)$_2$ + H$_2$CO**, obtained by PBEh-3c, PW6B95 and PW6B95 incl. COSMO RS

Compound	ΔH (PBEh-3c)	ΔG (PBEh-3c)	ΔH (PW6B95)	ΔG (PW6B95)	ΔH (PW6B95) + COSMO RS	ΔG (PW6B95) + COSMO RS
1-(py) + py + H$_2$CO	124.68	65.35	113.69	54.36	92.36	42.27
1-(py)$_2$ + H$_2$CO	0.00	0.00	0.00	0.00	0.00	0.00
TS1	57.05	102.84	56.62	102.41	66.35	105.72
INT1	-61.97	-3.12	-47.59	11.26	-49.65	5.12
1-(OCH$_2$)-(py)$_2$ + py	24.03	24.03	29.14	29.15	8.15	11.24

Table S4.6: Numerical data for the involved structures in the reaction of **1-(py)$_2$** and formaldehyde (H_2CO), obtained by PBEh-3c, PW6B95 and PW6B95 incl. COSMO RS.

	Compound	Final Gibbs free energy [Eh]	Final entropy term [Eh]	**Final entropy term [kJ mol^{-1}]**	Total enthalpy **H** [Eh]	Total correction [Eh]	**Total correction [kJ mol^{-1}]**	final singlepoint energy [Eh]	**final singlepoint energy [kJ mol^{-1}]**	**H [kJ mol^{-1}] = E_{el} (SP) + total corr. (FREQ) + k_BT**	**G [kJ mol^{-1}] = H - final entropy term (FREQ)**	**ΔH [kJ mol^{-1}]**	**ΔG (295.15K) [kJ mol^{-1}]**	**H [kJ mol^{-1}]**	**G (295.15K) [kJ mol^{-1}]**
		! PBEh-3c Grid5 OPT TightSCF FREQ						PW6B95/def2-QZVPP				COSMO RS		solvent corrected values	
absolute values	**H_2CO**	-114.245036	0.025446	66.81	-114.219591	0.030515	80.12	-114.689604	-301117.51	-301037.39	-301104.20	-19.65	-10.50	-301057.04	-301114.70
	py	-247.665670	0.032455	85.21	-247.633215	0.095842	251.63	-248.715831	-653003.33	-652751.69	-652836.90	-27.27	-18.41	-652778.97	-652855.31
	1-(py)	-4971.093881	0.084484	221.81	-4971.009397	0.228642	600.30	-4982.834894	-13082431.22	-13081830.92	-13082052.73	-114.40	-105.93	-13081945.32	-13082158.67
	1-(py)$_2$	-5218.784440	0.094341	247.69	-5218.690099	0.328052	861.30	-5231.597596	-13735557.60	-13734696.30	-13734943.99	-120.35	-112.26	-13734816.65	-13735056.25
	TS1	-5332.990305	0.102346	268.71	-5332.887959	0.360428	946.30	-5346.267495	-14036623.38	-14035677.08	-14035945.79	-130.27	-119.45	-14035807.34	-14036065.24
	INT1	-5333.030664	0.097370	255.65	-5332.933293	0.364215	956.25	-5346.310974	-14036737.53	-14035781.29	-14036036.93	-142.06	-128.90	-14035923.34	-14036165.83
	1-(OCH_2)-(py)$_2$	-5085.354652	0.087329	229.28	-5085.267323	0.265351	696.68	-5097.562893	-13383649.54	-13382952.86	-13383182.14	-133.72	-122.26	-13383086.58	-13383304.41
summed values	**1-(py) + py + H_2CO**	-5333.004587	0.142384	373.83	-5332.862203	0.354999	932.05	-5346.240329	-14036552.06	-14035620.01	-14035993.84	-161.32	-134.84	-13383002.37	-13383273.37
	1-(py)$_2$ + H_2CO	-5333.029476	0.119787	314.50	-5332.909689	0.358568	941.42	-5346.287199	-14036675.11	-14035733.69	-14036048.19	-140.00	-122.76	-14035873.69	-14036170.96
	TS1	-5332.990305	0.102346	268.71	-5332.887959	0.360428	946.30	-5346.267495	-14036623.38	-14035677.08	-14035945.79	-130.27	-119.45	-14035807.34	-14036065.24
	INT1	-5333.030664	0.097370	255.65	-5332.933293	0.364215	956.25	-5346.310974	-14036737.53	-14035781.29	-14036036.93	-142.06	-128.90	-14035923.34	-14036165.83
	1-(OCH_2)-py + py	-5333.020322	0.119783	314.49	-5332.900538	0.361193	948.31	-5346.278724	-14036652.86	-14035704.55	-14036019.04	-160.99	-140.68	-14035865.55	-14036159.72

4.4 Reaction of **1-C** with formaldehyde

The dissociation of the PPh_2-sidearm is only slightly endergonic, and the subsequent insertion of formaldehyde into the P-Si pocket proceeds *via* an easily accessible transition state (ΔG^* = 71.1 kJ mol^{-1}). The overall reaction is exergonic by 50.7 kJ mol^{-1}.

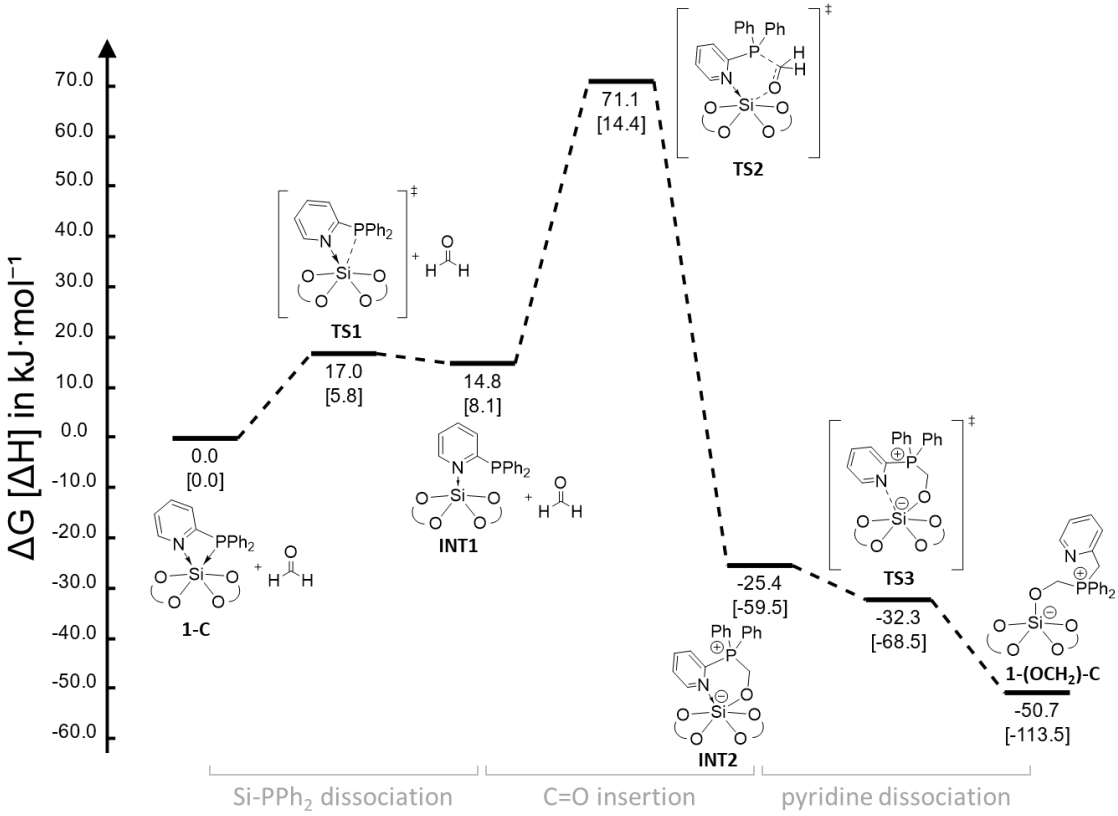

Fig. S4.5: Reaction coordinate for the formaldehyde activation with **1-C** using density functional theory. Calculations were carried out at the PW6B95-D3(BJ)/def2-QZVPP//PBEh-3c level of theory. The given values are free enthalpies and were obtained after considering the solvent environment (CH_2Cl_2) with the COSMO-RS scheme. The values in square brackets correspond to gas phase enthalpies.

Table S4.7: Summary of the energies relative to the ground state **1-C + H_2CO**, obtained by PBEh-3c, PW6B95 and PW6B95 incl. COSMO RS

Compound	ΔH (PBEh-3c)	ΔG (PBEh-3c)	ΔH (PW6B95)	ΔG (PW6B95)	ΔH (PW6B95) + COSMO RS	ΔG (PW6B95) + COSMO RS
1-C + H_2CO	0	0	0	0	0	0
TS1 + H_2CO	13.27	17.38	5.80	9.91	13.35	16.98
INT1 + H_2CO	15.19	13.59	8.15	6.54	16.27	14.76
TS2	8.44	62.68	14.43	68.67	26.86	71.10
INT2	-68.17	-13.30	-59.47	-4.61	-72.93	-25.39
TS3	-77.73	-20.54	-68.45	-11.27	-81.88	-32.32
1-(OCH_2)-C	-117.75	-61.99	-113.50	-57.74	-98.38	-50.72

Table S4.8: Numerical data for the involved structures in the reaction of **1-C** and formaldehyde (H_2CO), obtained by PBEh-3c, PW6B95 and PW6B95 incl. COSMO RS.

	Compound	Final Gibbs free energy [Eh]	Final entropy term [Eh]	**Final entropy term [kJ mol^{-1}]**	Total enthalpy **H** [Eh]	Total correction [Eh]	**Total correction [kJ mol^{-1}]**	final singlepoint energy [Eh]	**final singlepoint energy [kJ mol^{-1}]**	**H [kJ mol^{-1}] = E_{el} (SP) + total corr. (FREQ) + k_BT**	**G [kJ mol^{-1}] = H - final entropy term (FREQ)**	**ΔH [kJ mol^{-1}]**	**ΔG (295.15K) [kJ mol^{-1}]**	**H [kJ mol^{-1}]**	**G (295.15K) [kJ mol^{-1}]**
		! PBEh-3c Grid5 OPT TightSCF FREQ						PW6B95/def2-QZVPP				COSMO RS		solvent corrected values	
absolute values	**H_2CO**	-114.245036	0.025446	66.81	-114.219591	0.030515	80.12	-114.69	-301117.51	-301037.39	-301104.20	-19.65	-10.50	-301057.04	-301114.70
	1-C	-5773.566918	0.105116	275.98	-5773.461802	0.417891	1097.17	-5788.04	-15196501.15	-15195403.97	-15195679.96	-133.26	-124.72	-15195537.23	-15195804.68
	TS1	-5773.560300	0.103551	271.87	-5773.456750	0.416992	1094.81	-5788.04	-15196492.99	-15195398.17	-15195670.05	-125.71	-117.65	-15195523.89	-15195787.70
	INT1	-5773.561742	0.105727	277.59	-5773.456016	0.417950	1097.33	-5788.04	-15196493.16	-15195395.83	-15195673.41	-125.13	-116.50	-15195520.96	-15195789.91
	TS2	-5887.788081	0.109902	288.55	-5887.678179	0.451533	1185.50	-5902.73	-15497612.44	-15496426.94	-15496715.49	-140.47	-132.79	-15496567.41	-15496848.28
	INT2	-5887.817022	0.109665	287.93	-5887.707357	0.453670	1191.11	-5902.76	-15497691.95	-15496500.84	-15496788.77	-166.36	-156.00	-15496667.20	-15496944.77
	TS3	-5887.819779	0.108782	285.61	-5887.710997	0.452499	1188.04	-5902.76	-15497697.86	-15496509.82	-15496795.43	-166.34	-156.27	-15496676.16	-15496951.70
	1-(OCH_2)-C	-5887.835566	0.109324	287.03	-5887.726242	0.453473	1190.59	-5902.78	-15497745.46	-15496554.87	-15496841.90	-137.79	-128.20	-15496692.66	-15496970.10
summed values	**1-C + H_2CO**	-5887.811955	0.130562	342.79	-5887.681393	0.448406	1177.29	-5902.73	-15497618.66	-15496441.37	-15496784.16	-152.91	-135.22	-15496594.28	-15496919.38
	TS1 + H_2CO	-5887.805337	0.128997	338.68	-5887.676340	0.447507	1174.93	-5902.73	-15497610.50	-15496435.57	-15496774.25	-145.36	-128.15	-15496580.93	-15496902.40
	INT2 + H_2CO	-5887.806779	0.131173	344.39	-5887.675606	0.448466	1177.45	-5902.73	-15497610.67	-15496433.22	-15496777.62	-144.79	-127.00	-15496578.01	-15496904.61
	TS2	-5887.788081	0.109902	288.55	-5887.678179	0.451533	1185.50	-5902.73	-15497612.44	-15496426.94	-15496715.49	-140.47	-132.79	-15496567.41	-15496848.28
	INT3	-5887.817022	0.109665	287.93	-5887.707357	0.453670	1191.11	-5902.76	-15497691.95	-15496500.84	-15496788.77	-166.36	-156.00	-15496667.20	-15496944.77
	TS3	-5887.819779	0.108782	285.61	-5887.710997	0.452499	1188.04	-5902.76	-15497697.86	-15496509.82	-15496795.43	-166.34	-156.27	-15496676.16	-15496951.70
	1-(OCH_2)-C	-5887.835566	0.109324	287.03	-5887.726242	0.453473	1190.59	-5902.78	-15497745.46	-15496554.87	-15496841.90	-137.79	-128.20	-15496692.66	-15496970.10

4.5 Reaction of **1-(PPh$_3$)$_2$** with formaldehyde

The dissociation of one PPh$_3$ is almost thermoneutral and entropy-driven, thus much less unfavorable in comparison to the dissociation of pyridine from **1**-(pyridine)$_2$ (cf. Figure S4.4).

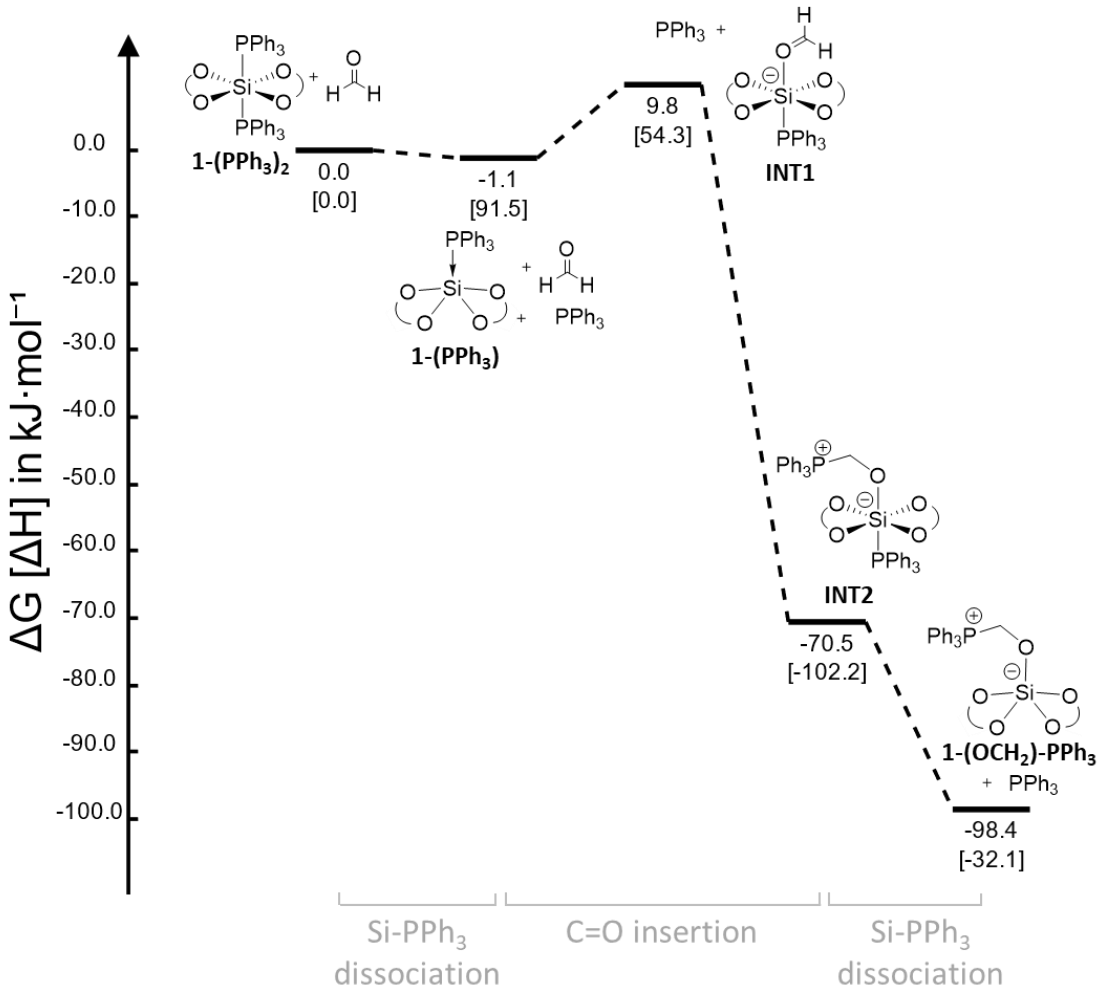

Fig. S4.6: Reaction coordinate for the formaldehyde activation with **1-(PPh$_3$)$_2$** using density functional theory. Calculations were carried out at the PW6B95-D3(BJ)/def2-QZVPP//PBEh-3c level of theory. The given values are free enthalpies and were obtained after considering the solvent environment (CH_2Cl_2) with the COSMO-RS scheme. The values in square brackets correspond to gas phase enthalpies.

Table S4.9: Summary of the energies relative to the ground state **1-(PPh$_3$)$_2$ + H$_2$CO**, obtained by PBEh-3c, PW6B95 and PW6B95 incl. COSMO RS.

Compound	ΔH (PBEh-3c)	ΔG (PBEh-3c)	ΔH (PW6B95)	ΔG (PW6B95)	ΔH (PW6B95) + COSMO RS	ΔG (PW6B95) + COSMO RS
1-(PPh$_3$)$_2$ + H$_2$CO	0.00	0.00	0.00	0.00	0.00	0.00
1-(PPh$_3$) + PPh$_3$ + H$_2$CO	100.42	32.53	91.53	23.64	58.99	-1.10
INT1 + PPh3	51.23	33.31	54.29	36.37	28.83	9.82
INT2	-105.64	-51.10	-102.16	-47.62	-121.05	-70.49
1-(OCH$_2$)-PPh$_3$ + PPh$_3$	-33.78	-48.48	-32.07	-46.76	-85.62	-98.40

Table S4.10: Numerical data for the involved structures in the reaction of **1-(PPh_3)$_2$** and formaldehyde (H_2CO), obtained by PBEh-3c, PW6B95 and PW6B95 incl. COSMO RS.

	Compound	Final Gibbs free energy [Eh]	Final entropy term [Eh]	**Final entropy term [kJ mol^{-1}]**	Total enthalpy **H** [Eh]	Total correction [Eh]	**Total correction [kJ mol^{-1}]**	final singlepoint energy [Eh]	**final singlepoint energy [kJ mol^{-1}]**	**H [kJ mol^{-1}] = E_{el} (SP) + total corr. (FREQ) + k_BT**	**G [kJ mol^{-1}] = H - final entropy term (FREQ)**	**ΔH [kJ mol^{-1}]**	**ΔG (295.15K) [kJ mol^{-1}]**	**H [kJ mol^{-1}]**	**G (295.15K) [kJ mol^{-1}]**
		! PBEh-3c Grid5 OPT TightSCF FREQ						PW6B95/def2-QZVPP				COSMO RS		solvent corrected values	
absolute values	**H_2CO**	-114.245036	0.025446	66.81	-114.219591	0.030515	80.12	-114.689604	-301117.51	-301037.39	-301104.20	-19.65	-10.50	-301057.04	-301114.70
	PPh_3	-1034.118852	0.058289	153.04	-1034.060562	0.297843	781.99	-1037.857753	-2724895.16	-2724113.17	-2724266.21	-51.49	-44.03	-2724164.66	-2724310.24
	1-(PPh_3)$_2$	-6791.672280	0.138576	363.83	-6791.533705	0.731469	1920.47	-6809.871131	-17879314.20	-17877393.73	-17877757.56	-131.66	-125.39	-17877525.38	-17877882.94
	1-(PPh_3)	-5757.541040	0.106145	278.68	-5757.434895	0.430297	1129.74	-5771.975186	-15154318.77	-15153189.03	-15153467.71	-112.71	-106.09	-15153301.74	-15153573.80
	INT2	-6905.936780	0.143248	376.10	-6905.793532	0.766606	2012.72	-6924.604267	-18180546.01	-18178533.28	-18178909.38	-170.19	-158.75	-18178703.47	-18179068.13
	1-(OCH_2)-PPh_3	-5871.816929	0.111328	292.29	-5871.705600	0.465674	1222.63	-5886.716728	-15455572.65	-15454350.02	-15454642.31	-153.36	-143.49	-15454503.39	-15454785.81
	INT1	-5871.785780	0.112559	295.52	-5871.673220	0.464425	1219.35	-5886.682587	-15455483.01	-15454263.66	-15454559.19	-125.27	-118.40	-15454388.94	-15454677.59
summed values	**1-(PPh_3)$_2$ + H_2CO**	-6905.917317	0.164021	430.64	-6905.753295	0.761985	2000.59	-6924.560734	-18180431.71	-18178431.12	-18178861.76	-151.31	-135.89	-18178582.43	-18178997.65
	1-(PPh_3) + PPh_3 + H_2CO	-6905.904928	0.189880	498.53	-6905.715048	0.758656	1991.85	-6924.522542	-18180331.44	-18178339.59	-18178838.12	-183.85	-160.62	-18178523.44	-18178998.74
	INT1 + PPh3	-6905.904631	0.170848	448.56	-6905.733783	0.762269	2001.34	-6924.540340	-18180378.17	-18178376.83	-18178825.39	-176.77	-162.44	-18178553.60	-18178987.83
	INT2	-6905.936780	0.143248	376.10	-6905.793532	0.766606	2012.72	-6924.604267	-18180546.01	-18178533.28	-18178909.38	-170.19	-158.75	-18178703.47	-18179068.13
	1-(OCH_2)-PPh_3 + PPh_3	-6905.935780	0.169618	445.33	-6905.766163	0.763517	2004.61	-6924.574481	-18180467.80	-18178463.19	-18178908.52	-204.86	-187.52	-18178668.05	-18179096.05

5. NMR spectra

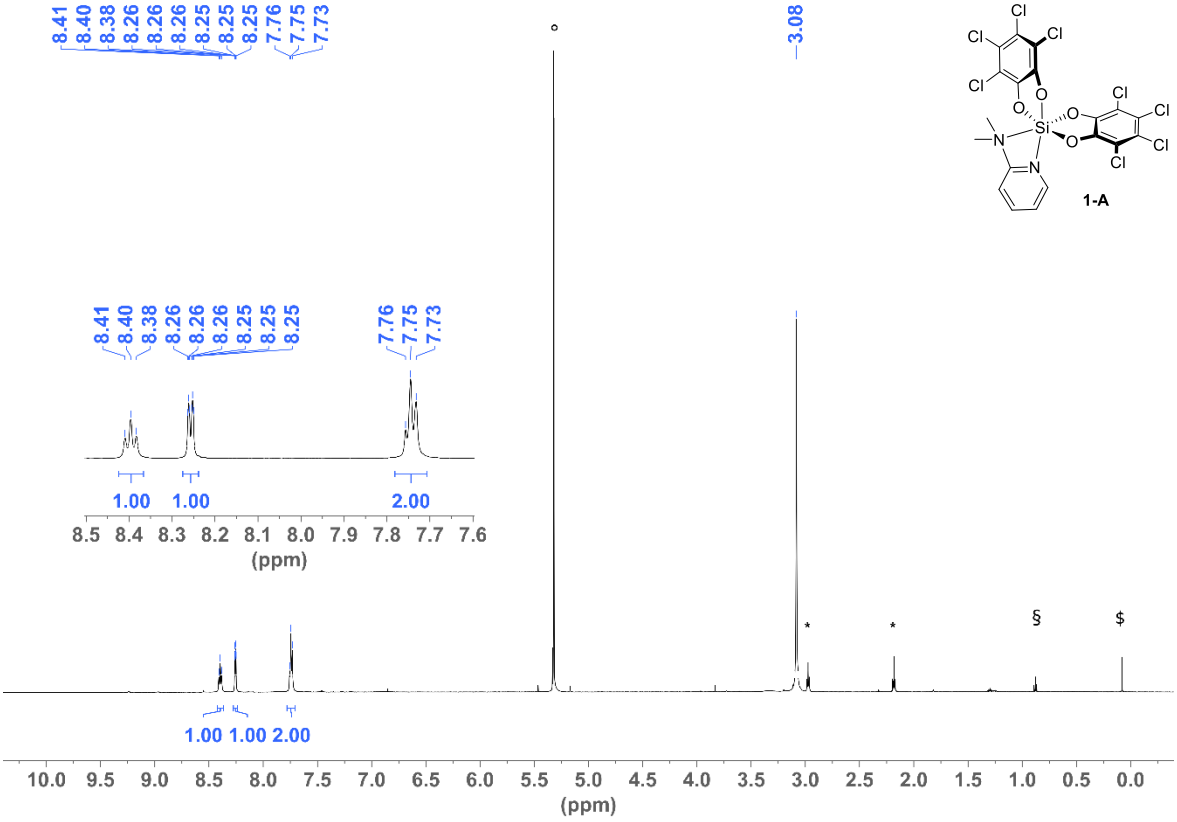

Figure S5.1: ^{1}H NMR (600 MHz, CD_2Cl_2, RT) of **1-A**. Residual proton signals marked with ° (solvent), * (sulfolane), § (pentane) and $ (grease).

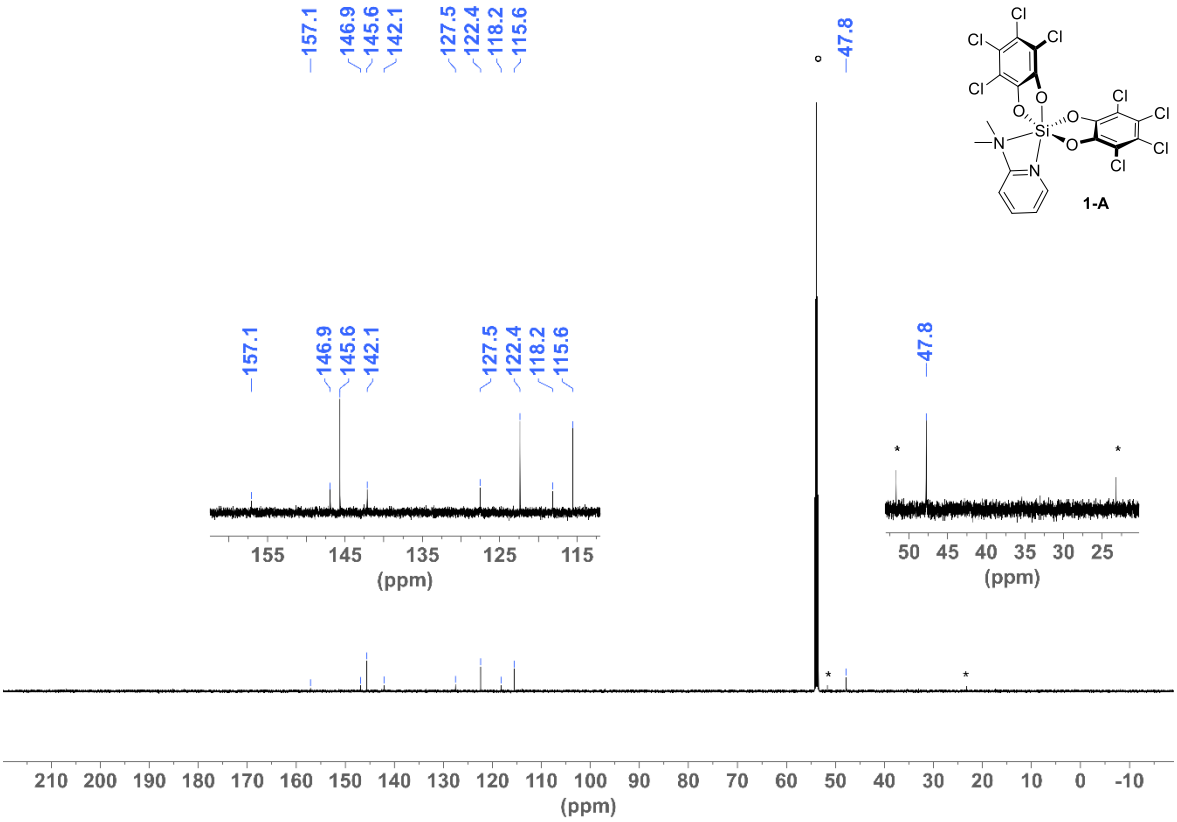

Figure S5.2: ^{13}C NMR (151 MHz, CD_2Cl_2, RT) of **1-A**. Residual carbon signals marked with ° (solvent) and * (sulfolane).

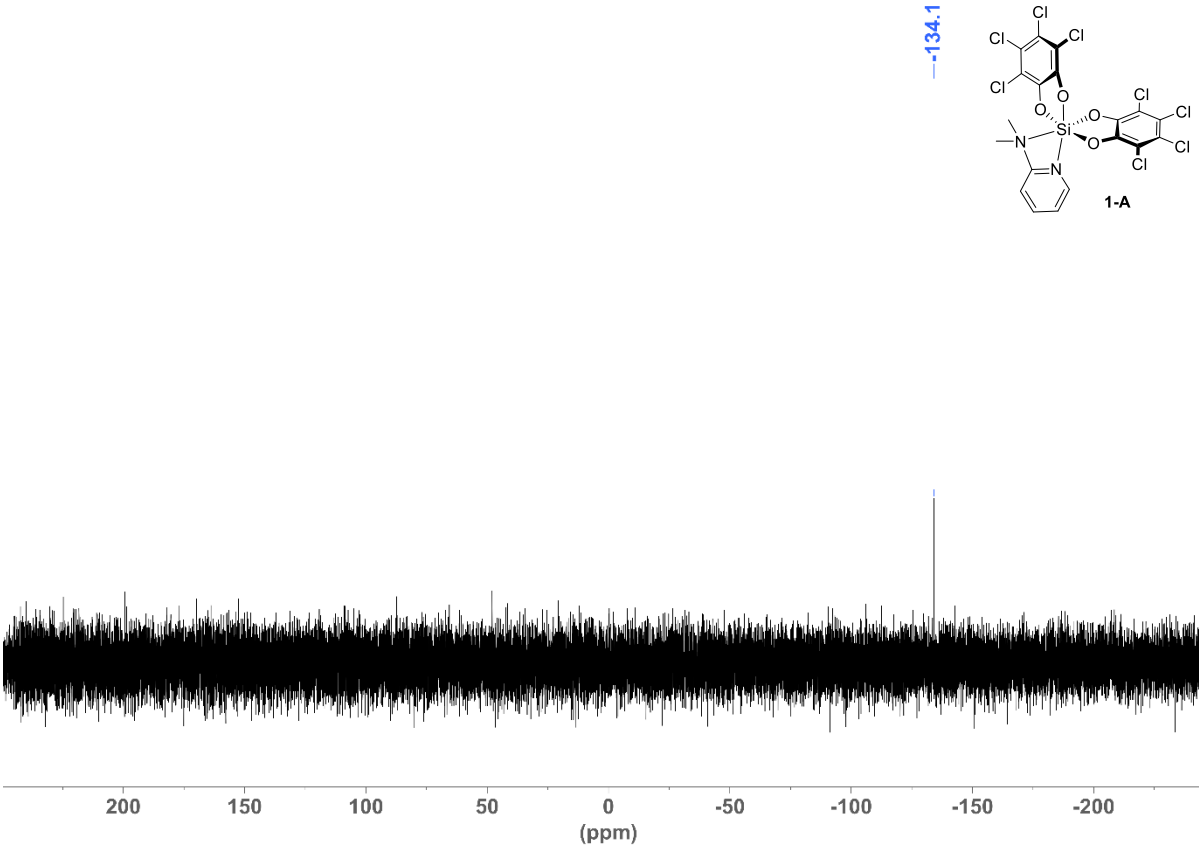

Figure S5.3: ^{29}Si NMR (119 MHz, CD_2Cl_2, RT) of **1-A**.

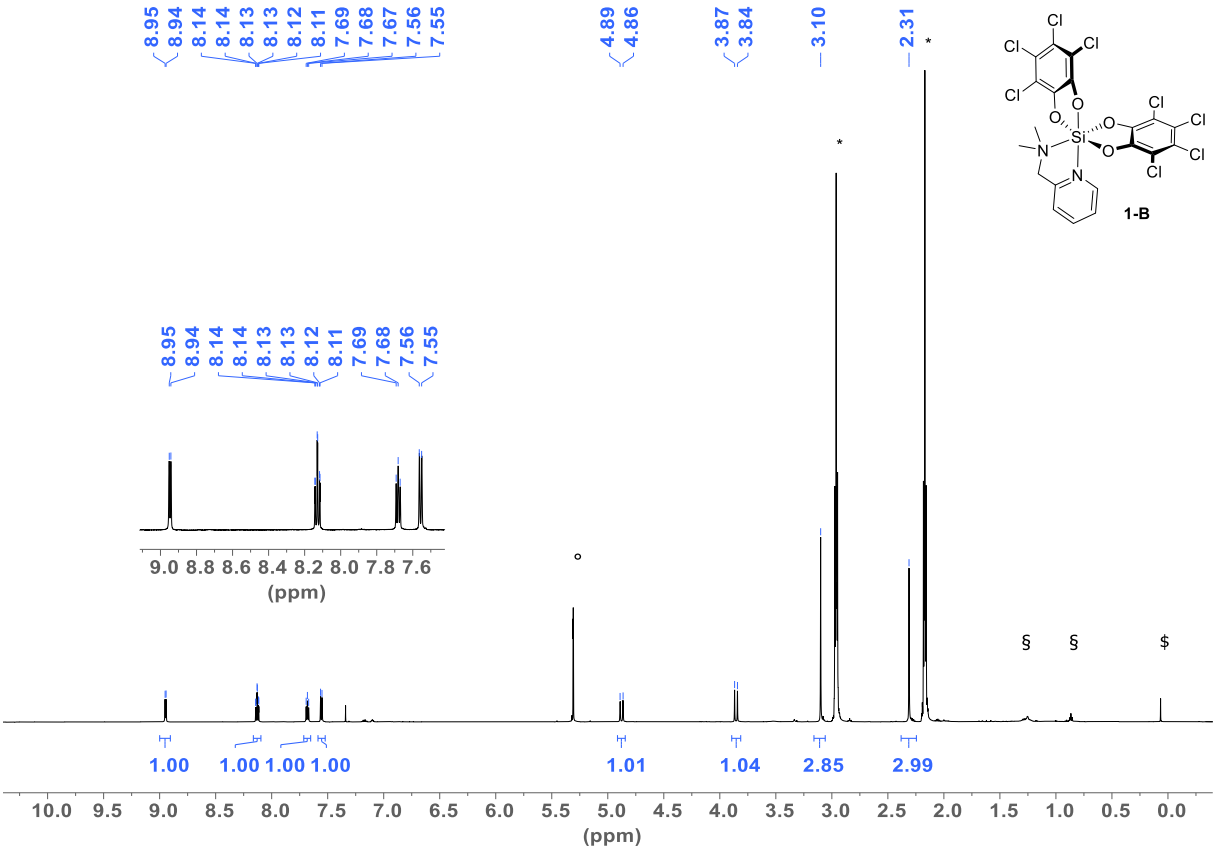

Figure S5.4: ^{1}H NMR (600 MHz, CD_2Cl_2, RT) of **1-B**. Residual proton signals marked with ° (solvent), * (sulfolane), § (pentane) and $ (grease).

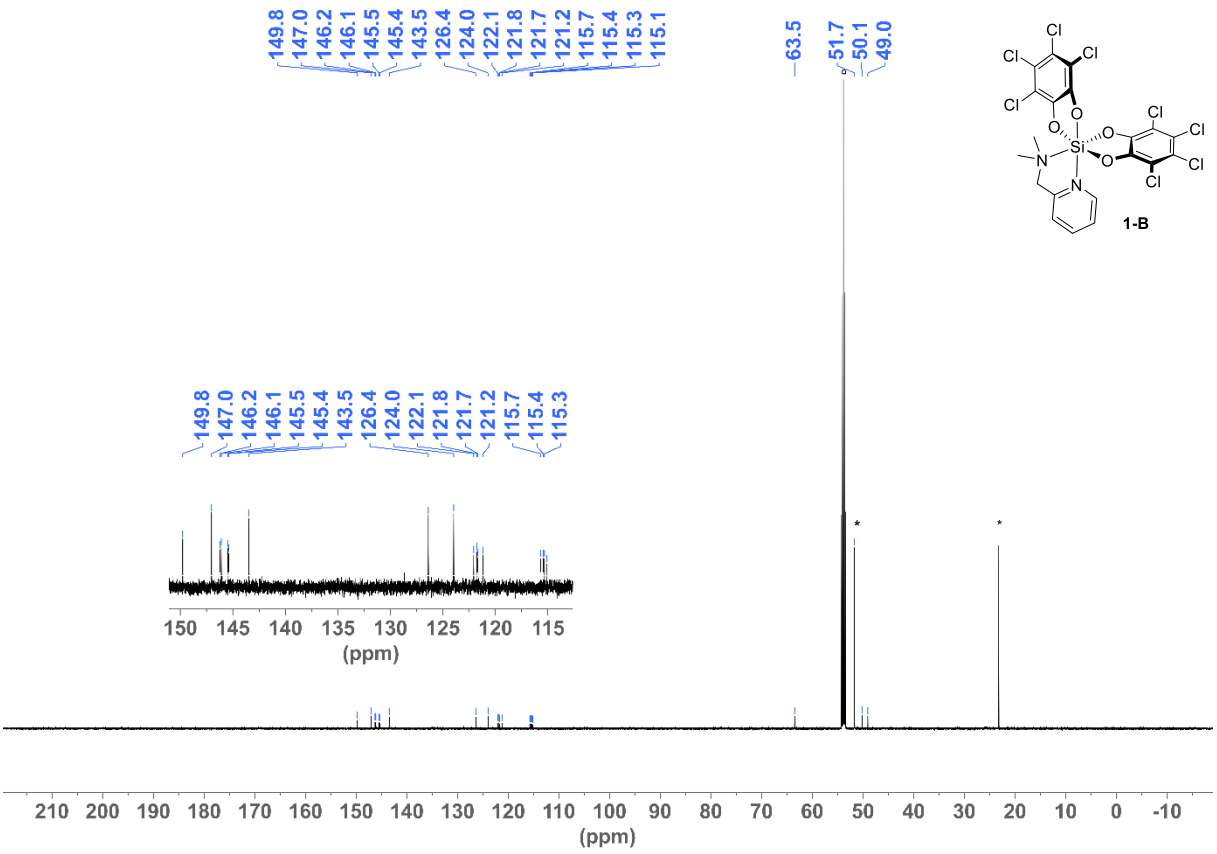

Figure S5.5: ^{13}C NMR (151 MHz, CD_2Cl_2, RT) of **1-B** . Residual carbon signals marked with ° (solvent) and * (sulfolane).

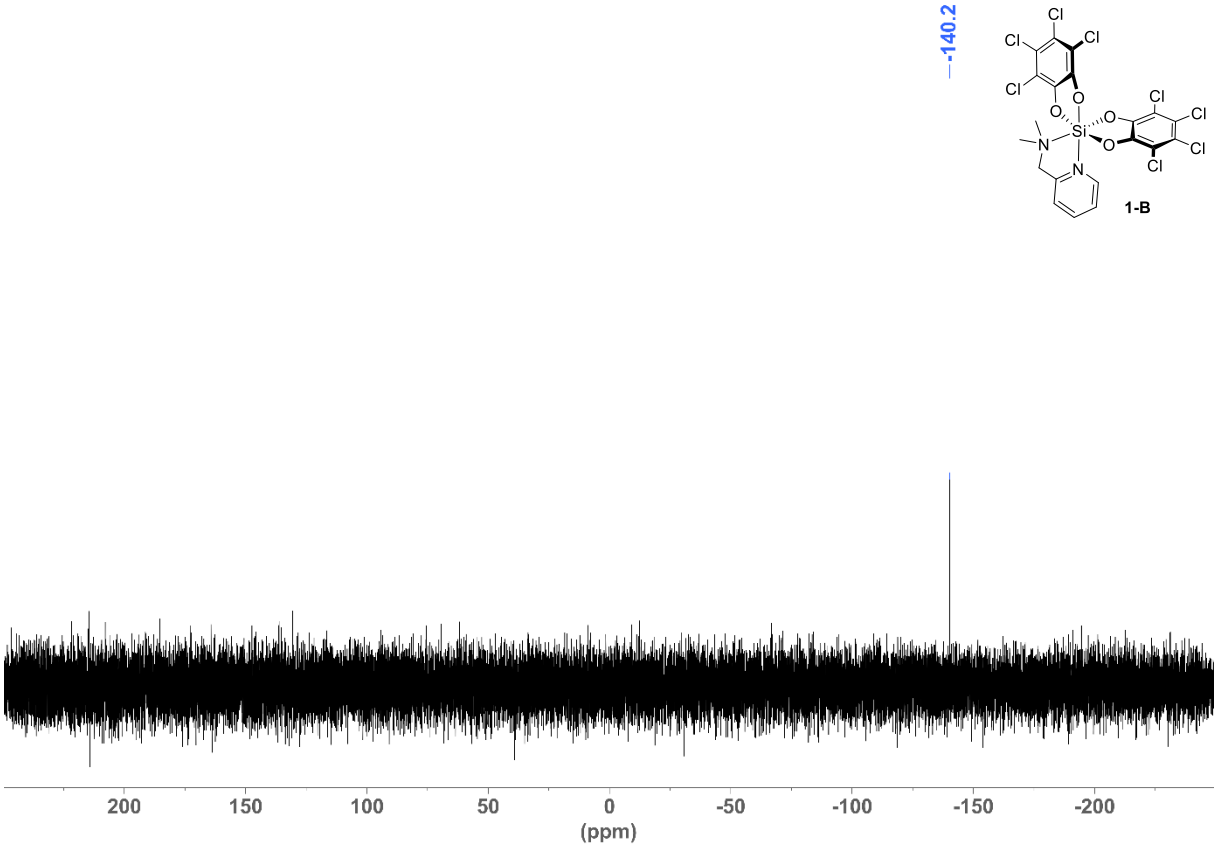

Figure S5.6: ^{29}Si NMR (119 MHz, CD_2Cl_2, RT) of **1-B**.

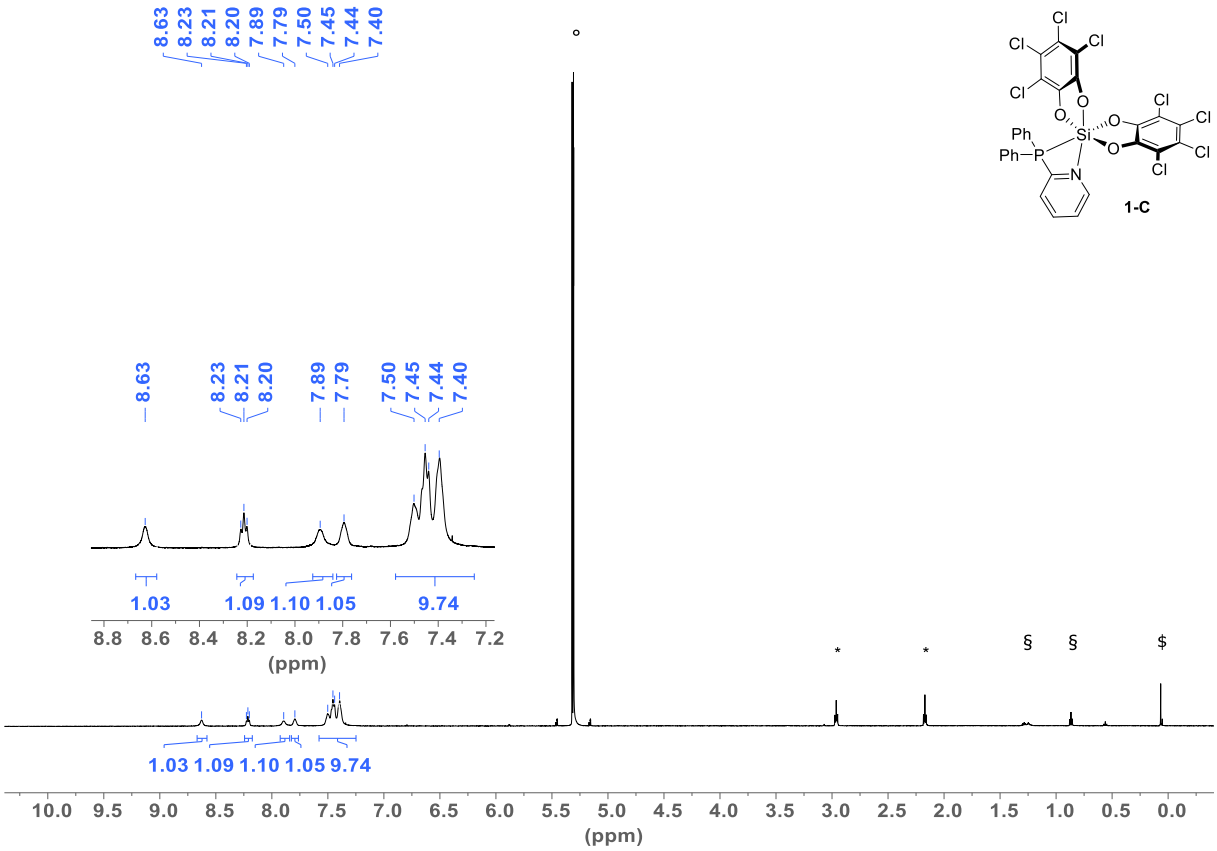

Figure S5.7: ^{1}H NMR (600 MHz, CD_2Cl_2, RT) of **1-C**. Residual proton signals marked with ° (solvent), * (sulfolane), § (pentane) and $ (grease).

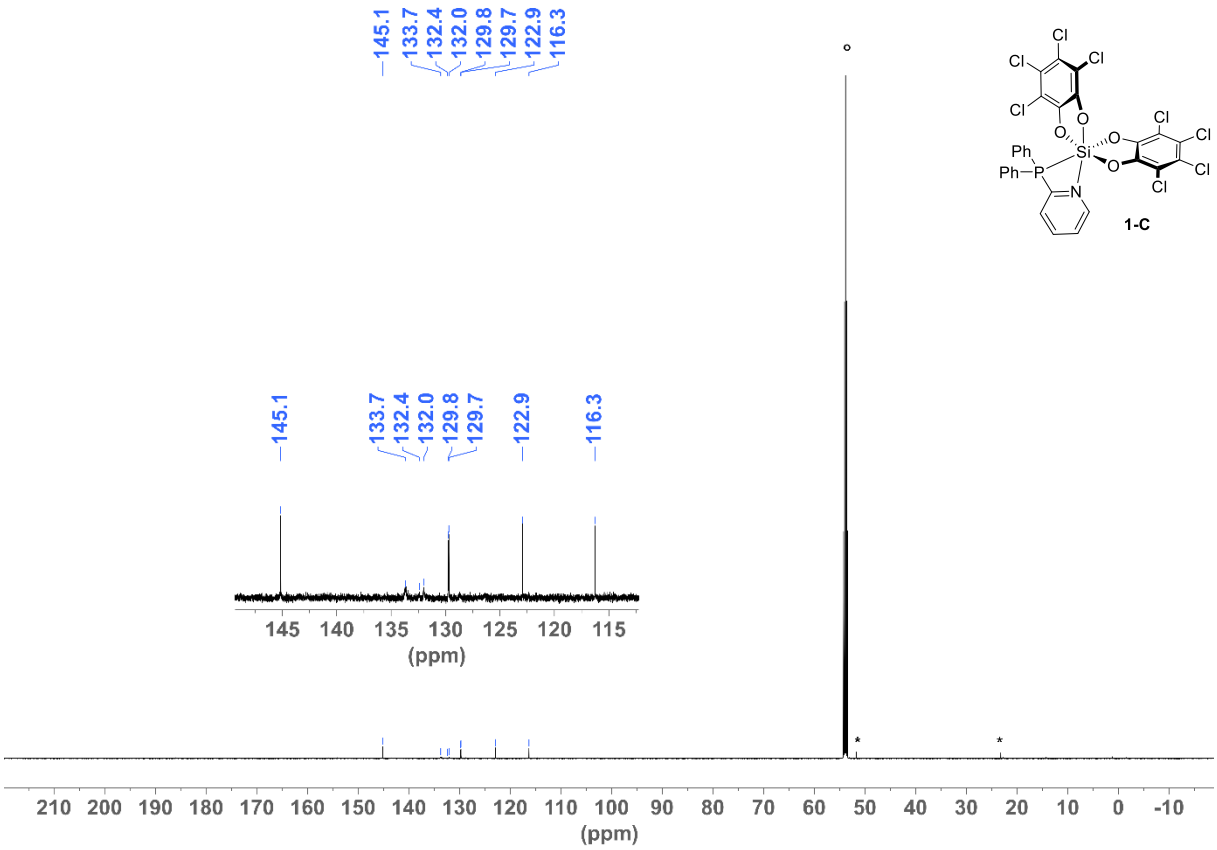

Figure S5.8: ^{13}C NMR (151 MHz, CD_2Cl_2, RT) of **1-C**. Residual carbon signals marked with ° (solvent) and * (sulfolane).

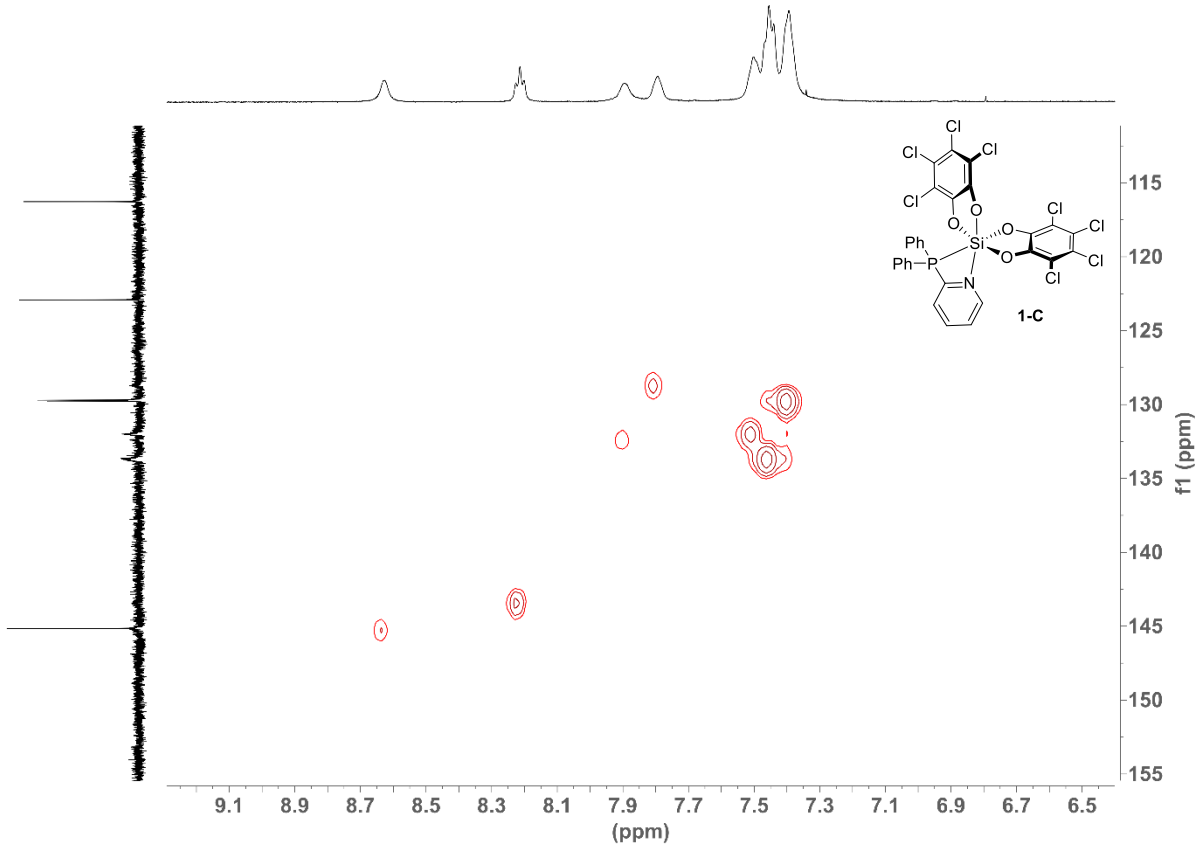

Figure S5.9: Aromatic region of ^{1}H-^{13}C-HSQC NMR (600 MHz, 151 MHz, CD_2Cl_2, RT) of **1-C**.

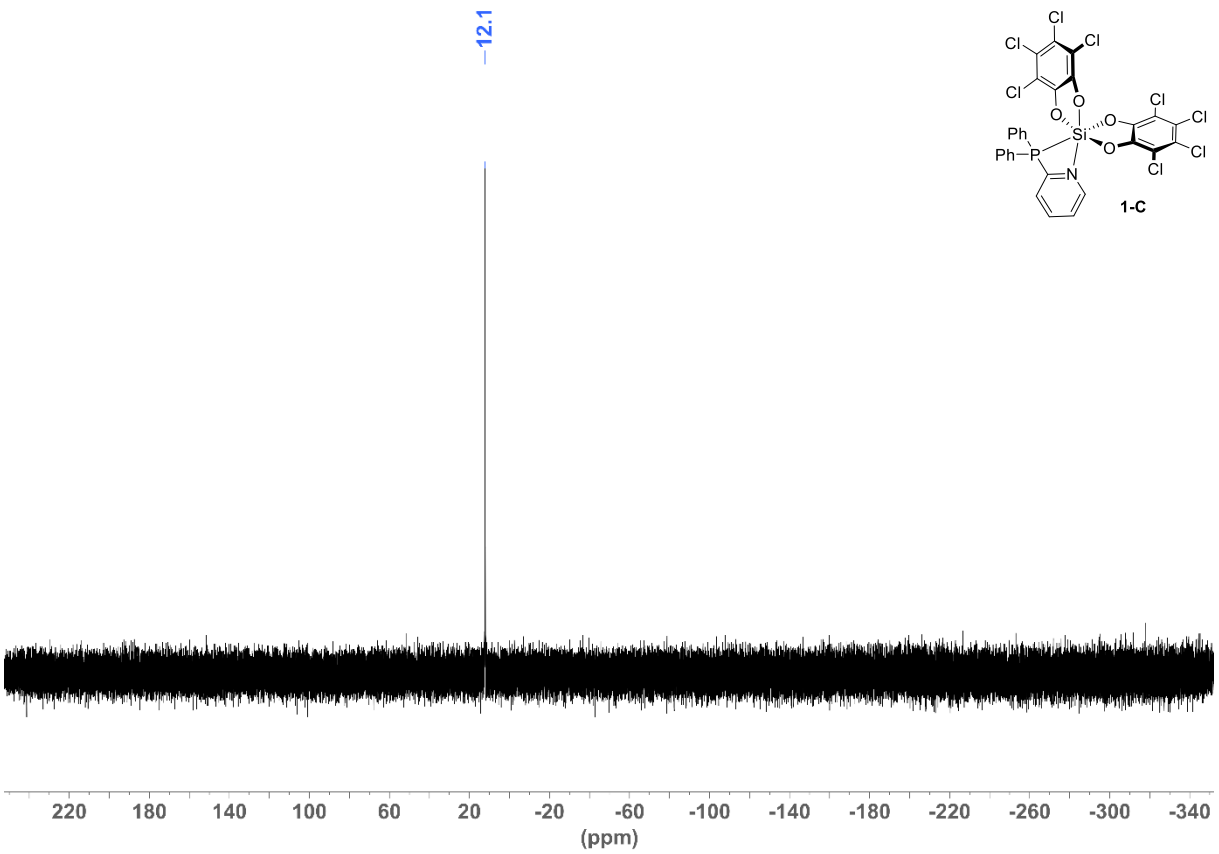

Figure S5.10: ^{31}P NMR (243 MHz, CD_2Cl_2, RT) of **1-C**.

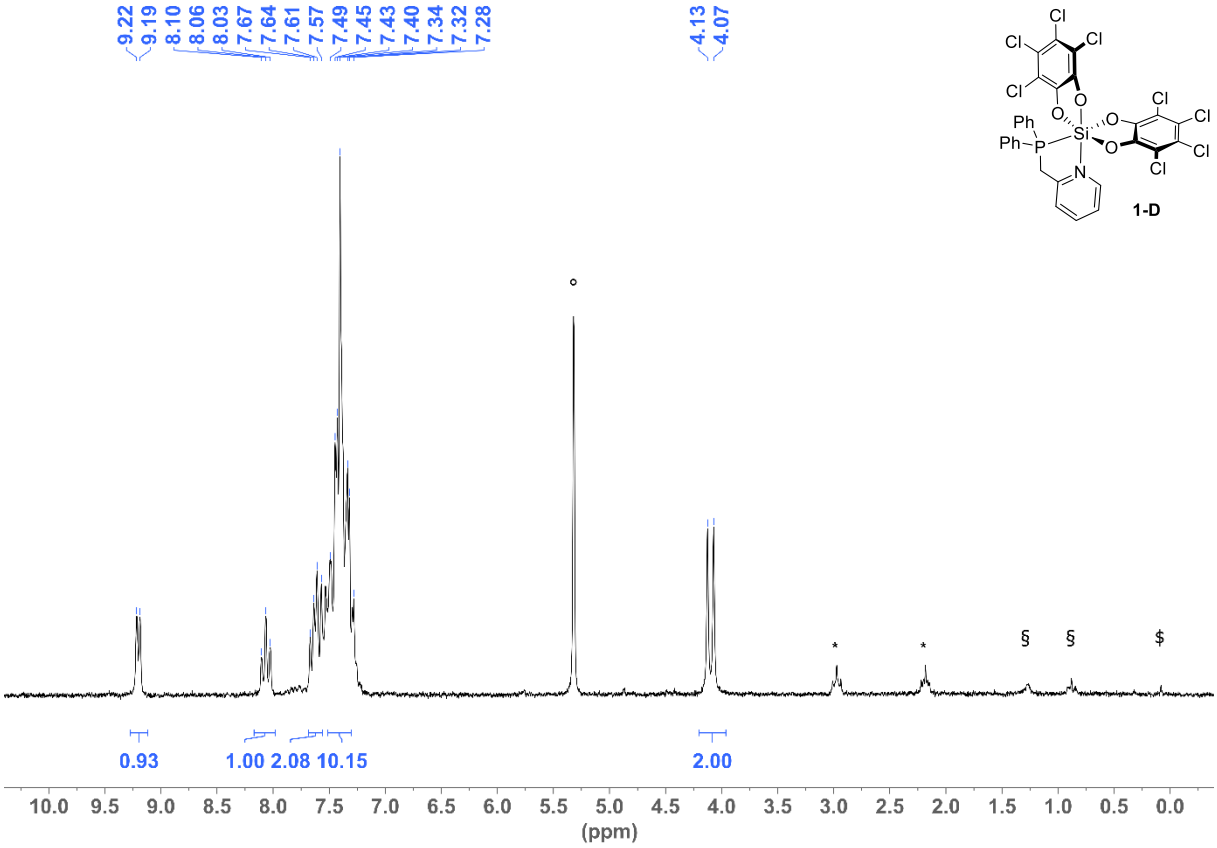

Figure S5.11: ^{1}H NMR (200 MHz, CD_2Cl_2, RT) of **1-D**. Residual proton signals marked with ° (solvent), * (sulfolane), § (pentane) and $ (grease).

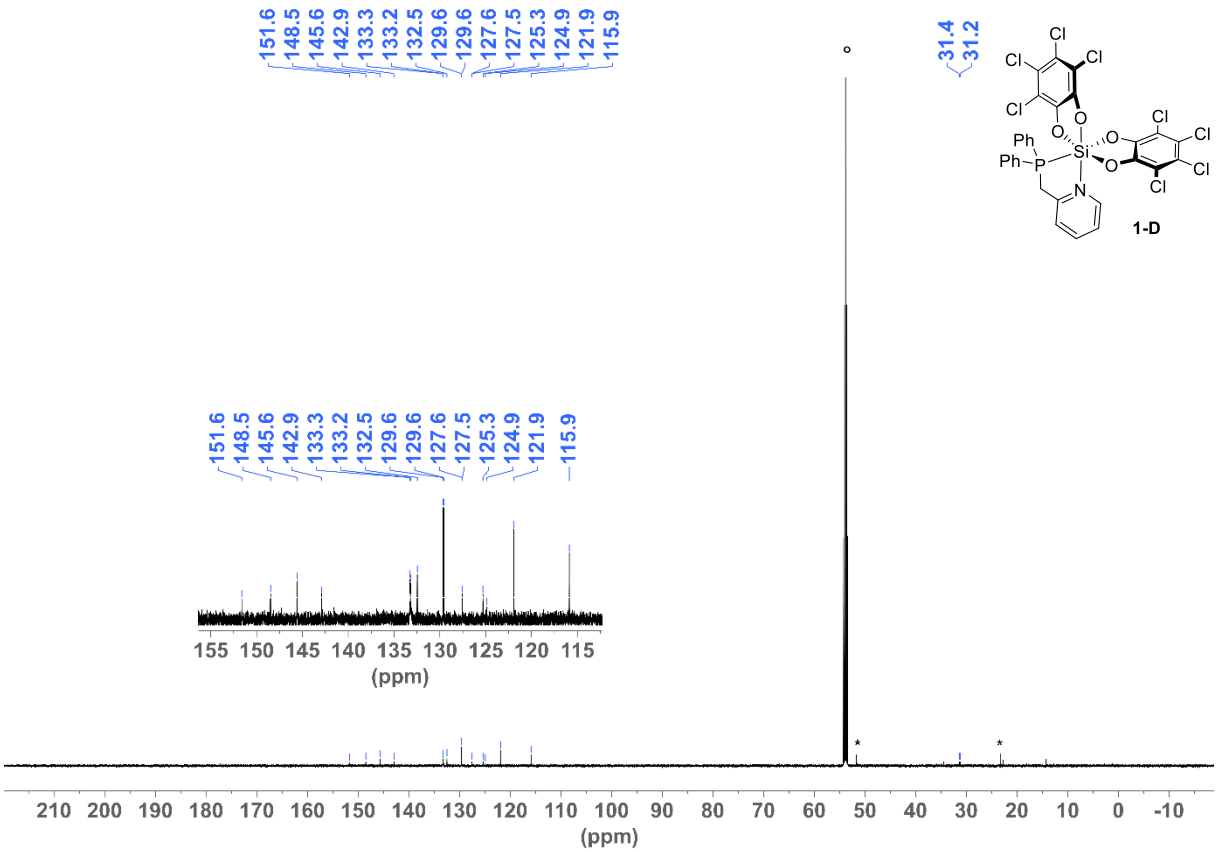

Figure S5.12: ^{13}C NMR (151 MHz, CD_2Cl_2, RT) of **1-D**. Residual carbon signals marked with ° (solvent) and * (sulfolane).

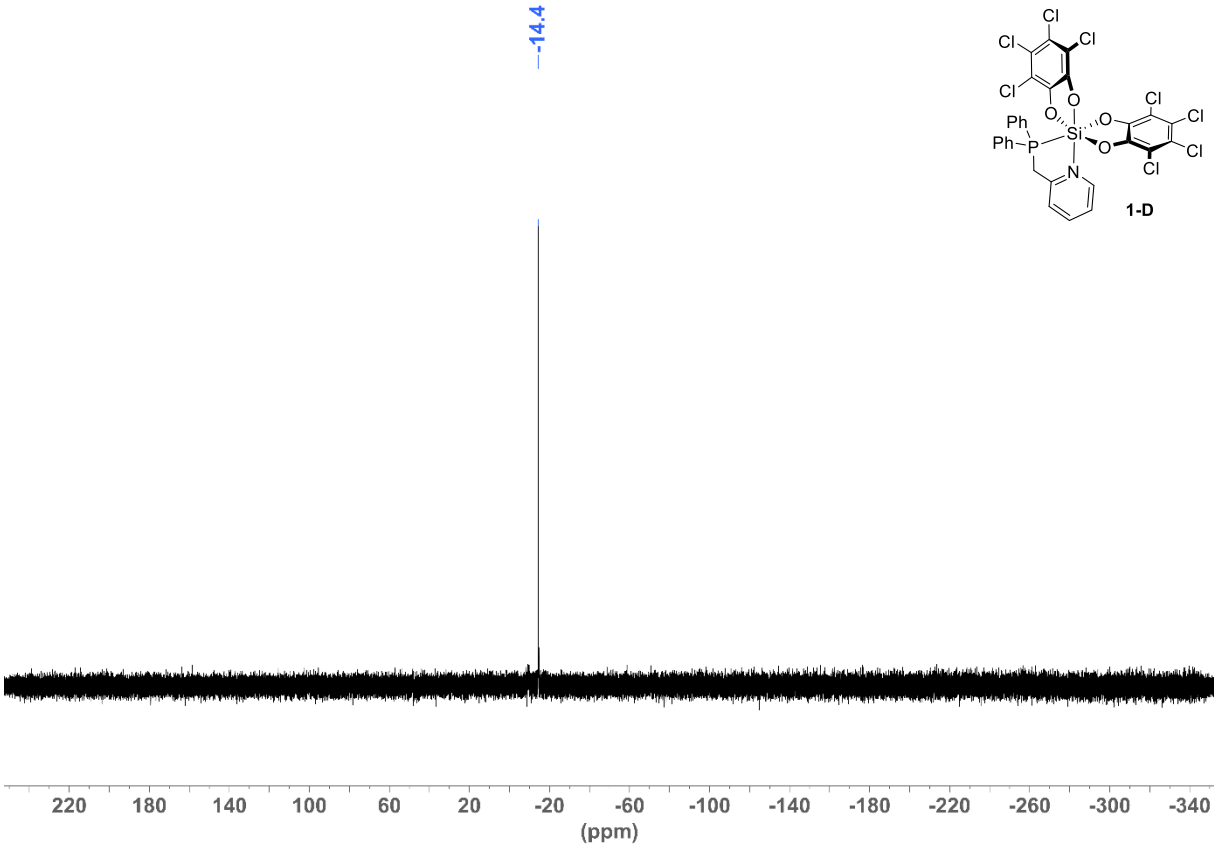

Figure S5.13: ^{31}P NMR (243 MHz, CD_2Cl_2, RT) of **1-D**.

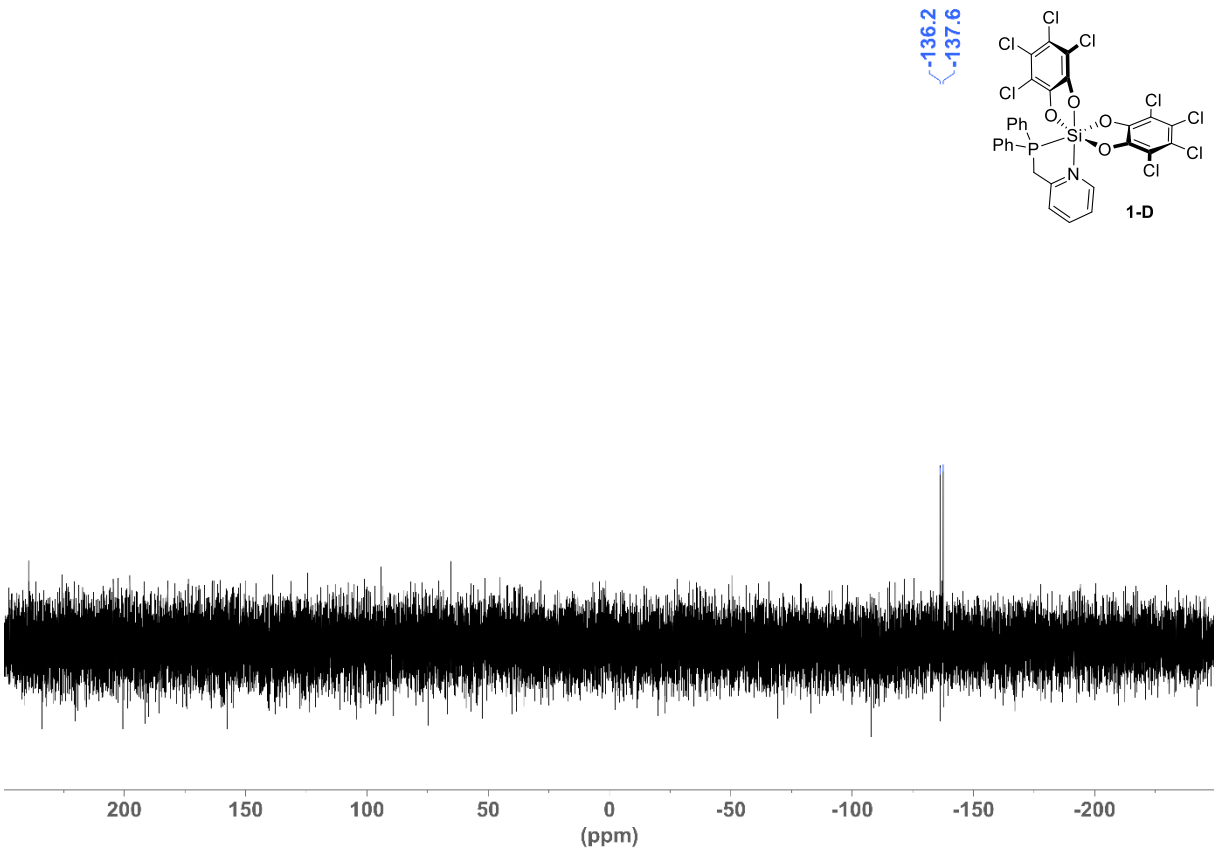

Figure S5.14: ^{29}Si NMR (119 MHz, CD_2Cl_2, RT) of **1-D**.

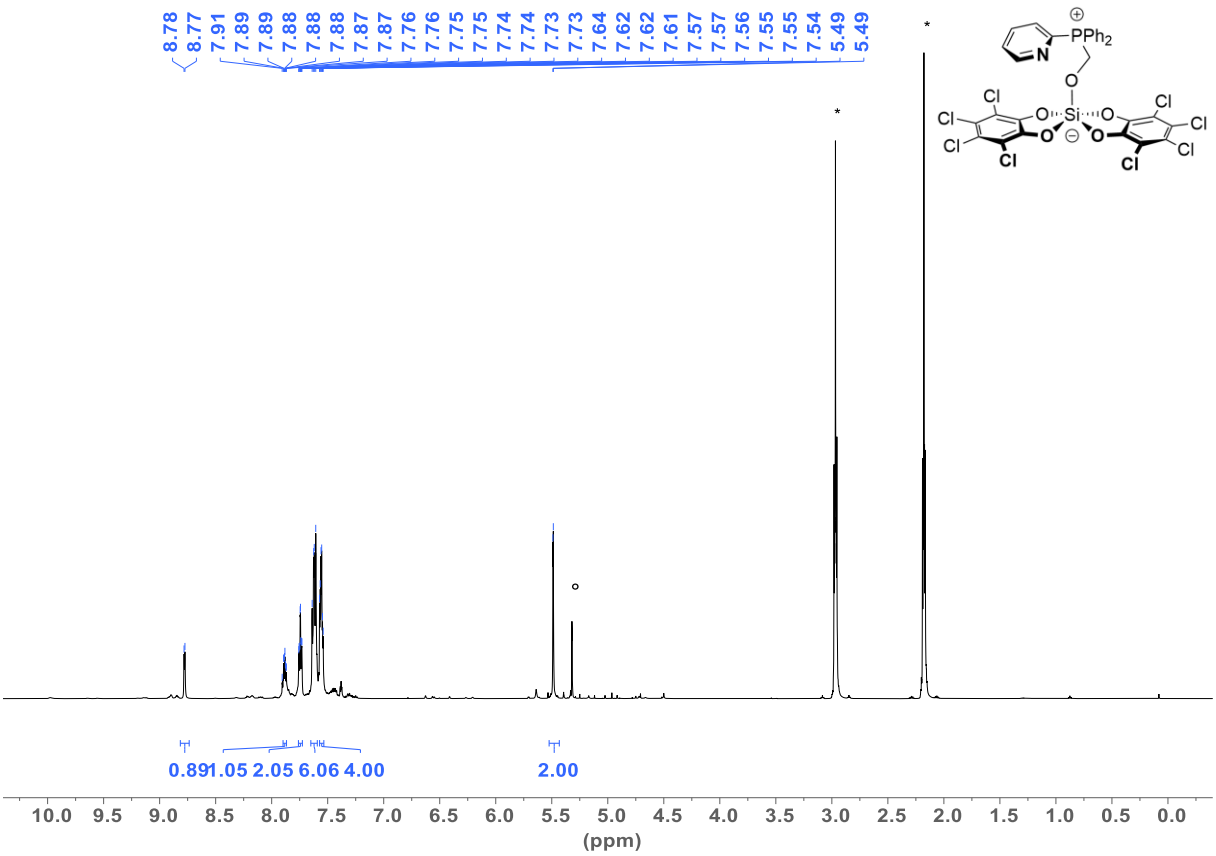

Figure S5.15: ^{1}H NMR (600 MHz, CD_2Cl_2, RT) of **1-(OCH$_2$)-C**. Residual proton signals marked with ° (solvent), * (sulfolane).

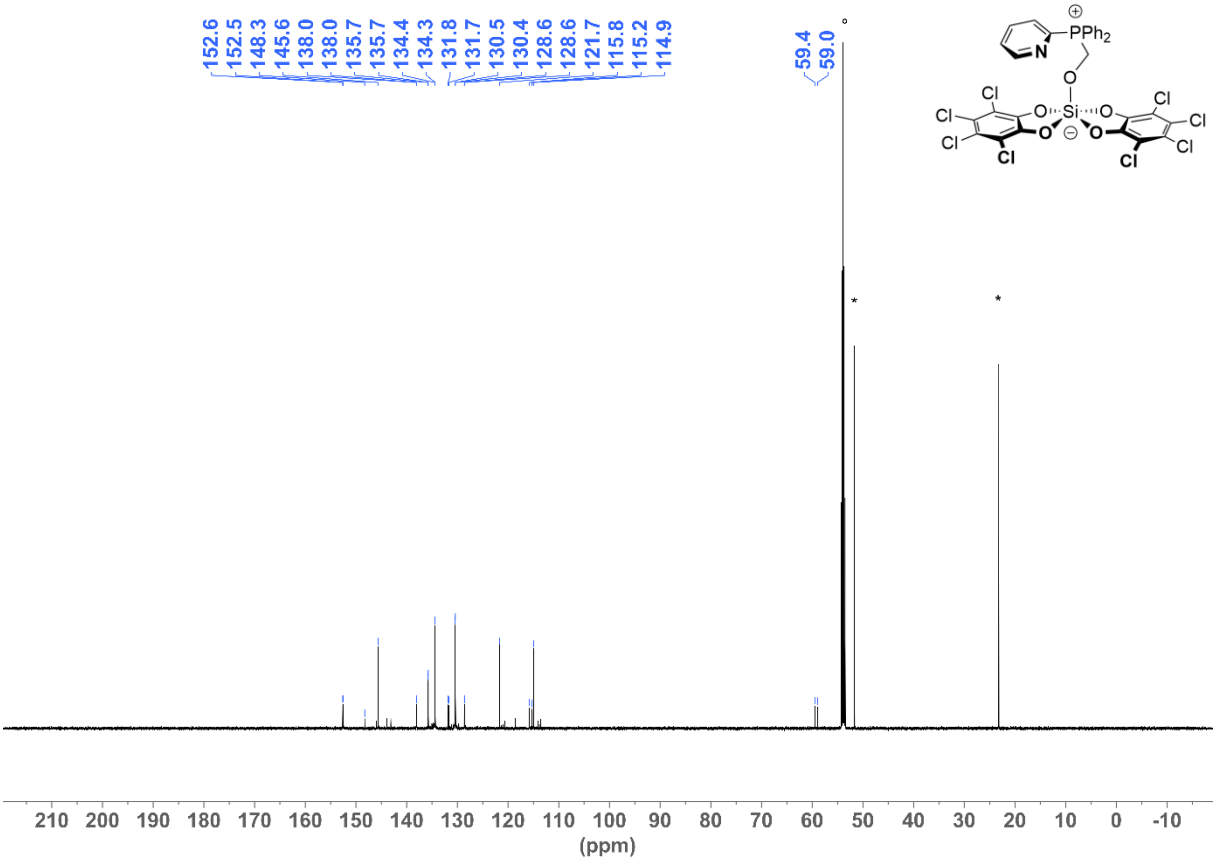

Figure S5.16: ^{13}C NMR (151 MHz, CD_2Cl_2, RT) of **1-(OCH$_2$)-C**. Residual carbon signals marked with ° (solvent) and * (sulfolane).

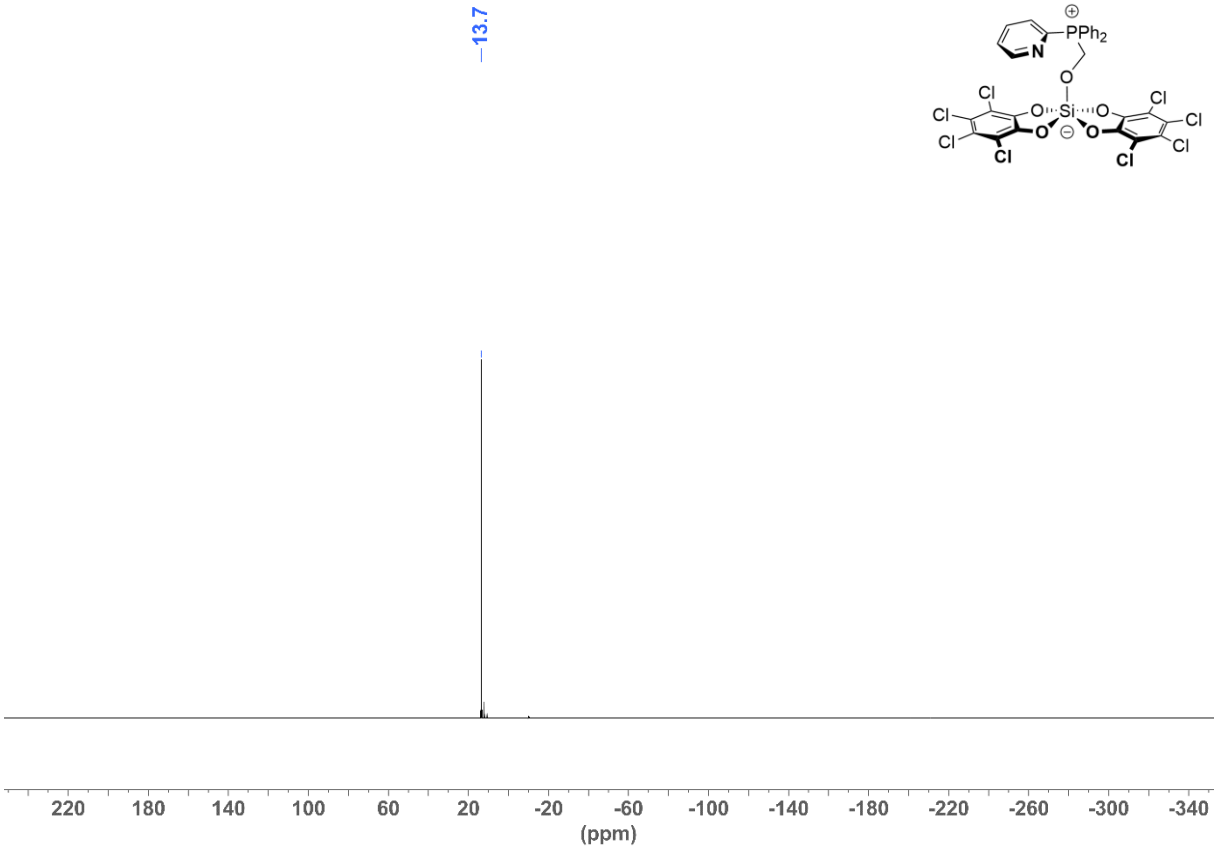

Figure S5.17: ^{31}P NMR (243 MHz, CD_2Cl_2, RT) of **1-(OCH$_2$)-C**.

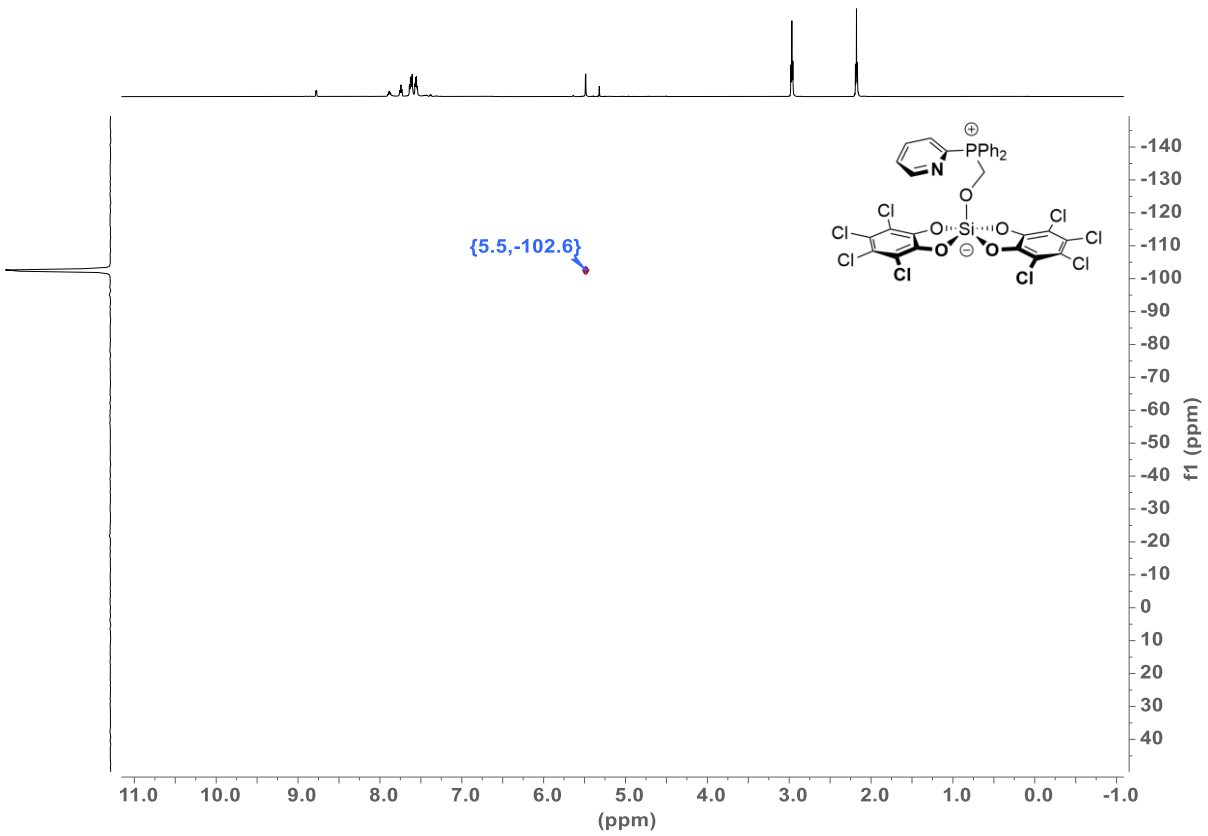

Figure S5.18: ^{1}H-^{29}Si-HMBC NMR (600 MHz, CD_2Cl_2, RT) of **1-(OCH$_2$)-C**.

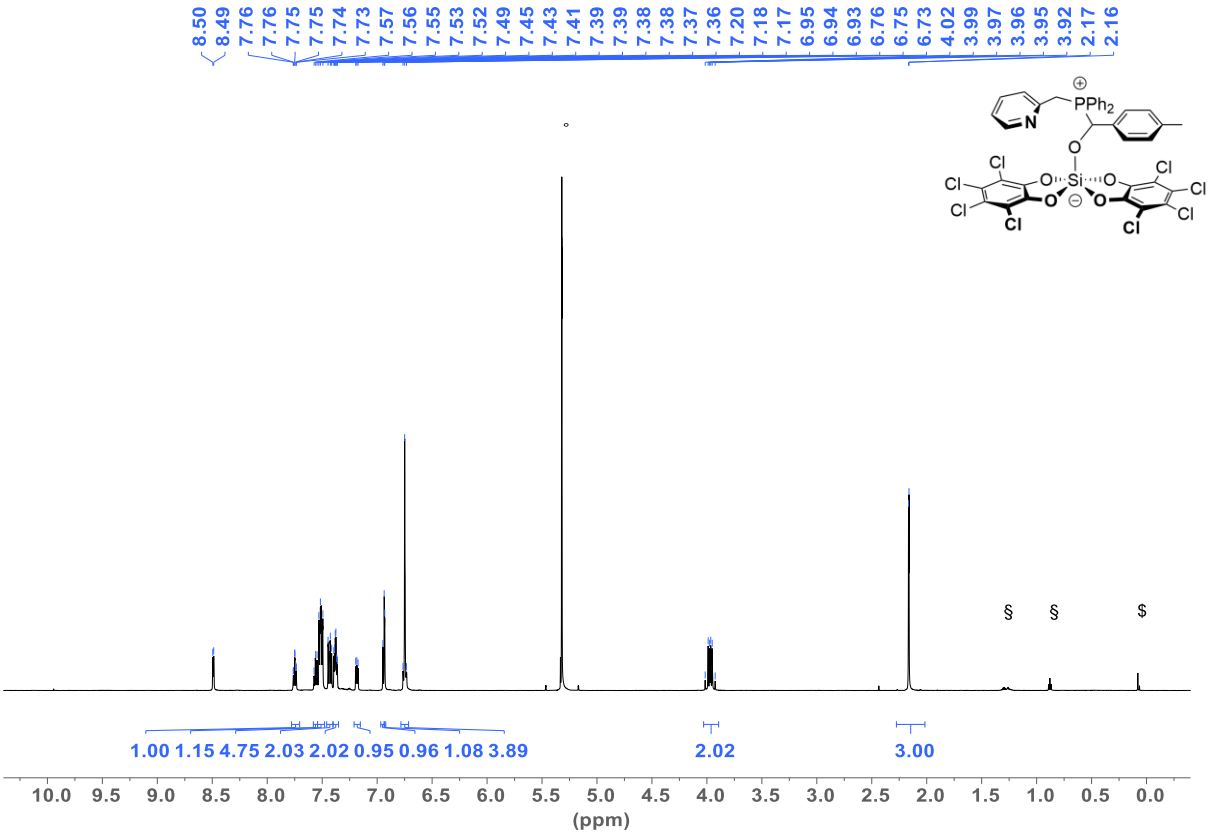

Figure S5.19: ^{1}H NMR (600 MHz, CD_2Cl_2, RT) of **1-(*p*-Me-BA)-D**. Residual proton signals marked with ° (solvent), § (pentane) and $ (grease).

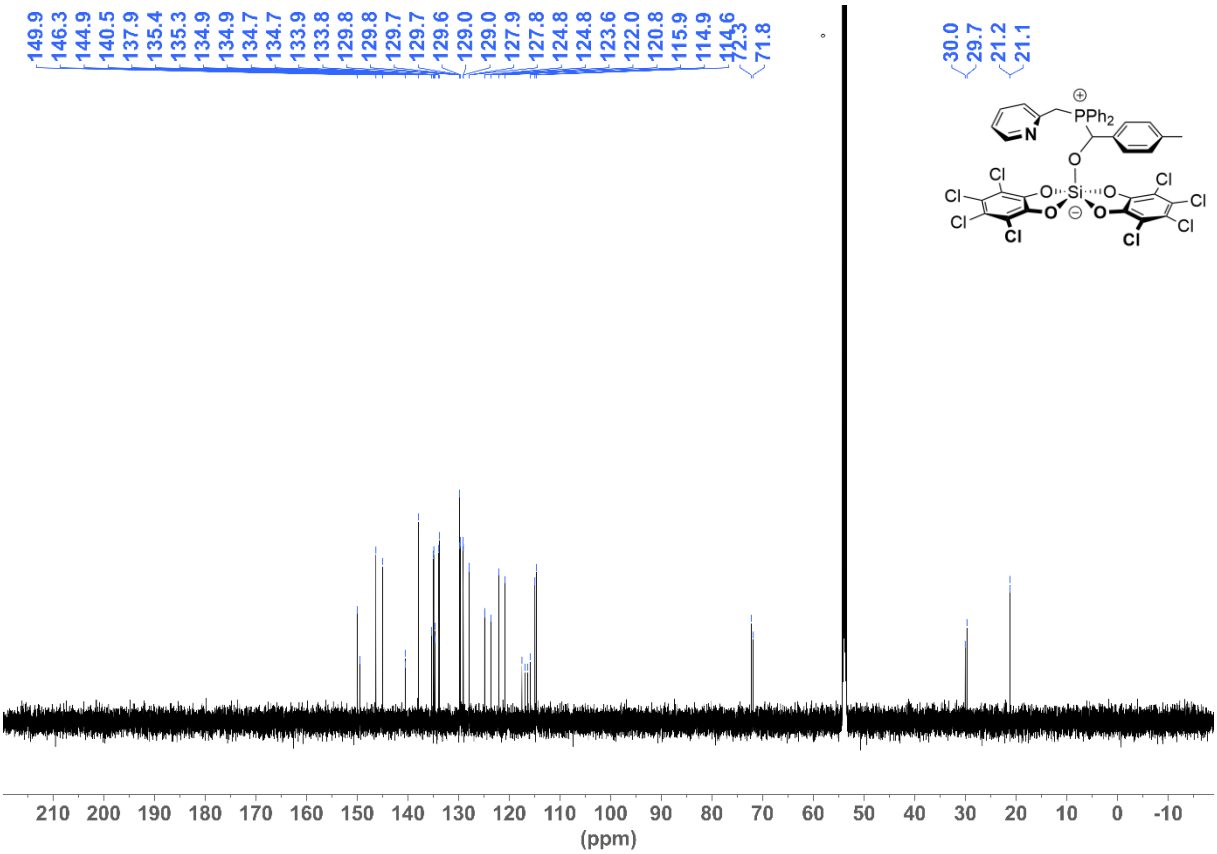

Figure S5.20: ^{13}C NMR (151 MHz, CD_2Cl_2, RT) of **1-(*p*-Me-BA)-D**. Residual carbon signals marked with ° (solvent).

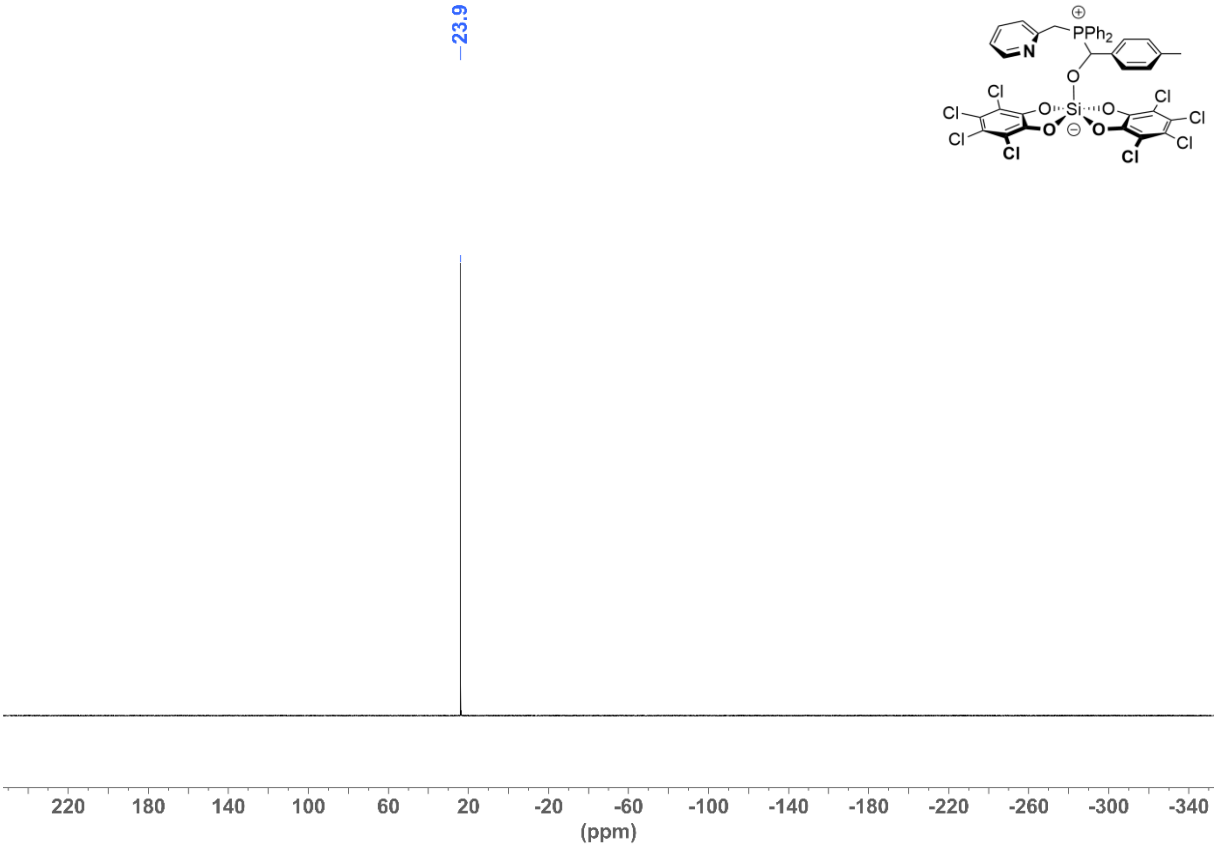

Figure S5.21: ^{31}P NMR (243 MHz, CD_2Cl_2, RT) of **1-(*p*-Me-BA)-D**.

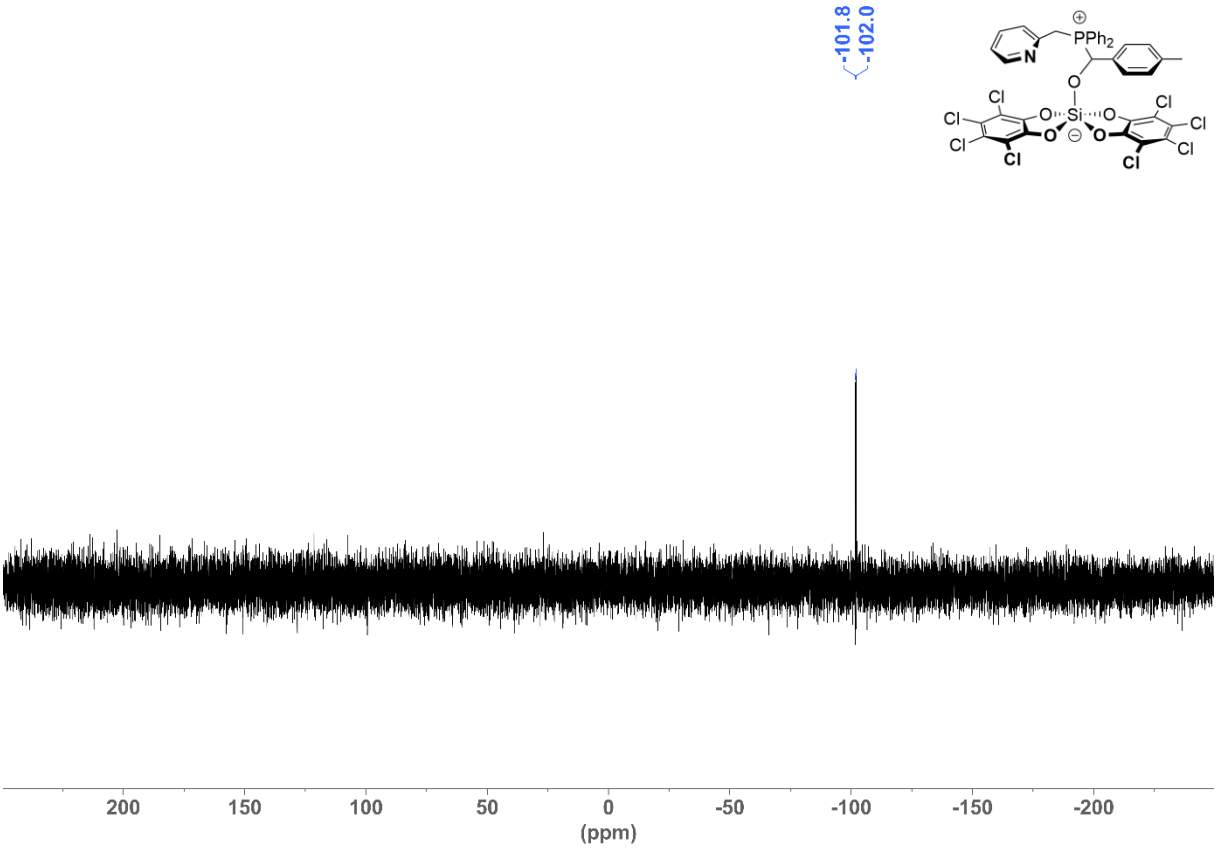

Figure S5.22: ^{29}Si NMR (119 MHz, CD_2Cl_2, RT) of **1-(*p*-Me-BA)-D**.

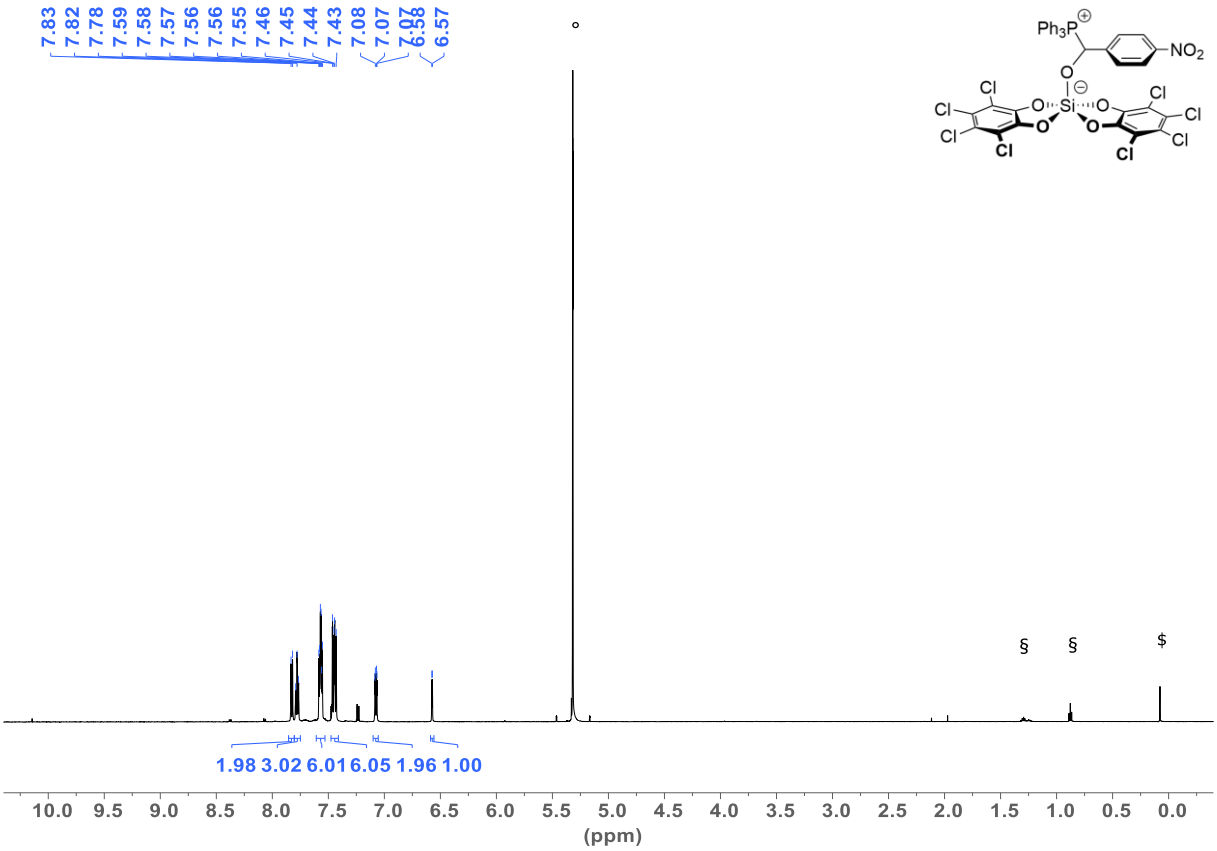

Figure S5.23: ^{1}H NMR (600 MHz, CD_2Cl_2, RT) of **1-(*p*-NO_2-BA)-PPh_3**. Residual proton signals marked with ° (solvent), § (pentane) and $ (grease).

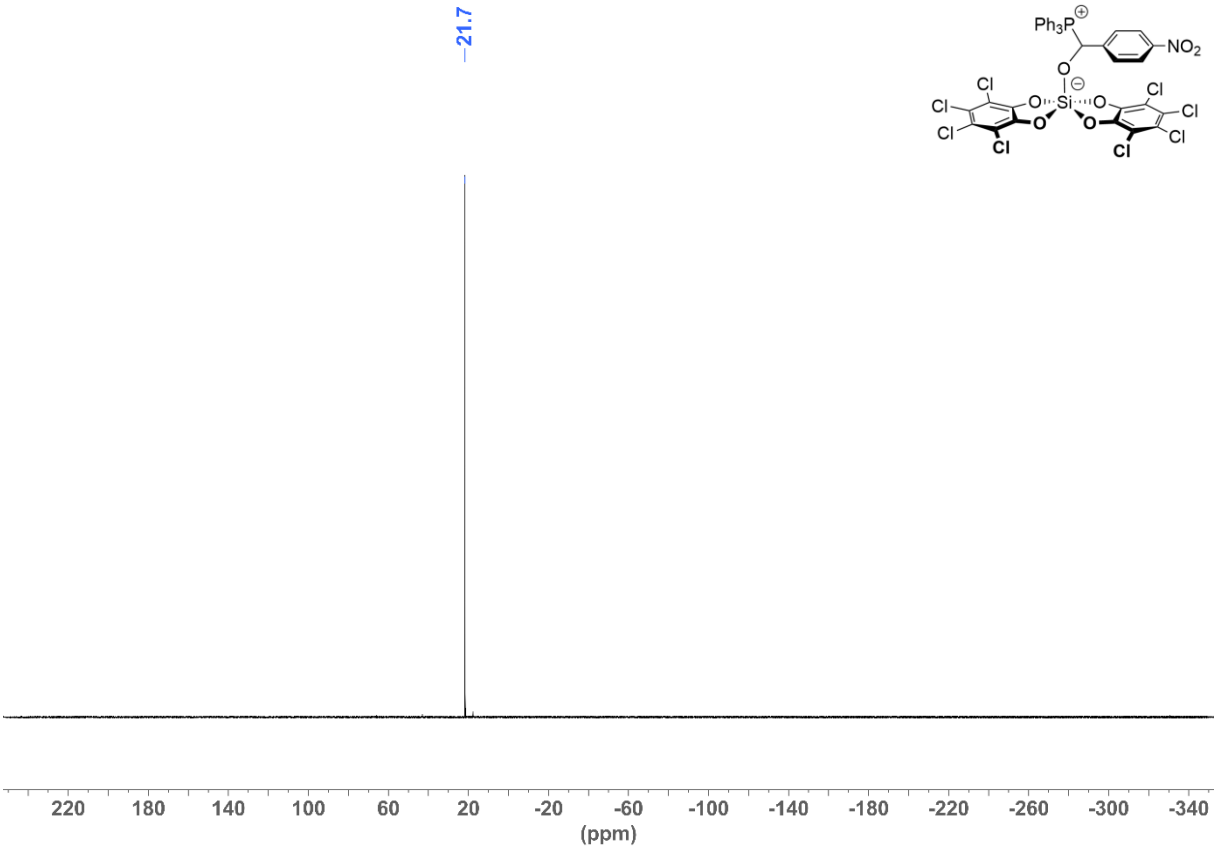

Figure S5.24: ^{31}P NMR (243 MHz, CD_2Cl_2, RT) of **1-(*p*-NO_2-BA)-PPh_3**.

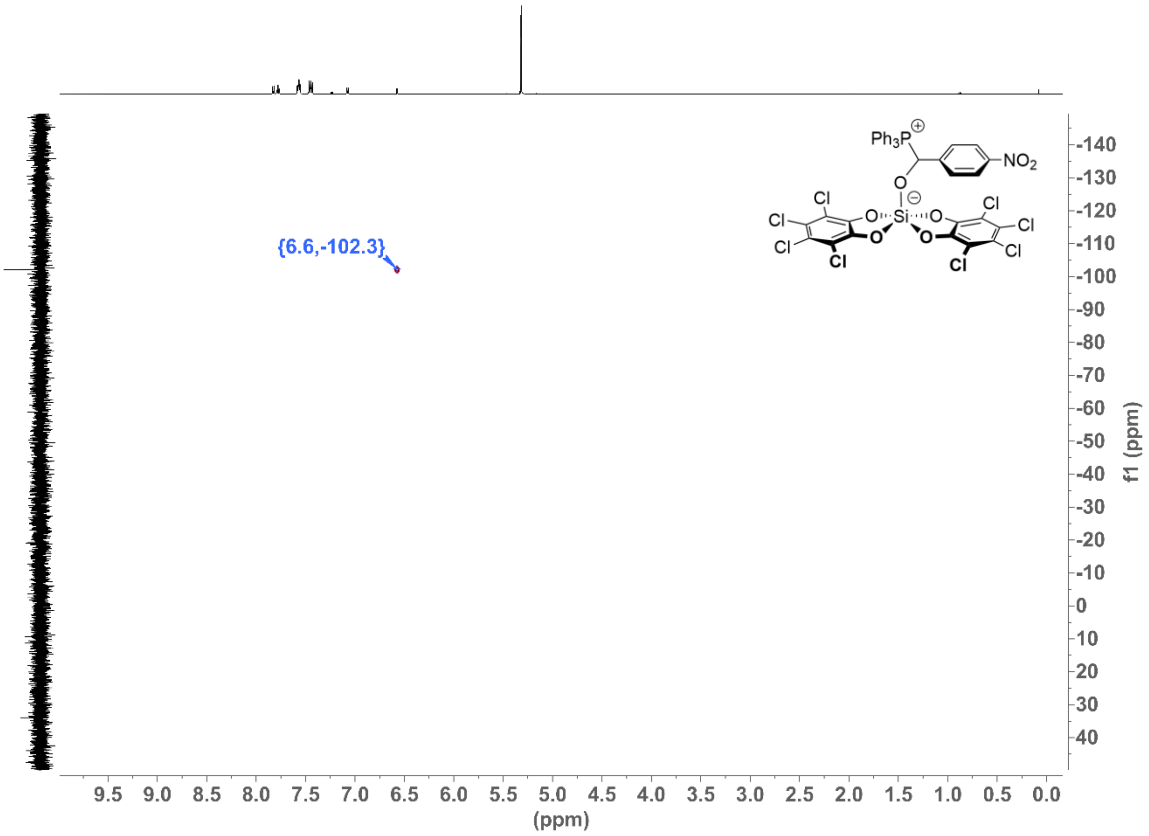

Figure S5.25: ^{1}H-^{29}Si-HMBC NMR (400 MHz, CD_2Cl_2, RT) of **1-(*p*-NO_2-BA)-PPh_3**.

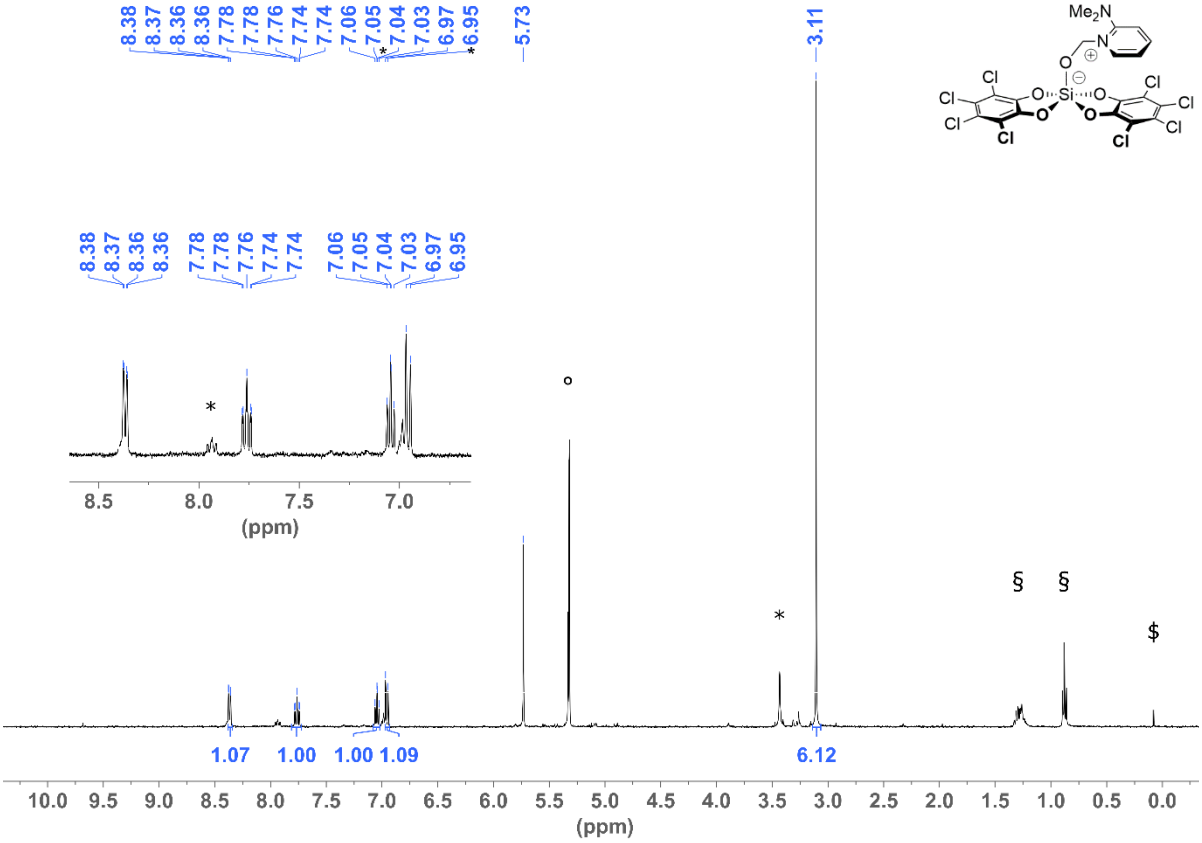

Figure S5.26: ^{1}H NMR (400 MHz, CD_2Cl_2, RT) of **1-(OCH_2)-A**. Residual proton signals marked with ° (solvent), * (impurity in **A**), § (pentane) and $ (grease).

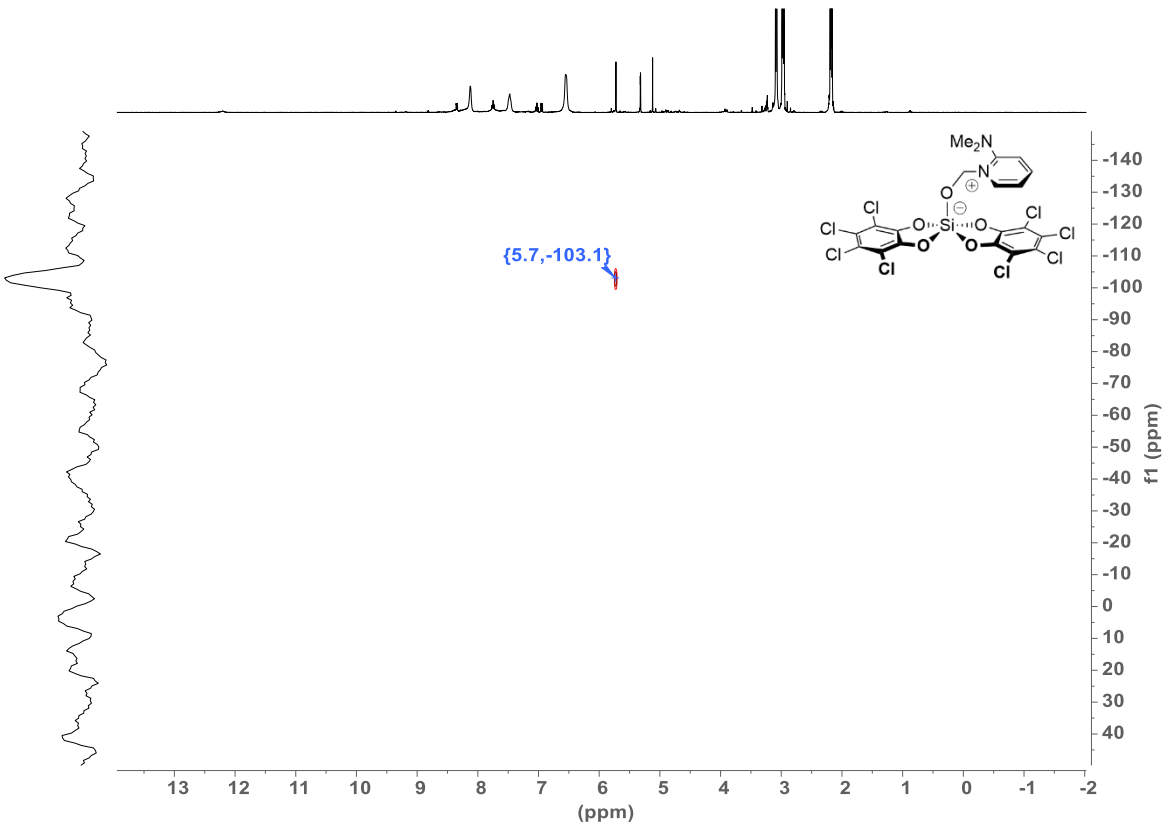

Figure S5.27: ^{1}H-^{29}Si-HMBC NMR (400 MHz, CD_2Cl_2, RT) of **1-(OCH_2)-A**.

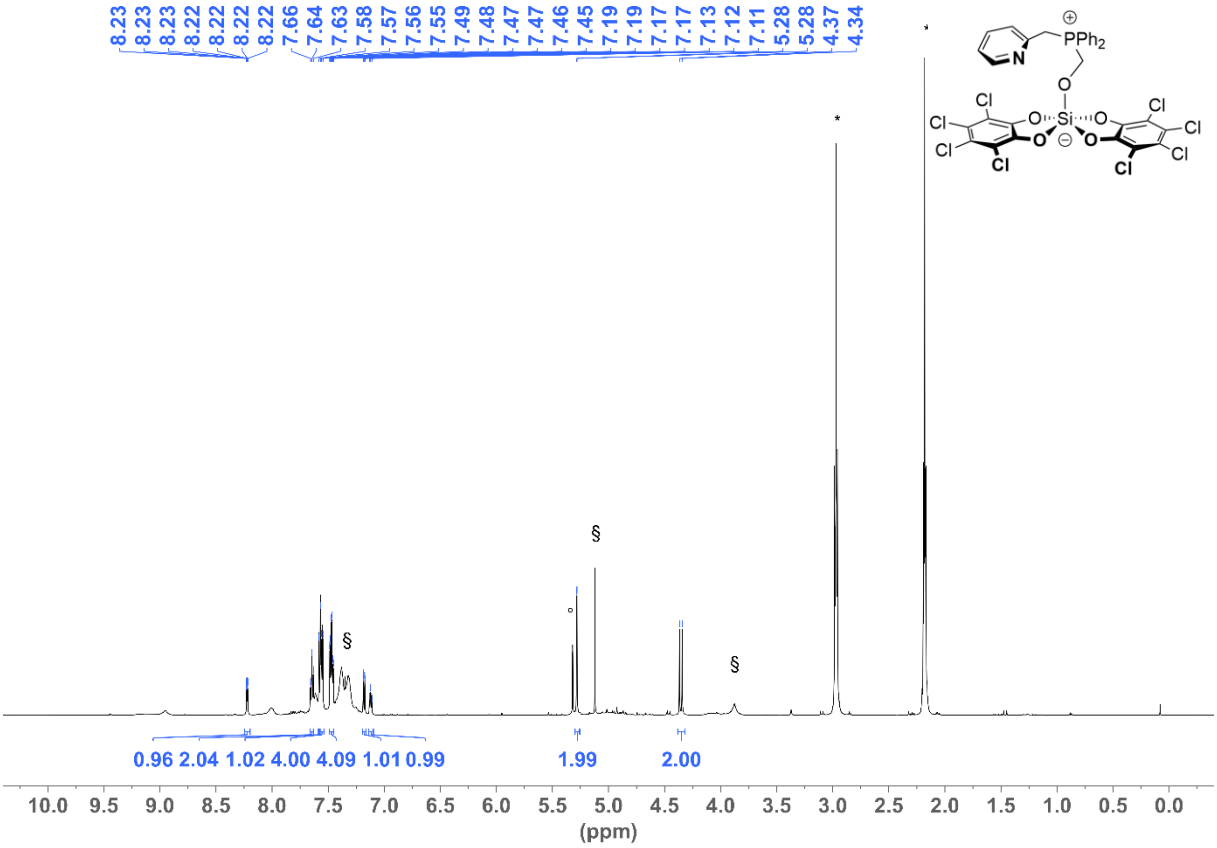

Figure S5.28: ^{1}H NMR (600 MHz, CD_2Cl_2, RT) of **1-(OCH$_2$)-D**. Residual proton signals marked with ° (solvent), § (unidentified byproduct) and * (sulfolane).

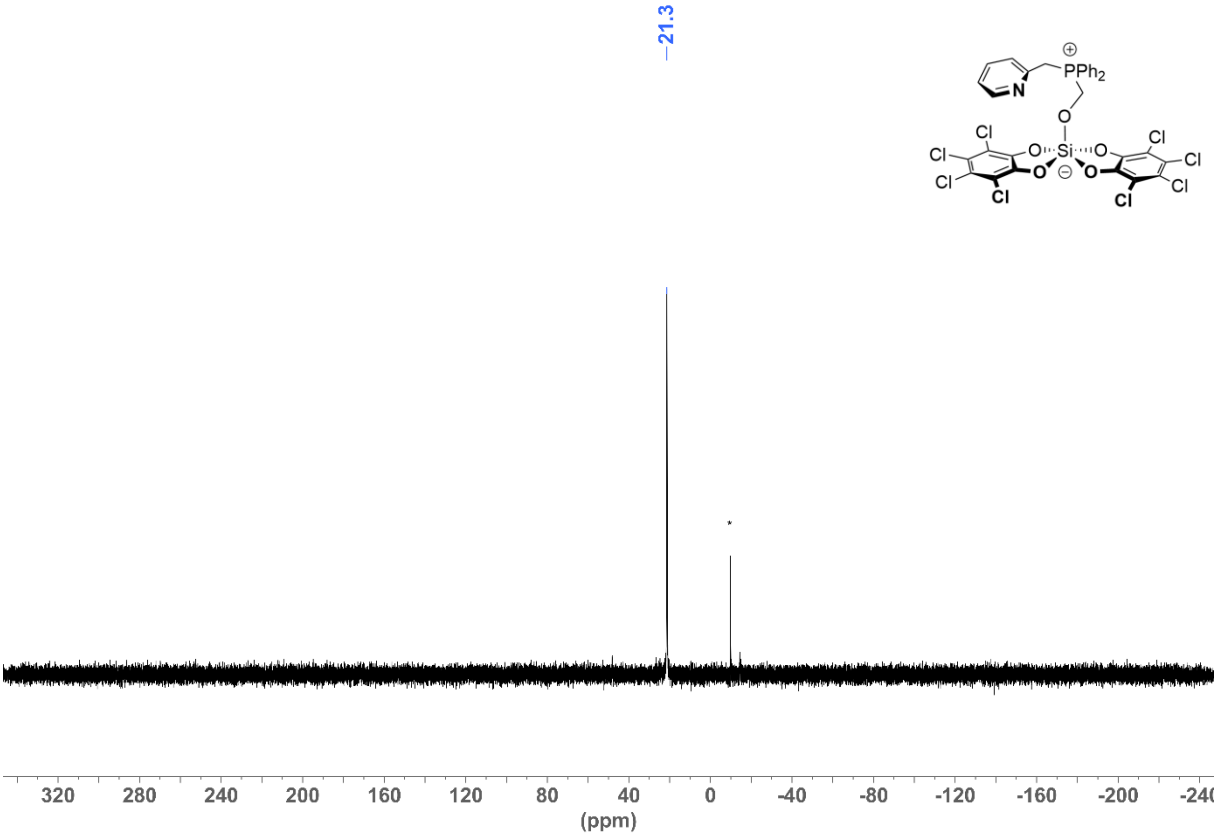

Figure S5.29: ^{31}P NMR (243 MHz, CD_2Cl_2, RT) of **1-(OCH$_2$)-D**. Phosphorus signal from excess **D** marked with *.

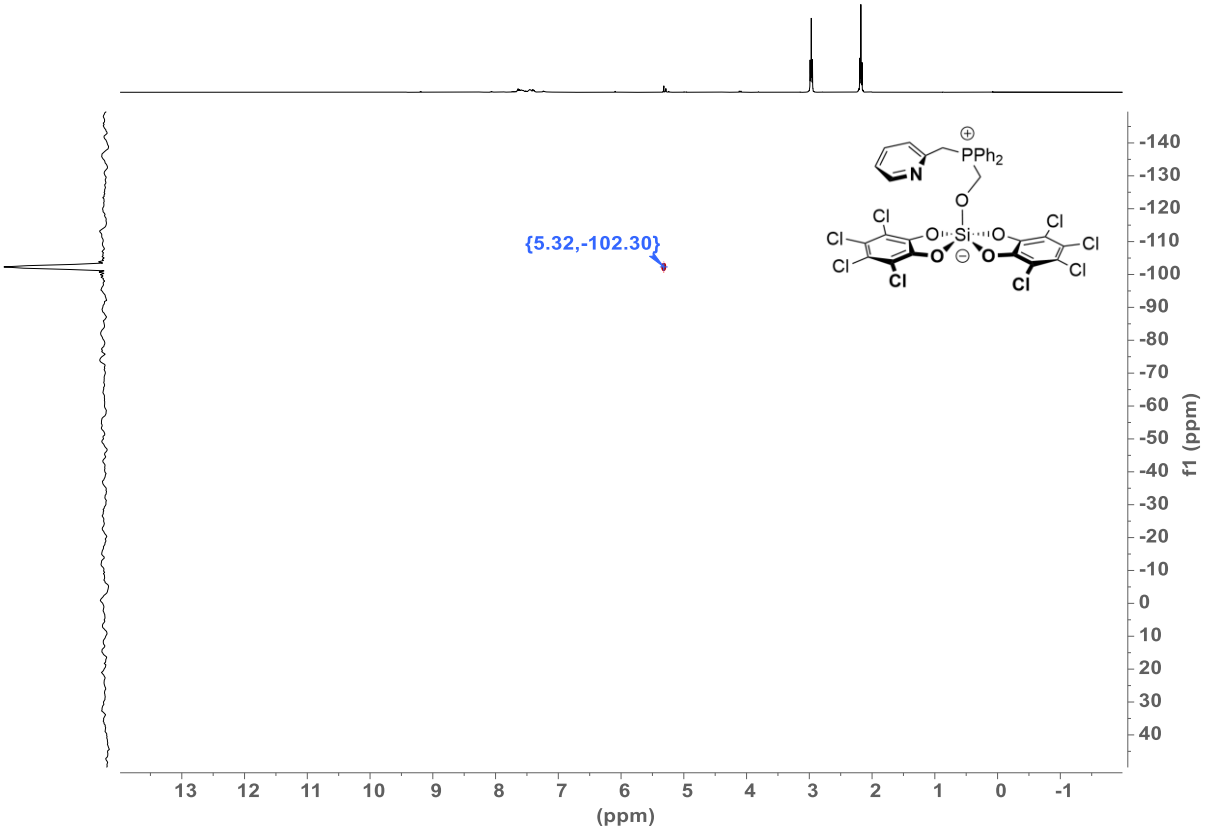

Figure S5.30: : ^{1}H-^{29}Si-HMBC NMR (600 MHz, CD_2Cl_2, RT) of **1-(OCH_2)-D**.

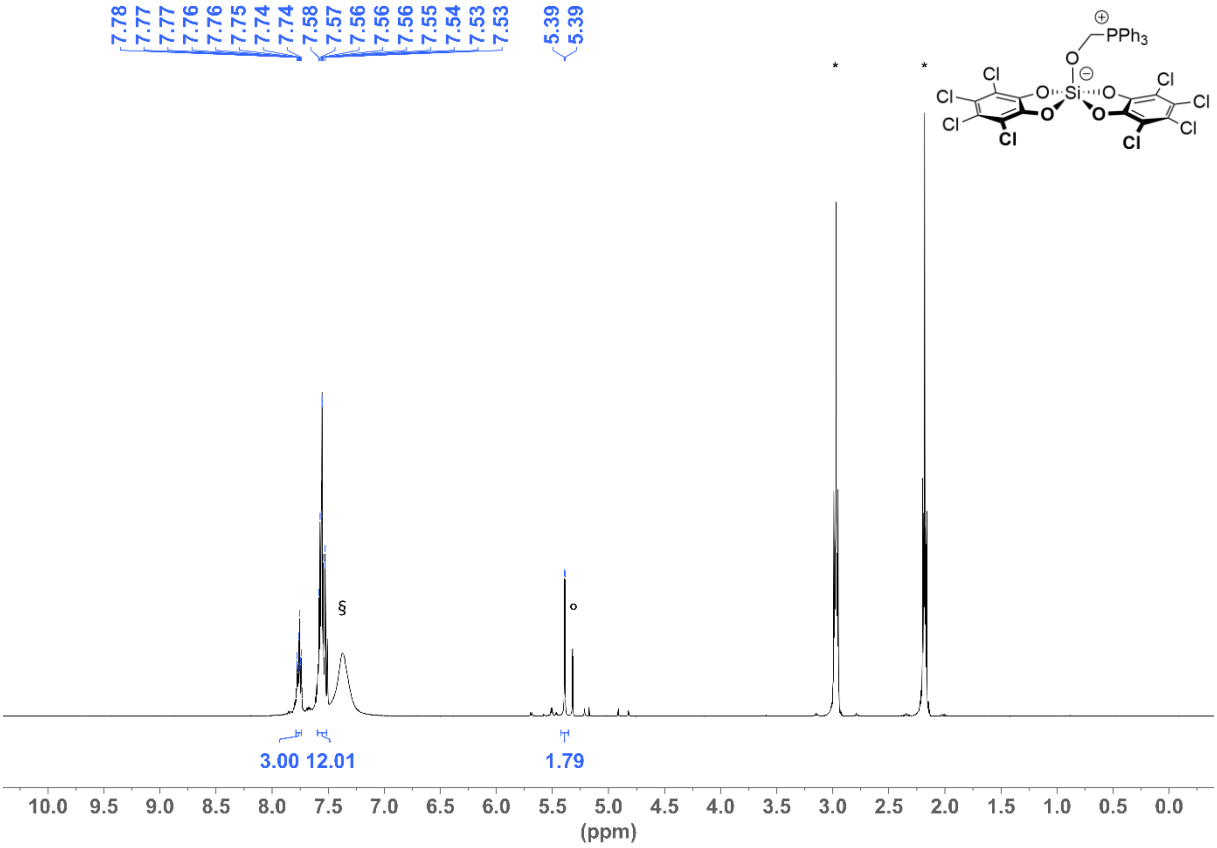

Figure S5.31: ^{1}H NMR (600 MHz, CD_2Cl_2, RT) of **1-(OCH$_2$)-PPh$_3$**. Residual proton signals marked with ° (solvent), * (sulfolane) and § (PPh_3).

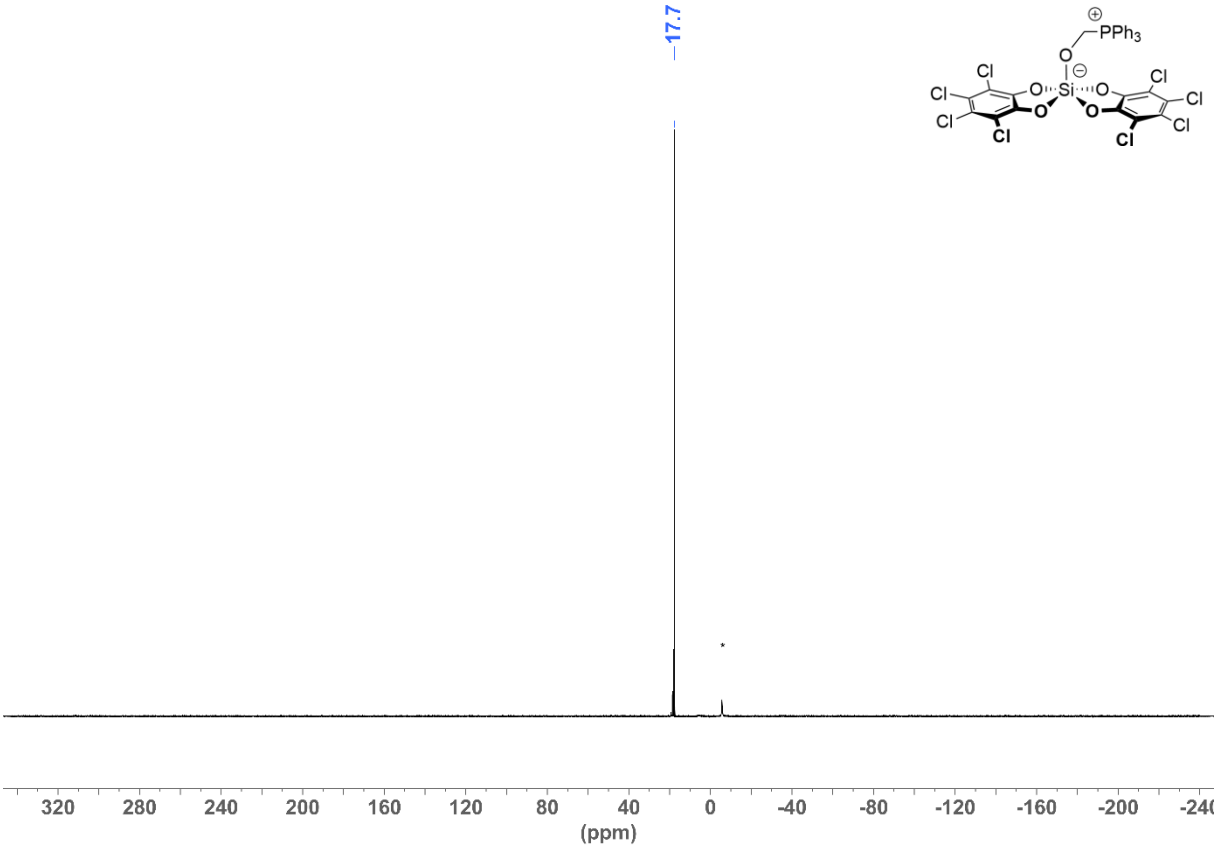

Figure S5.32: ^{31}P NMR (243 MHz, CD_2Cl_2, RT) of **1-(OCH$_2$)-PPh$_3$**. Phosphorus signal from excess PPh_3 marked with *.

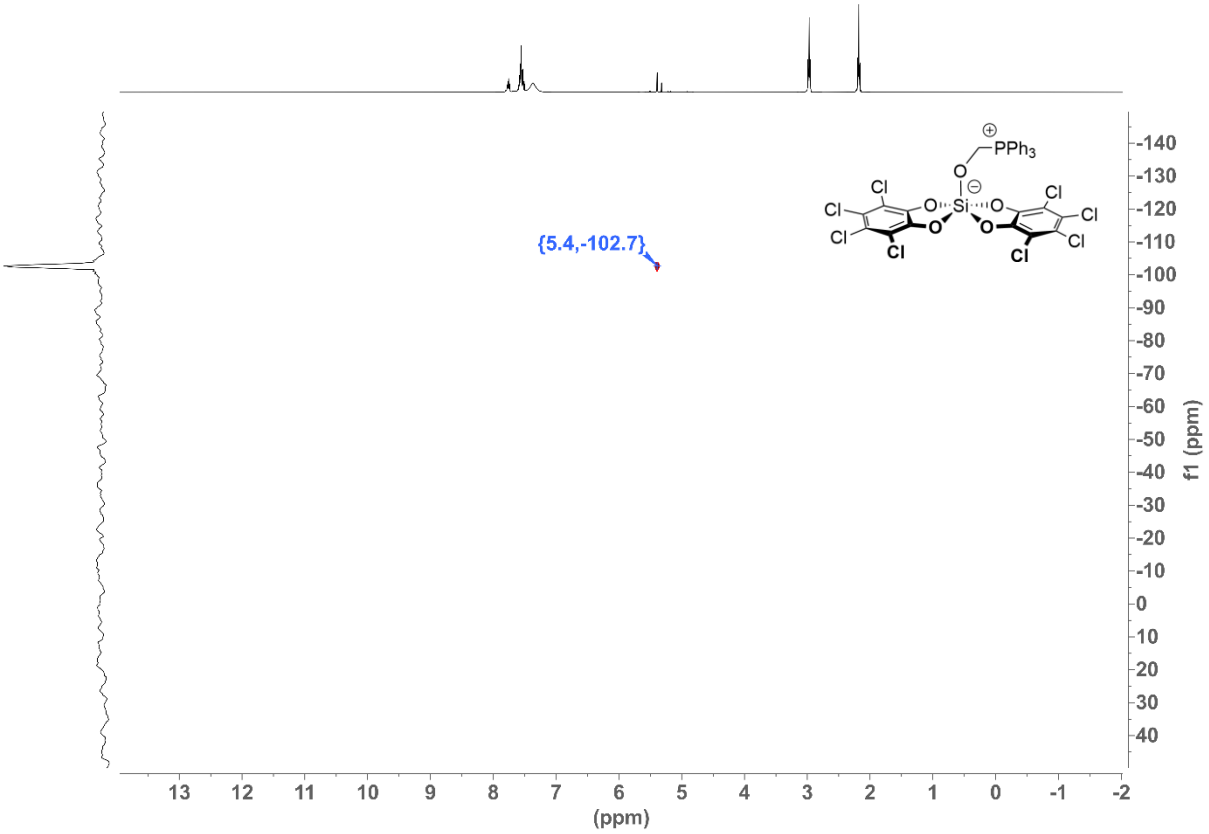

Figure S5.33: ^{1}H-^{29}Si-HMBC NMR (400 MHz, CD_2Cl_2, RT) of **1-(OCH_2)-PPh_3**.

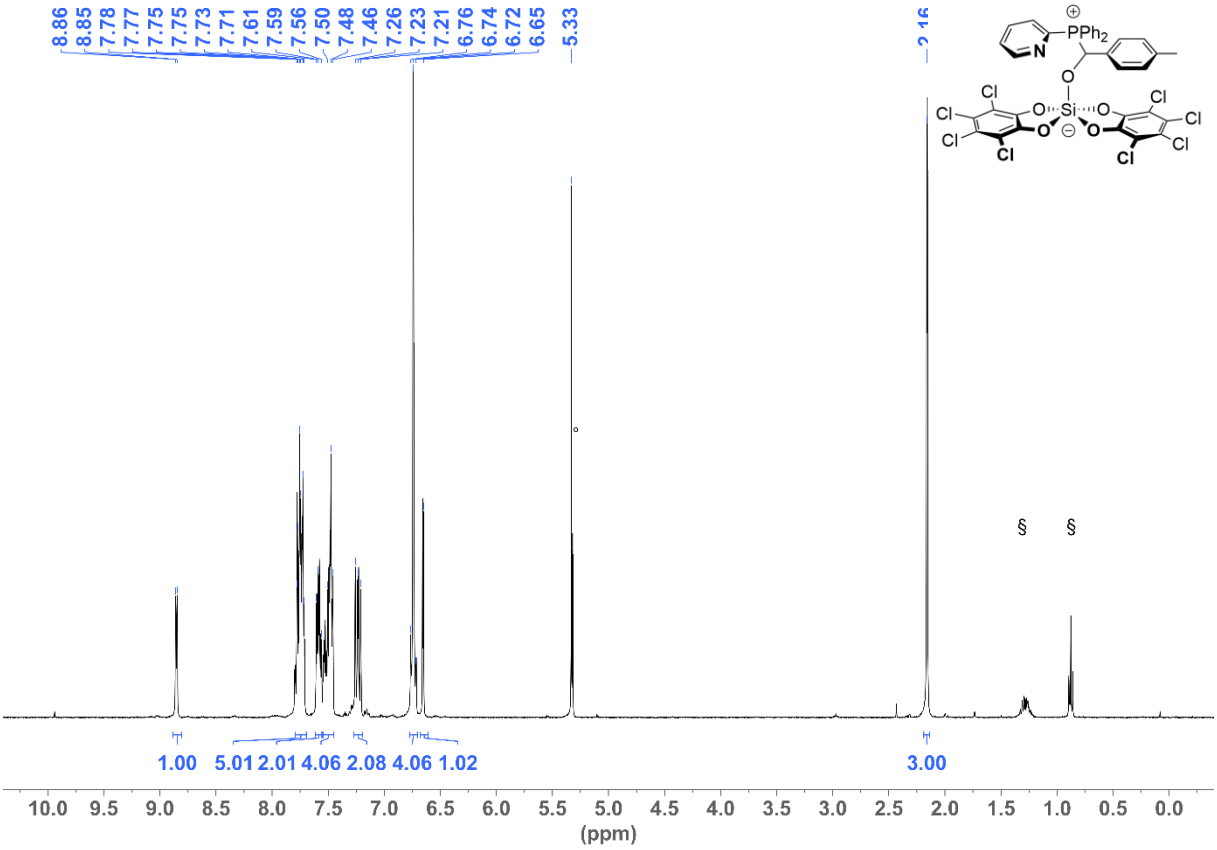

Figure S5.34: ^{1}H NMR (600 MHz, CD_2Cl_2, RT) of **1-(*p*-MeBA)-C**. Residual proton signals marked with ° (solvent) and § (pentane).

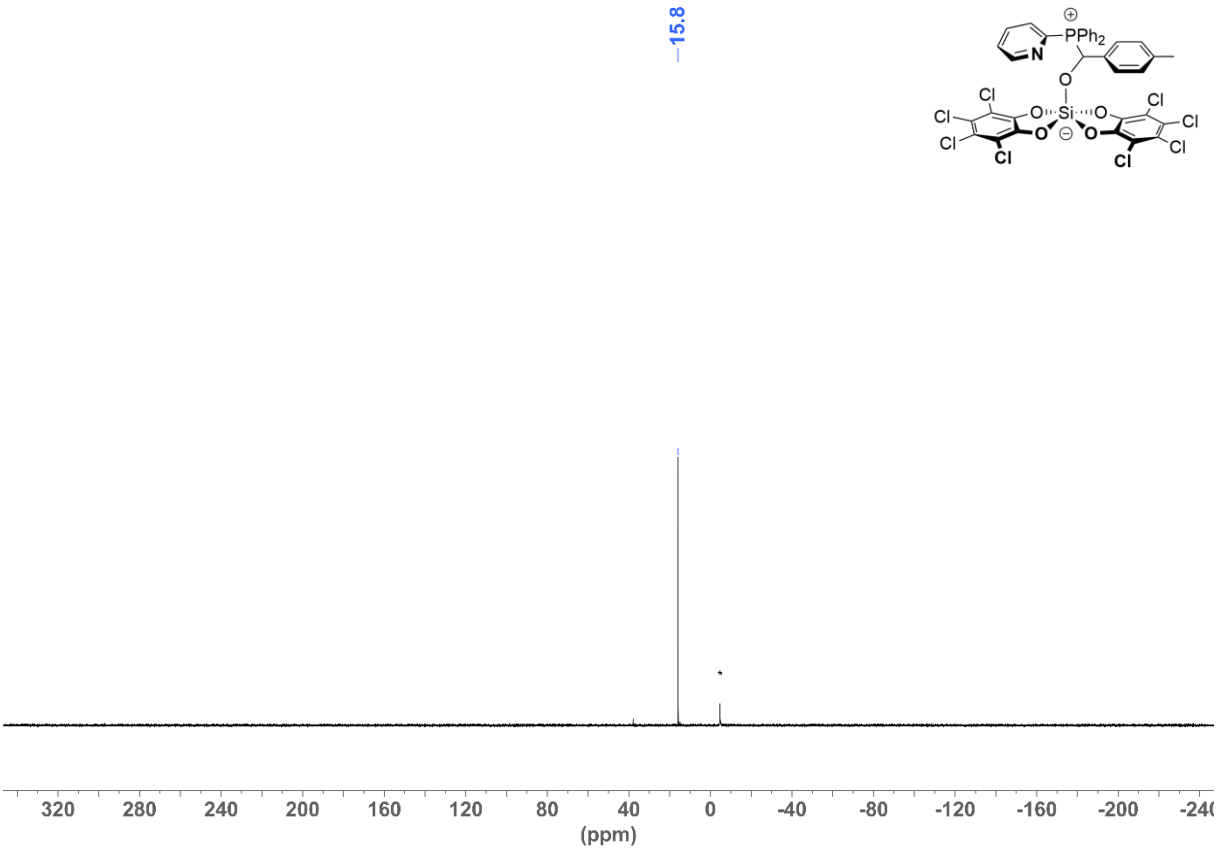

Figure S5.35: ^{31}P NMR (243 MHz, CD_2Cl_2, RT) of **1-(*p*-MeBA)-C**. Phosphorus signal from excess **C** marked with *.

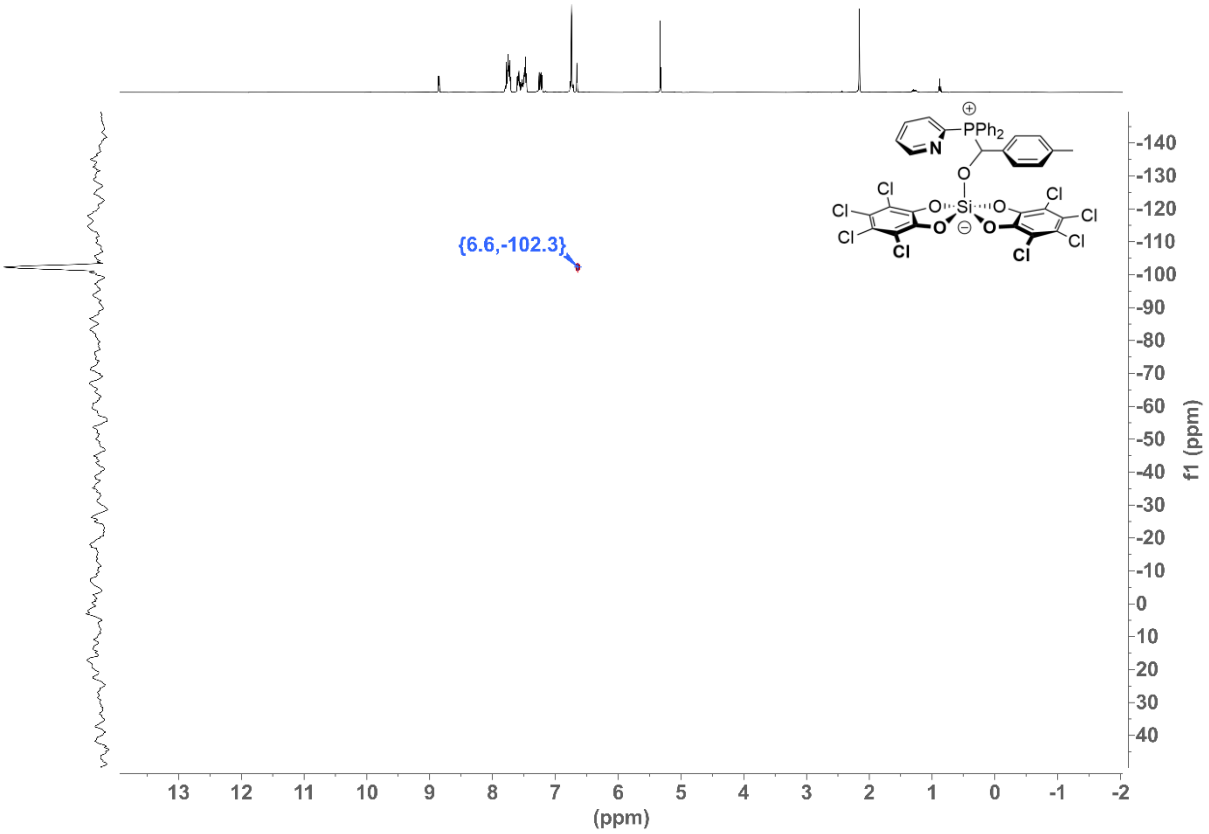

Figure S5.36: ^{1}H-^{29}Si-HMBC NMR (400 MHz, CD_2Cl_2, RT) of **1-(*p*-MeBA)-C**.

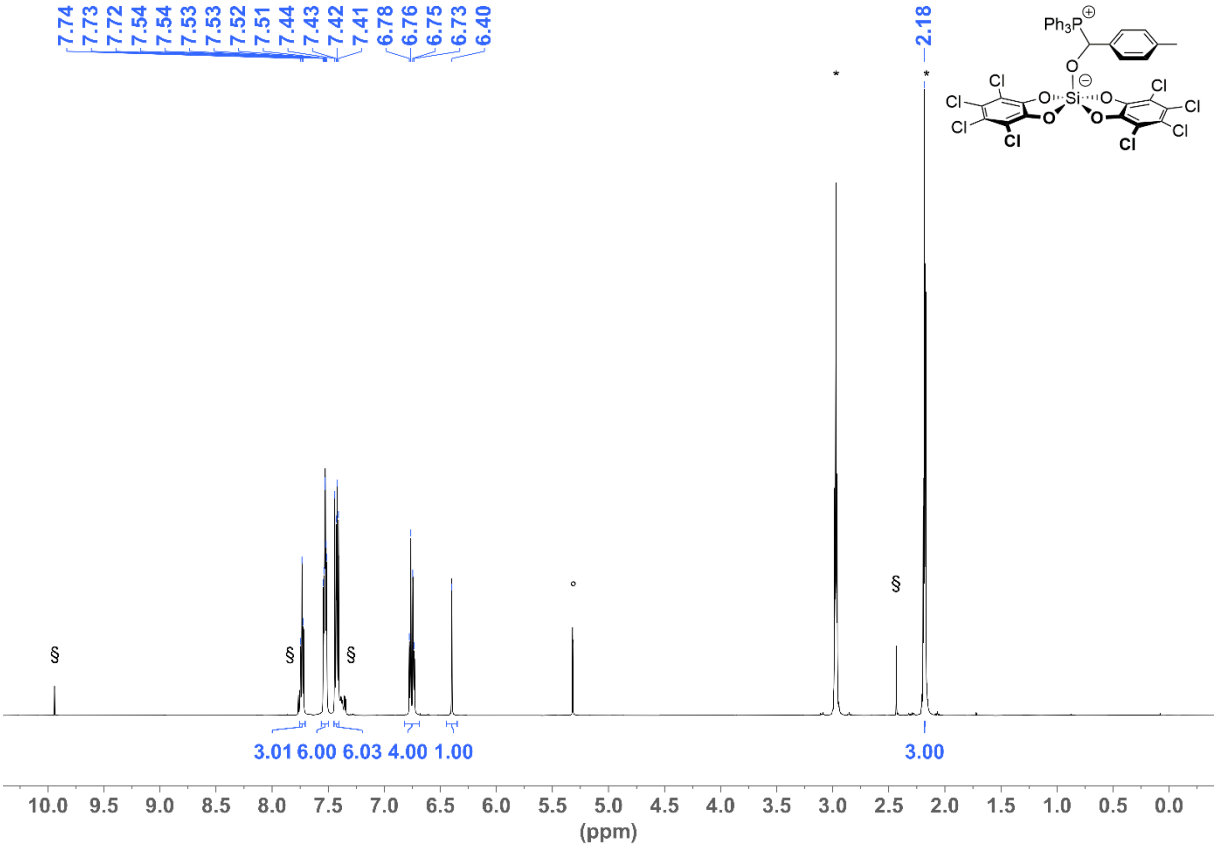

Figure S5.37: ^{1}H NMR (600 MHz, CD_2Cl_2, RT) of **1-(*p*-Me-BA)-PPh$_3$**. Residual proton signals marked with ° (solvent), * (sulfolane) and § (*p*-Me-BA).

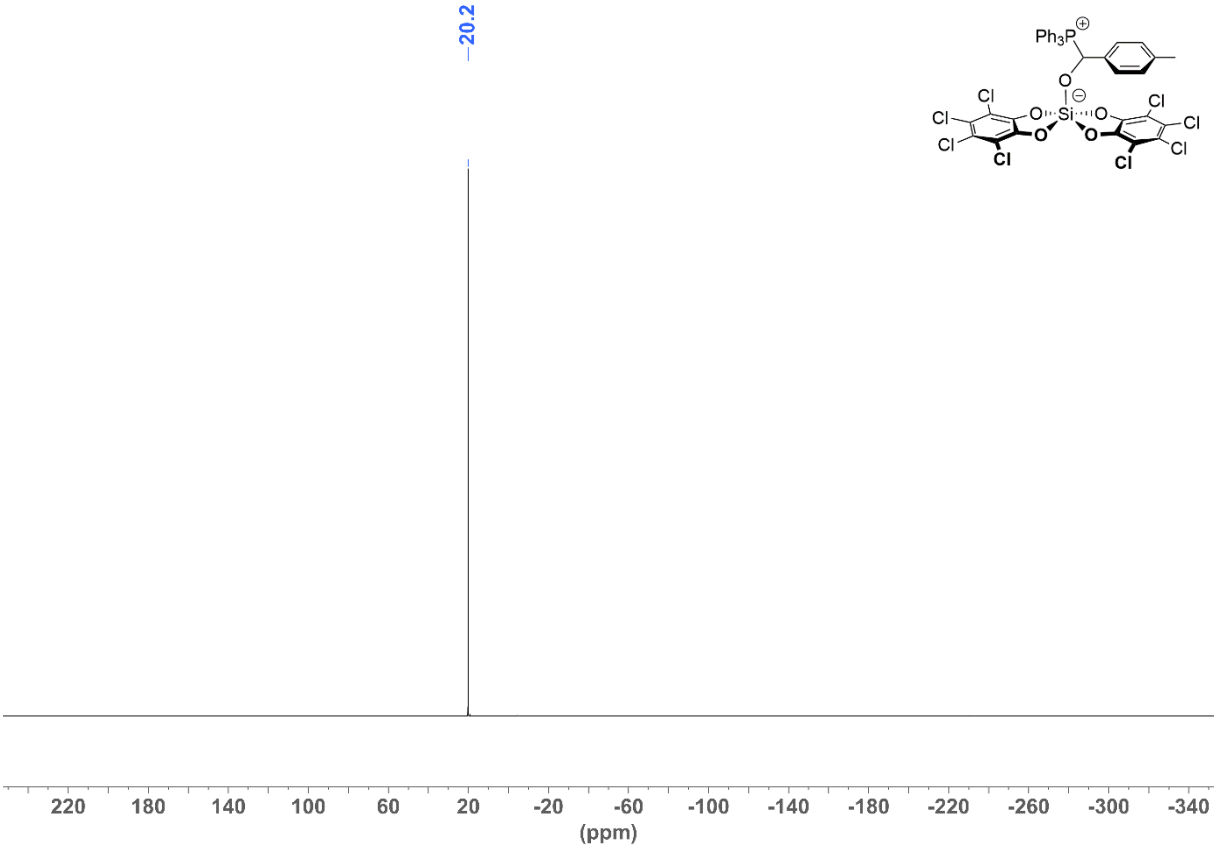

Figure S5.38: ^{31}P NMR (243 MHz, CD_2Cl_2, RT) of **1-(*p*-Me-BA)-PPh$_3$**. Phosphorus signal from excess PPh_3 marked with *.

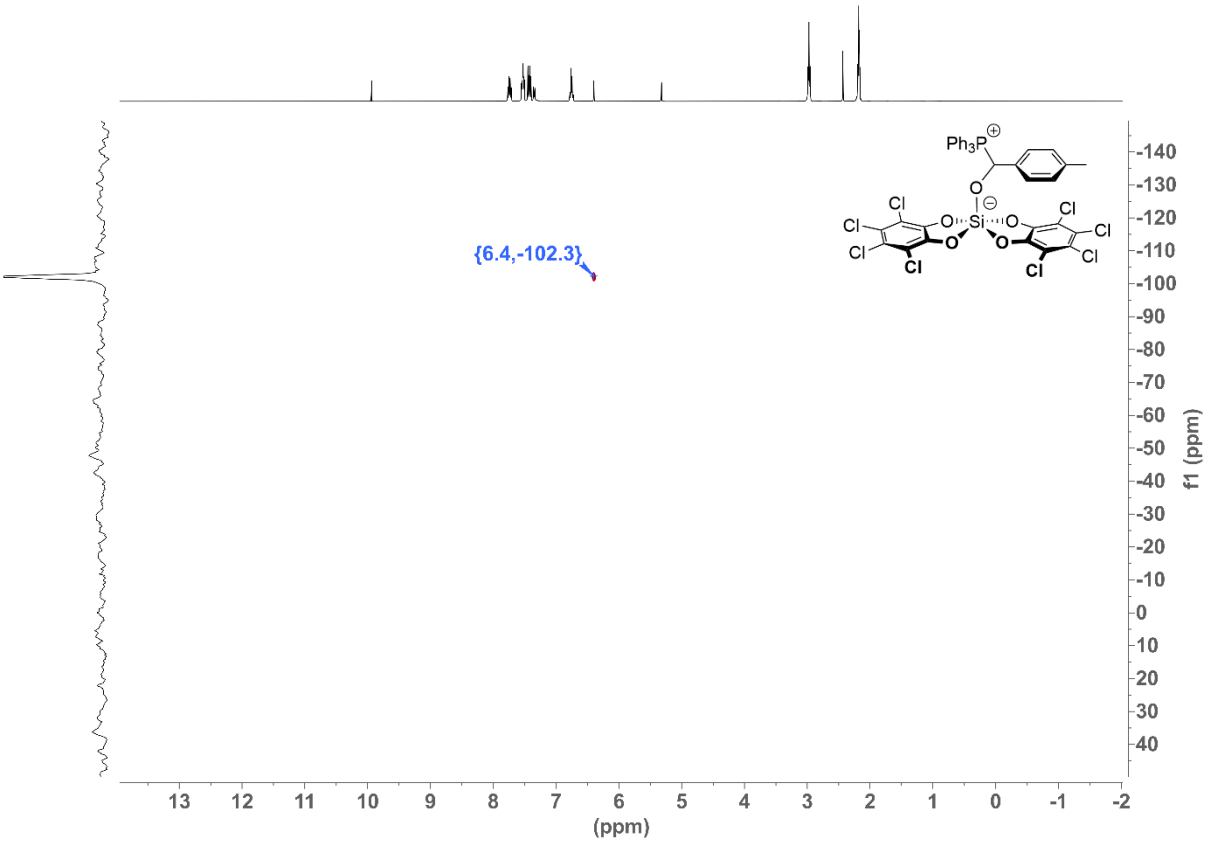

Figure S5.39: ^{1}H-^{29}Si-HMBC NMR (400 MHz, CD_2Cl_2, RT) of **1-(*p*-Me-BA)-PPh$_3$**.

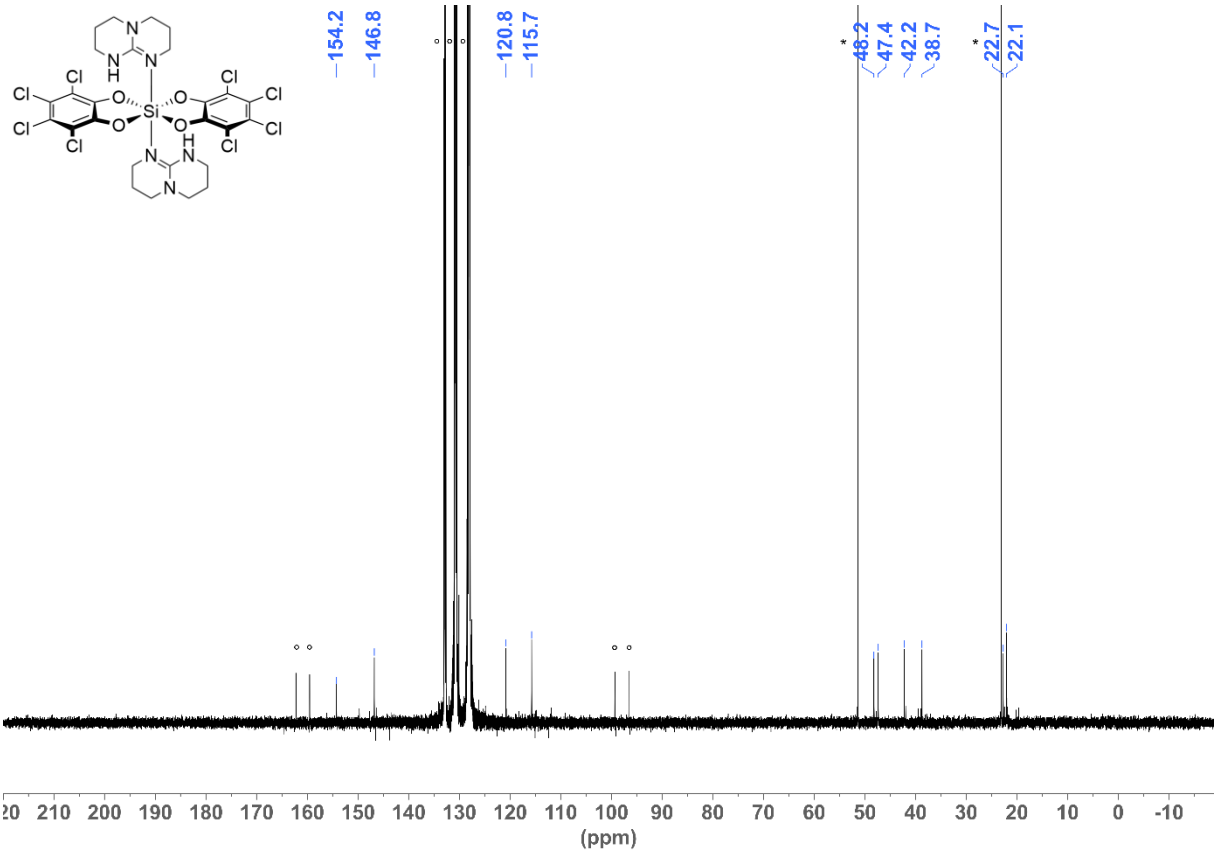

Figure S5.40: ^{13}C NMR (151 MHz, *o*-DCB, RT) of **1-(hppH)$_2$**. Residual proton signals marked with ° (solvent) and * (sulfolane).

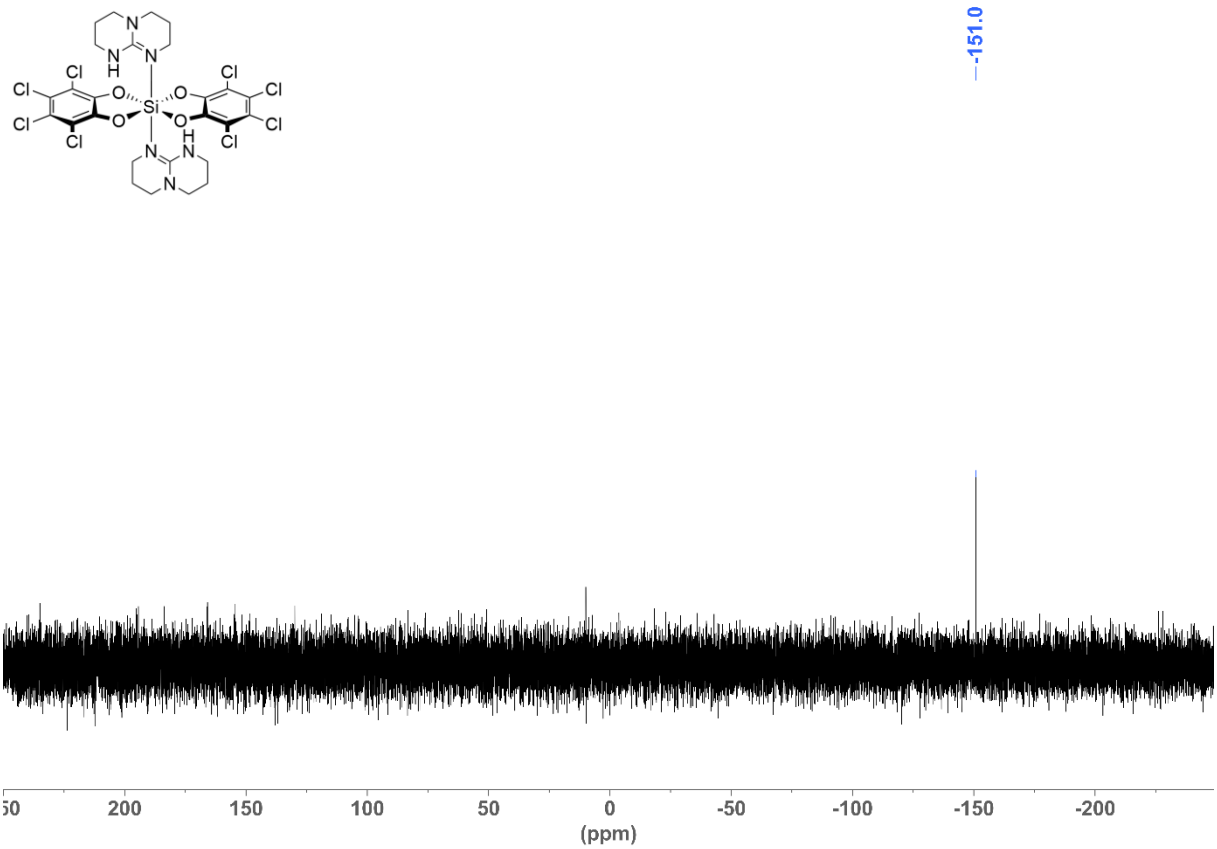

Figure S5.41: ^{29}Si NMR (119 MHz, *o*-DCB, RT) of **1-(hppH)$_2$**.

6. References

1. T. Thorwart, D. Roth and L. Greb, *Chemistry*, 2021, DOI: 10.1002/chem.202101138.
2. B.-S. Kim, J. Jiménez, F. Gao and P. J. Walsh, *Organic letters*, 2015, **17**, 5788–5791.
3. M. R. Willcott, *Journal of the American Chemical Society*, 2009, **131**, 13180-13180.
4. Z. Otwinowski and W. Minor, *Methods Enzymol*, 1997, **276**, 307-326.
5. SAINT, *Journal*, 2016.
6. G. M. Sheldrick, *Journal*, 2004-2014.
7. L. Krause, R. Herbst-Irmer, G. M. Sheldrick and D. Stalke, *Journal of Applied Crystallography*, 2015, **48**, 3-10.
8. G. M. Sheldrick, *Journal*, 2014-2018.
9. G. M. Sheldrick, *Acta Crystallographica Section A Foundations of Crystallography*, 2015, DOI: 10.1107/S2053273314026370, 3-8.
10. G. M. Sheldrick, *Journal*, 2012-2018.
11. W. Robinson and G. M. Sheldrick, *Journal*, 1988.
12. G. M. Sheldrick, *Acta Crystallographica Section A Foundations of Crystallography*, 2008, **64**, 112-122.
13. G. M. Sheldrick, *Acta Crystallographica Section C Structural Chemistry*, 2015, **71**, 3-8.
14. O. V. Dolomanov, L. J. Bourhis, R. J. Gildea, J. A. K. Howard and H. Puschmann, *Journal of Applied Crystallography*, 2009, **42**, 339-341.
15. C. B. Hübschle, G. M. Sheldrick and B. Dittrich, *J Appl Crystallogr*, 2011, **44**, 1281-1284.
16. I. J. Bruno, J. C. Cole, P. R. Edgington, M. Kessler, C. F. Macrae, P. McCabe, J. Pearson and R. Taylor, *Acta Crystallogr B*, 2002, **58**, 389-397.
17. C. F. Macrae, I. J. Bruno, J. A. Chisholm, P. R. Edgington, P. McCabe, E. Pidcock, L. Rodriguez-Monge, R. Taylor, J. van de Streek and P. A. Wood, *Journal of Applied Crystallography*, 2008, **41**, 466-470.
18. C. F. Macrae, P. R. Edgington, P. McCabe, E. Pidcock, G. P. Shields, R. Taylor, M. Towler and J. van de Streek, *Journal of Applied Crystallography*, 2006, **39**, 453-457.
19. C. F. Macrae, I. Sovago, S. J. Cottrell, P. T. A. Galek, P. McCabe, E. Pidcock, M. Platings, G. P. Shields, J. S. Stevens, M. Towler and P. A. Wood, *J Appl Crystallogr*, 2020, **53**, 226-235.
20. P. van der Sluis and A. L. Spek, *Acta Crystallographica Section A Foundations of Crystallography*, 1990, **46**, 194-201.
21. A. L. Spek, *Acta Crystallographica Section C Structural Chemistry*, 2015, **71**, 9-18.
22. A. L. Spek, *Journal*.
23. A. L. Spek, *Journal of Applied Crystallography*, 2003, 7-13.
24. F. Neese, *Wires. Comput. Mol. Sci.*, 2012, **2**, 73-78.
25. S. Grimme, J. G. Brandenburg, C. Bannwarth and A. Hansen, *J. Chem. Phys.*, 2015, **143**, 054107.
26. S. Grimme, *Chem-Eur. J.*, 2012, **18**, 9955-9964.
27. Y. Zhao and D. G. Truhlar, *J. Phys. Chem. A*, 2005, **109**, 5656-5667.
28. A. Schafer, C. Huber and R. Ahlrichs, *Journal of Chemical Physics*, 1994, **100**, 5829-5835.
29. F. Weigend, F. Furche and R. Ahlrichs, *The Journal of Chemical Physics*, 2003, **119**, 12753-12762.
30. F. Weigend and R. Ahlrichs, *Phys. Chem. Chem. Phys.*, 2005, **7**, 3297-3305.
31. S. Grimme, J. Antony, S. Ehrlich and H. Krieg, *J. Chem. Phys.*, 2010, **132**.
32. E. R. Johnson and A. D. Becke, *J. Chem. Phys.*, 2005, **123**.
33. A. D. Becke and E. R. Johnson, *J. Chem. Phys.*, 2005, **122**.
34. S. Grimme, S. Ehrlich and L. Goerigk, *J. Comput. Chem.*, 2011, **32**, 1456-1465.
35. K. Eichkorn, O. Treutler, H. Ohm, M. Haser and R. Ahlrichs, *Chem. Phys. Lett.*, 1995, **242**, 652-660.
36. F. Neese, F. Wennmohs, A. Hansen and U. Becker, *Chem. Phys.*, 2009, **356**, 98-109.
37. K. Eichkorn, F. Weigend, O. Treutler and R. Ahlrichs, *Theor. Chem. Acc.*, 1997, **97**, 119-124.

38. E. J. Baerends, T. Ziegler, A. J. Atkins, J. Autschbach, D. Bashford, O. Baseggio, A. Brces, F. M. Bickelhaupt, C. Bo, P. M. Boerritger, L. Cavallo, C. Daul, D. P. Chong, D. V. Chulhai, L. Deng, R. M. Dickson, J. M. Dieterich, D. E. Ellis, M. van Faassen, A. Ghysels, A. Giammona, S. J. A. van Gisbergen, A. Goez, A. W. Gtz, S. Gusarov, F. E. Harris, P. van den Hoek, Z. Hu, C. R. Jacob, H. Jacobsen, L. Jensen, L. Joubert, J. W. Kaminski, G. van Kessel, C. Knig, F. Kootstra, A. Kovalenko, M. Krykunov, E. van Lenthe, D. A. McCormack, A. Michalak, M. Mitoraj, S. M. Morton, J. Neugebauer, V. P. Nicu, L. Noodleman, V. P. Osinga, S. Patchkovskii, M. Pavanello, C. A. Peeples, P. H. T. Philipsen, D. Post, C. C. Pye, H. Ramanantoanina, P. Ramos, W. Ravenek, J. I. Rodrguez, P. Ros, R. Rger, P. R. T. Schipper, D. Schlns, H. van Schoot, G. Schreckenbach, J. S. Seldenthuis, M. Seth, J. G. Snijders and Sol, *Journal*.
39. E. Van Lenthe and E. J. Baerends, *J. Comput. Chem.*, 2003, **24**, 1142-1156.
40. F. Eckert and A. Klamt, *AlChE J.*, 2002, **48**, 369-385.
41. A. Klamt and M. Diedenhofen, *J. Comput. Aided Mol. Des.*, 2010, **24**, 357-360.
42. A. Klamt, *J. Phys. Chem.*, 1995, **99**, 2224-2235.
43. A. Klamt, B. Mennucci, J. Tomasi, V. Barone, C. Curutchet, M. Orozco and F. J. Luque, *Acc. Chem. Res.*, 2009, **42**, 489-492.